Distribution Agreement

In presenting this thesis or dissertation as a partial fulfillment of the requirements for an advanced degree from Emory University, I hereby grant to Emory University and its agents the non-exclusive license to archive, make accessible, and display my thesis or dissertation in whole or in part in all forms of media, now or hereafter known, including display on the world wide web. I understand that I may select some access restrictions as part of the online submission of this thesis or dissertation. I retain all ownership rights to the copyright of the thesis or dissertation. I also retain the right to use in future works (such as articles or books) all or part of this thesis or dissertation.

Signature:

_____ _____

Sarah M. L. Wilkening Date

Immobilization Methods for Binding Polyoxometalates onto Surfaces for Water Splitting Applications

By

Sarah Marie Lauinger Wilkening
Doctor of Philosophy

Chemistry

_____
Craig L. Hill, Ph.D.
Advisor

_____
Tianquan Lian, Ph.D.
Committee Member

_____
Khalid Salaita, Ph.D.
Committee Member

Accepted:

_____
Lisa A. Tedesco, Ph.D.
Dean of the James T. Laney School of Graduate Studies

_____
Date

Immobilization Methods for Binding Polyoxometalates onto Surfaces for Water Splitting Applications

By

Sarah Marie Lauinger Wilkening
B.S., Manchester College, 2012

Advisor: Craig L. Hill, Ph.D.

An abstract of a dissertation submitted to the Faculty of the James T. Laney School of Graduate Studies of Emory University in partial fulfillment of the requirements for the degree of Doctor of Philosophy in Chemistry
2017

Abstract

Immobilization Methods for Binding Polyoxometalates onto Surfaces for Water Splitting Applications

By

Sarah Marie Lauinger Wilkening

Photoelectrochemical conversion of solar light into hydrogen fuel through water splitting is the technological pathway to fuel with low or no CO_2 emissions. The water oxidation half reaction of water splitting requires a durable and efficient catalyst. All-inorganic polyoxometalate (POM) water oxidation catalysts (WOCs) are oxidatively, hydrolytically and thermally stable, and can aid in the multi-electron process required to split water. Homogenous POM WOCs have been studied in a variety of conditions with photosensitizers and sacrificial electron acceptors and are becoming more understood; however, these homogenous catalysts behave differently when bound to a surface. Cost-effective thin-film and nanoparticle semiconductor materials are optimal photoelectrochemical materials that, when combined with POM WOCs, are a potential new hybrid material for water splitting systems.

The general goals of this thesis are to (1) immobilized POM WOCs onto light absorbing surfaces for solar-driven water oxidation; (2) stabilize the POM WOC on the light absorbing surface using an atomic layer deposition protection layer; (3) electrochemically evaluate the stability of these species when immobilized via silylation on metal oxide surfaces or via Nafion on glassy carbon electrodes; and (4) evaluate the stability of these homogenous species through early-time kinetic measurements of oxygen generation and oxidant consumption.

Prior to this work, immobilization techniques resulted in little POM WOC stability on the surface. The first part of this thesis discloses the silylation technique which results in high surface coverage of the POM while maintaining water oxidation activity. In the follow-up research, the immobilized POM is further stabilized with nanometers of protection using atomic layer deposition (ALD). The end of the thesis reports on the early-time kinetic studies by light-driven oxygen generation combined with oxidant consumption of several POM WOCs and the stability assessment of an electrocatalyst immobilized on glassy carbon electrodes for water oxidation.

Immobilization Methods for Binding Polyoxometalates onto Surfaces for Water Splitting Applications

By

Sarah Marie Lauinger Wilkening
B.S., Manchester College, 2012

Advisor: Craig L. Hill, Ph.D.

A dissertation submitted to the Faculty of the James T. Laney School of Graduate Studies of Emory University in partial fulfillment of the requirements for the degree of Doctor of Philosophy in Chemistry
2017

TABLE OF CONTENTS

LIST OF TABLES

CHAPTER 1

CHAPTER 3

CHAPTER 4

LIST OF FIGURES

CHAPTER 1

CHAPTER 2

CHAPTER 3

CHAPTER 4

IMMOBILIZATION METHODS FOR BINDING POLYOXOMETALATES ONTO SURFACES FOR WATER SPLITTING APPLICATIONS

CHAPTER 1

Background of Photocatalysts and Water Oxidation Catalysts

with Quishi Yin, Yurii V. Geletii, and Craig L Hill

Published in part in: Lauinger S. M., Yin, Q., Geletii, Y. V., Hill, C. L. "Polyoxometalate Multi-Electron Catalysts in Solar Fuel Production" *Advances in Inorganic Chemistry*. **2017**, 69, Chapter 5

1.1 Introduction and Outlook

Much of our world's energy comes from consuming fossil fuels. According to Thomas Princen, "for the planet to sustain a livable future –for humans, at least—the only viable strategy is never to extract [fossil fuels]."[1] The high-energy lifestyle that we have become accustomed to due to our fossil fuel dependency will not be possible when a switch to renewable energy takes over. True, fossil fuels—until recently—have been easy-to-get, cheap, and a high-density energy form for the ever-increasing energy demand. Unfortunately, burning oil has also been the cause of toxic substances dispersed throughout the planet, erosion of soil, acidification of the oceans, and damage to the underground aquifers. Continued extraction, refining, combustion, and dispersion of the remaining fossil fuels will magnify these effects.

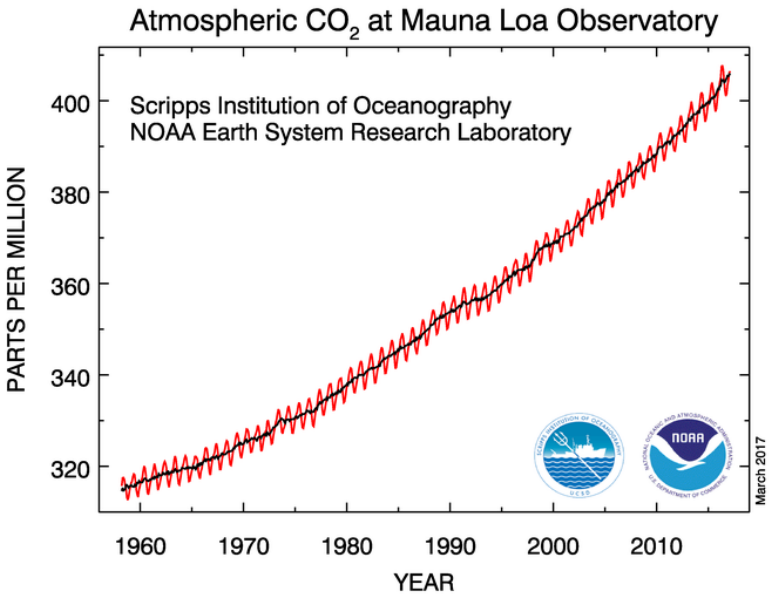

Figure 1.1 Annual atmospheric CO_2 emissions in ppm as measured by the Mauna Loa Observatory (www.esrl.noaa.gov).

Possibly the most consequential result of current technologies for energy production is the increased carbon dioxide content in the atmosphere, warming the planet and increasing polution. To date, there are several alternative energy sources available, but to generate enough energy to fulfill the demand of the growing population through these avenues remains insufficient.

Energy sources have been defined in three broad categories: chemical and photophysical energy, nuclear reactions, and thermomechanical.[2] More specifically, chemical and photophysical energy generates heat and electricity from redox reactions (typically a hydrocarbon) or light illumination. The energy from chemical reactions is in the form of breaking and/or forming chemical bonds. Nuclear reactions create energy by splitting large nuclei or fusing light nuclei. Thermomechanical energy sources include wind, solar, hydro, or geothermal—all of which have a low carbon emission.

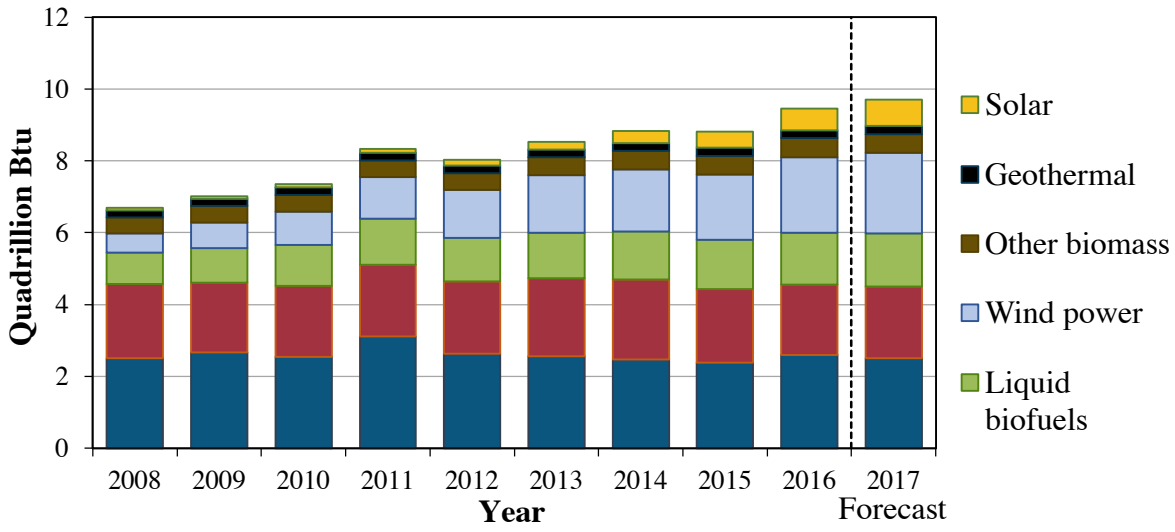

Figure 1.2 U.S. renewable energy supply in quadrillion British thermal units from 2008 to 2017. Note: Hydropower value excludes pumped storage generation; liquid biofuels includes both ethanol and waste biodiesel; other biomass includes landfill gas and other non-wood waste. Source: U.S. Energy Information Administration (Dec. 2016).

Wind energy has become a promising pollution-free energy source to replace fossil fuel-generated electricity; however, some major drawbacks to wind energy are the diffuse nature of the source and the large numbers of wind generators that are required in order to generate useful amounts of electricity.

Solar energy uses the powerful supply of photons from the sun. Dr. Craig Hill and others have said many times that the energy provided by the sun in 80 minutes is enough to supply the world's energy demand for one year.[3] Solar panels and photovoltaics (PV) are a reliable source of electricity; however, the highest efficiency of a PV cell remains 14-22% under sun simulated light, requiring large areas of solar panels similar to wind turbine farms.[4-5]

Hydropower energy generates electricity from the gravitational potential of moving water. Many countries have invested in man-made waterfall dams. Like most renewable sources of energy, hydropower could not compete with low-cost fossil fuel consumption; however, to date, hydropower is the most dominant renewable energy source used for electricity.

Geothermal power can be found from the accumulation of heat from radioactive decay seeping out from various gradients in the planet. There are very few locations where this energy can be found and extracted for generation of heat.

Each energy source has limitations and unwanted characteristics. With the majority of the planet's energy coming from fossil fuels and nuclear sources, mankind must continue working on sustainable energy sources while simultaneously dealing with the issue of CO_2 sequestration.[2]

Of all these sources for generating heat and electricity, there is a desire for a high-density hydrocarbons-free fuel for vehicle use. Hydrogen is an attractive fuel for several reasons: hydrogen can be generated from many precursors, its oxidation product is water, the H_2 bond carries a great deal of energy, it is lightweight, and highly abundant. Yet, among all these positive attributes, storage remains a problem.[6] Of the many sources available for renewable energy, chemical energy integrated with solar energy is a promising combination for sustainable fuel production.

1.2 Photocatalysis

In Nature, light is converted into energy during photosynthesis as photon absorption promotes electron transfer through a series of electron acceptors in the photosystems, sequentially converting ATP and NADPH into consumable energy products. Mimicking Nature's process has led to the development of photovoltaic (PV) and photoelectrochemical cells (PECs) to produce fuel and energy from light. Photovoltaics come in many forms and have been shown to facilitate the conversion of photon energy into electricity,[7] but they lack the ability to convert this photon energy into chemical fuel. The conversion of light into chemical energy in a PEC is achieved at the interface between the two phases of the semiconductor/liquid junction, which results in long-lived charge separation and overall efficient energy conversion.

Photocatalysis is the "acceleration of a photoreaction by the presence of a catalyst."[8] In a homogenous catalyst system, the photoexcitation process typically occurs in an adsorbate or photosensitizer molecule, which then interacts with the catalyst substrate

to initiate the chemical reaction. When the photoexcitation takes place on a heterogeneous catalyst, such as a semiconductor, the photoreaction takes place on the substrate surface.

Semiconductors are easily understood in terms of band theory at its fundamental level.[9] Similar to atoms being composed of electrons in orbitals, in a solid, the electrons are distributed into varying energy bands, where the electrons occupy these bands from lowest to highest energy. The lowest energy band with vacant electronic states is called the conduction band and the highest energy band in which electrons are present is the valence band (figure 1.3). The difference in band structure of materials results in the different properties of insulators, conductors, and semiconductors. The band gap is defined by the different energies between the valence and conduction bands. Electrons cannot exist in the band gap, but must reside in either the conduction or the valence band.

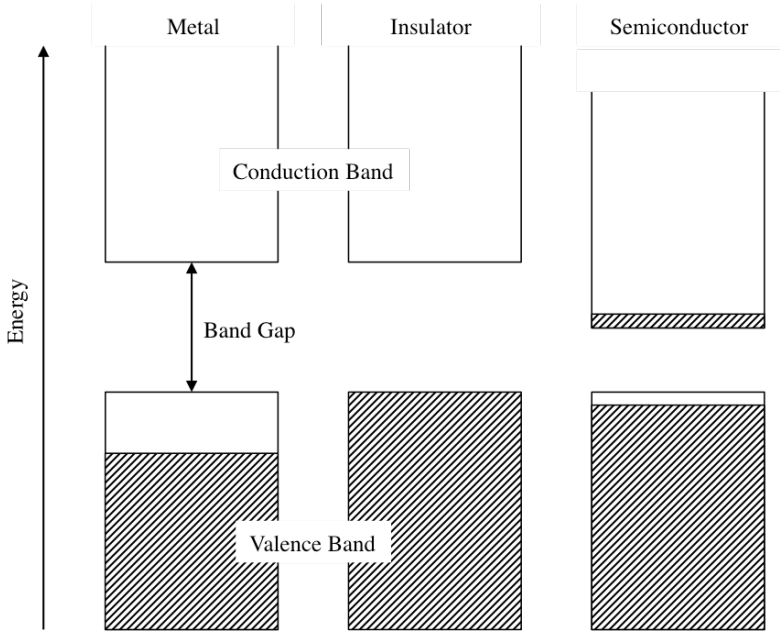

Figure 1.3 Schematic illustration of energy band gaps of metals, insulators, and semiconductors with filled in band representing the filled or mostly filled valence band and the white band representing the empty or mostly empty conduction band.

In a metal, the electrons fill a portion of the valence band and are delocalized, or freely moving across all atoms throughout the material. This allows metal materials to act as a conductor. Having partially filled bands allows for electrons to move between nearby empty bands. In an insulating material, such as plastic, the valence band is filled and the conduction band is too far away in energy, precluding the free flow of electrons. Semiconductors are unique in that the size of the band gap is small enough that electrons from the valence band can access the conduction band upon stimulation (heat, light, etc.).

The greatest shortcoming of semiconductor/liquid junctions for energy conversion is the stability and efficacy of the semiconductor's solar radiation absorption range. Semiconductors such as Si, GaAs, and MoSe2 have an ideal band gap (1.1 - 1.7 eV), but are oxidatively unstable and easily undergo corrosion under illumination.[10] Conversely, semiconductors with large band gaps, such as TiO_2 and WO_3 are stable but the optical energy threshold is high and lies in the ultraviolet region. Solutions to this obstacle have been extensively pursued in recent years.[11-16]

One method to overcome the stability limitation of semiconductors is by altering the redox reagents in solution, which compete kinetically with the corrosion of small band gap semiconductors such as Si, Ge, InP, GaAs, and InSb.[17-20] In another direction, some research uses non-aqueous electrolytes and solvents to prevent corrosion.[21]

Surface modification of semiconductors is generally done through doping or immobilization methods. Doping introduces impurity atoms in a controlled manner in order to change the properties of the material. Doping of semiconductors tunes the band gap energy by introducing new allowed energy states within the band gap. These energy levels

enhance conductivity, shift the Fermi level, and increase electron trapping sites depending on the concentration and type of dopant.[22] Electron donor impurities (n-type) create energy states near the conduction band, whereas, electron acceptor impurities (p-type) create states near the valence band.

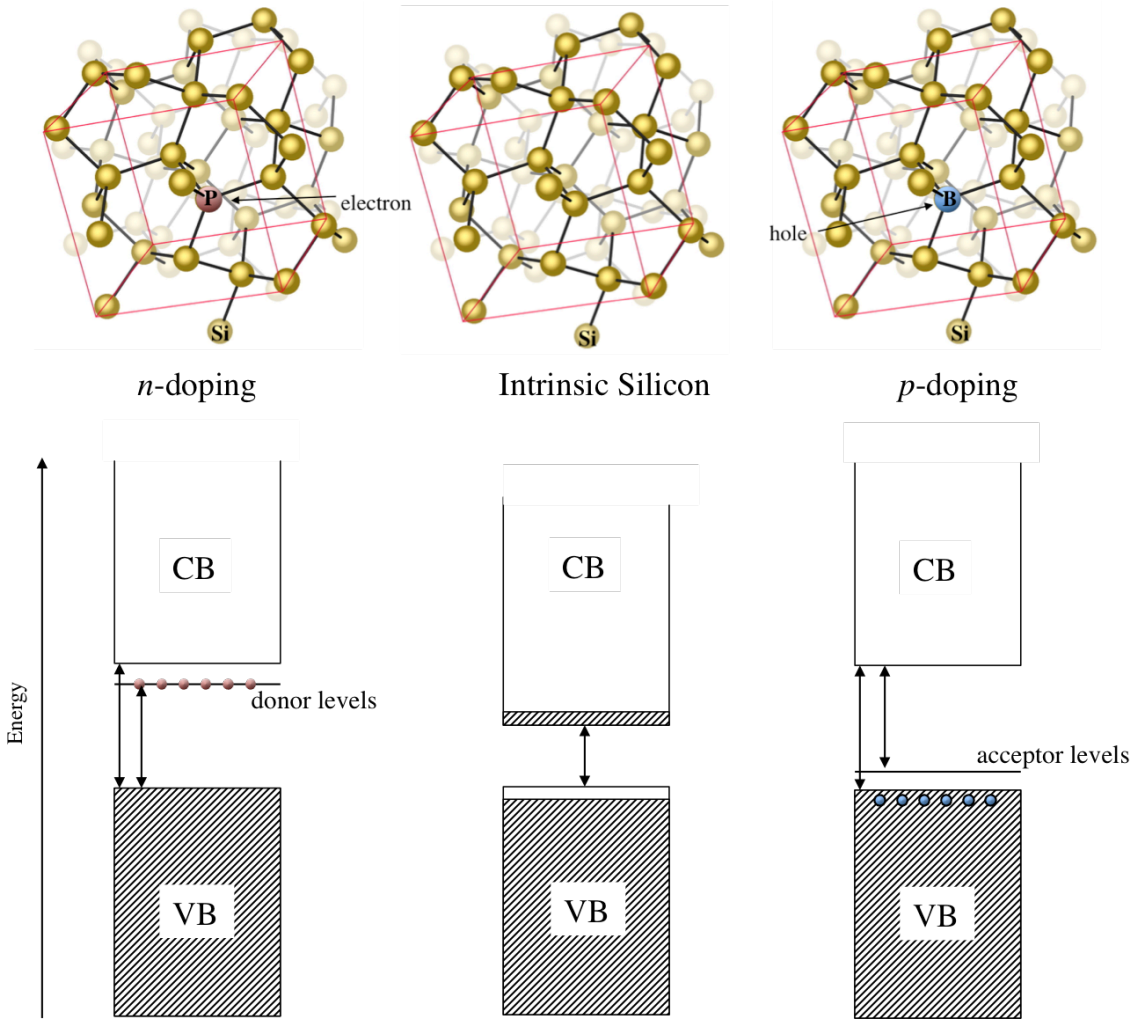

Figure 1.4 Adding covalently bonded phosphorus atoms as *n*-dopants and boron atoms as *p*-dopants into crystalline silicon matrix generates donor and acceptor levels, respectively. VB denotes the valence band and CB its conduction band.

Immobilization methods to enhance the light absorbing properties of inorganic semiconductors have been investigated for several decades. In 1980, Spitler and Parkinson layered dyes onto layered semiconductor materials WS_2, $MoSe_2$, WSe_2, and SnS_2.[23-25] The dyes were comprised of cyanine dyes that have visible light absorption ranges from 520 to 835 nm (Figure 1.4 a). [24] However, Spitler and Parkinson suggest that there is a limit for dye coverage and that the surface state densities and electron injection rates decrease with high dye coverage.[26]

In another approach, O'Regan and Grätzel researched a low-cost and highly efficient solar cell by associating the photosensitizer $Ru(bpy)_2(dppz\text{-}R)(PF_6)_2$ (bpy = bipyridyl, dppz-R = 11-(diethoxyphosphorylmethyl)dipyrido[3,2,2',3'-]phenazine) (Figure 1.4 b) to TiO_2 semiconductor.[27] The nanocrystalline surface of the TiO_2 resulted in an increased surface area for high loading of the photosensitizer. The system was considered long-lived in acetonitrile (around 825 ns), but was instantly quenched in aqueous systems.[28]

Most research in the area of dye-sensitized solar cells anchors photosensitizing molecules with carboxylate[29] and phosphonic acid groups.[30-39] Anchoring Ru-based sensitizers onto semiconductors has been extensively studied. In 2004, Wang et al., functionalized TiO_2 with an amphiphilic polypyridyl ruthenium complex (*cis*-$Ru(dpbpy)(dnbpy)(NCS)_2$) (dpbpy = 4,4'-diphosphonic acid-2,2'-bipyridine, dnbpy = 4,4'-dinonyl-2,2'-bipyridine) (Figure 1.5 c) in order to sensitize the TiO_2 material for visible light absorption.[40]

In 2010, Orlandi et al., first developed a triad system composed of semiconductor, chromophore and catalyst.[41] The semiconductor photoelectrodes were sensitized using $[Ru(bpy)_2(dpbpy)]^{2+}$ (Figure 1.5 d). In a later study, transient absorption measurements

revealed that the electron injection from the catalyst to the dye and then into the semiconductor generates long-lived charge separated states.[42] Following this research, Fielden et al., refined the triadic system by replacing the $[Ru(bpy)_2(dpbpy)]^{2+}$ with a new $[Ru(5\text{-crownphen})_2(H_2dpbpy)]$ dye (Figure 1.5 e).[43] This novel dye out-performed the previous photosensitizer by absorbing light more strongly and increasing stability of the system.

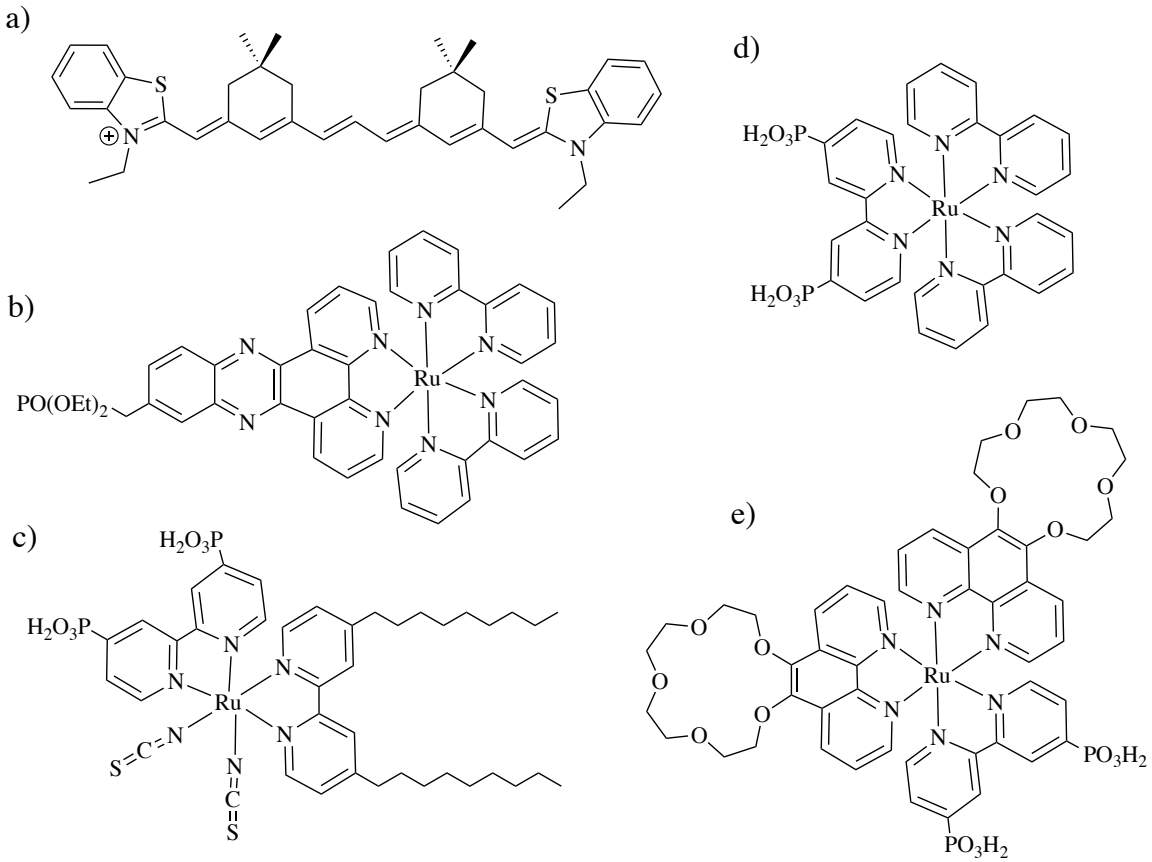

Figure 1.5 Dye compounds used to sensitize semiconductor surfaces for water oxidation.

1.3 Water Splitting and Challenges in Solar Energy Generation

There are three main technologies developed towards water splitting devices.[44] These three are photovoltaic-electrolyzer combinations, photocatalyst colloids, and photoelectrochemical devices. A general scheme for a device would require three major components: a photosensitizer for absorbing sun light with a long-lived charge separation in order to sequester the photoexcited electron and generate a hole; a proton reduction catalyst for hydrogen evolution; and a water oxidation catalyst to oxidize water into protons and oxygen gas (figure 1.6). For these device designs, the components must be independently efficient, stable, and scalable. To date, separate components have been studied and refined in conditions separate from other components, thus the system remains to share common or compatible conditions.

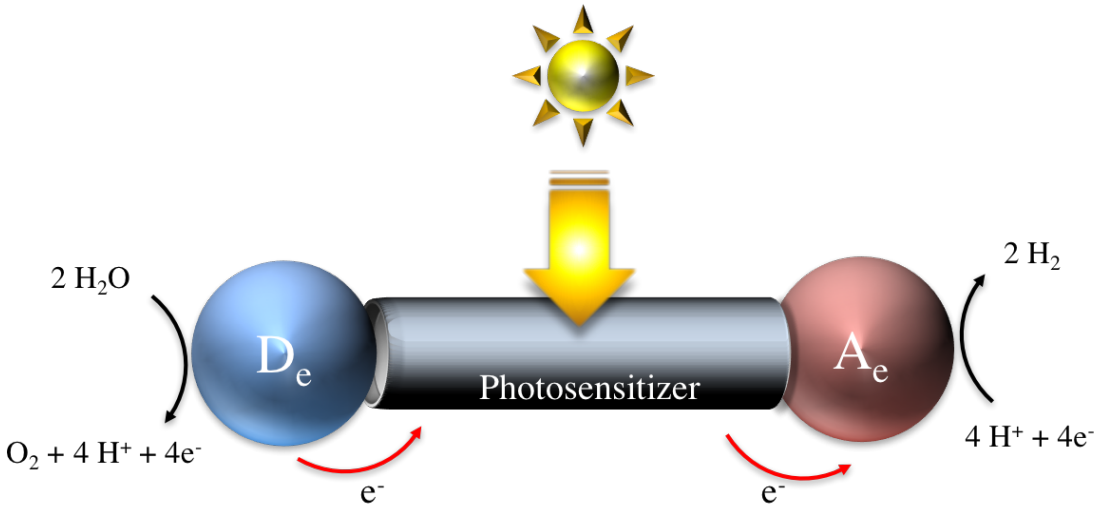

Figure 1.6 Scheme of a proton-coupled electron transfer (PCET) system with three components: a photosensitizer separation unit, an electron donor (D_e) for water oxidation, and an electron acceptor (A_e) for proton reduction. Arrows indicate the flow of electrons (red), energy (yellow), and catalytic pathway (black).

Photocatalytic water splitting, generating hydrogen and oxygen, provides a sustainable and green method for carbon-free fuel.[45] Of the two half reactions for water splitting, water oxidation is the most demanding of the two reactions and up-hill, requiring 1.23 V *vs*. NHE at pH 0 to initiate the four-electron and four-proton oxidation of water to oxygen (eq. 1.1 and 1.2).

Oxidation: $2\ H_2O(l) \rightleftarrows 4\ H^+(aq) + O_2(g) + 4\ e^-$ (1.1)

Reduction: $4\ H^+(aq) + 4\ e^- \rightleftarrows 2\ H_2(g)$ (1.2)

Overall: $2\ H_2O(l) + h\nu\ (for\ photocatalysis) \rightarrow O_2(g) + 2\ H_2(g)$ (1.3)

The half reactions of water splitting are pH dependent and higher pH values will shift the potential for water splitting to lower voltages according to the Nernst equation. In contrast, the thermodynamics of the overall reaction (eq 1.3) is independent of pH and depends on temperature and ionic strength under standard conditions ($\Delta G = 4.92$).[46] Because the water reduction step is less energy-demanding and many materials have been researched to mediate this process, the current research is focused on efficient and stable water oxidation catalysts and materials. At pH 14, only 0.40 V and 0.83 V *vs*. NHE are required for water oxidation and water reduction, respectively. In these conditions, water splitting is much more attainable; however, very few catalysts or materials are stable under such alkaline conditions.

Catalysts are either molecular or material. The most common bulk material catalysts consist of platinum surfaces or transition metal oxides such as RuO_2 and IrO_2. These materials have been shown to have the best performance for water oxidation;

however, they are rare and expensive. Therefore, research towards more earth abundant materials is underway.

1.4 Hydrogen Evolution Reaction Catalysts

The most highly active hydrogen evolution reaction (HER) catalysts are composed of Pt or alloys of Pt.[47] Non-noble catalyst cathodes stable in acidic conditions include molybdenum disulfides[48] and modifications thereof,[49-52] carbide, nitride, and boride catalysts.[53-56] Much research has been performed on an alkaline stable Ni-Mo and Ni-Mo-Cd hydrogen evolution catalysts that are now used commercially in alkaline electrolysis systems.[57-59]

1.5 Oxygen Evolution Reaction Catalysts

Heterogeneous water oxidation catalysts (WOCs) are made up of metal oxides that can withstand high potentials to oxidize water and are typically known to be stable, yet slow for oxygen evolution. Molecular catalysts are generally selective and faster. The most acid-stable oxygen evolution reaction (OER) catalysts constitute combinations of rare Ir or Ru metal oxides. To date, no efficient molecular acid-stable water oxidation catalysts have been reported. Variations of cobalt oxide and nickel hydroxide compounds have been found to be stable in alkaline conditions.[60-65]

In 1972, Fujishima and Honda studied the water oxidation and photosensitizing properties of TiO_2 electrodes.[66] The large band gap of TiO_2 (E_g = 3.2 eV) requires ultra violet radiation for water oxidation and limits its worth when developing a device functioning within the solar spectrum. Much research has been done over the past three

decades to expand the absorption range of TiO_2 to within the visible region. Metal oxides such as WO_3[67-68] and ZnO[69] have band gaps too large for use as photoanodes; however other metal oxides with smaller band gaps have been identified and studied, including α-Fe_2O_3[70-72] and $BiVO_4$.[73] These metal oxide photoanodes generally fail in efficiency even if the band gap is within the solar spectrum due to poor charge transport within the materials resulting in fast electron-hole recombination and slow kinetics.

Cobalt oxides have been thoroughly investigated for water oxidation properties in a range of structures and conditions. Nocera et al. developed a Co^{II} phosphate (CoP_i) catalyst that was electrochemically deposited on a film and active for water oxidation in phosphate buffer with very little change in activity over a long period of time.[61] From this work, cobalt oxide water oxidation catalysis took off. Dau et al., studied CoO_6 octahedra,[74] Pandey et al., explored Co_3O_4 clusters in silica scaffolds,[75] Dismukes et al., studied Co_4O_2 cubic cores,[76] and Wang et al., researched Co_3O_4 nanoparticles.[77]

Molecular catalysts exhibit much more selectivity and speed for water oxidation. The first molecular water oxidation catalyst disclosed was Meyer's "Blue Dimer" with a ruthenium core (Figure 1.7 a).[78] Since then, many other Ru-based organometallic compounds have been developed for water oxidation catalysis.[79-83] Iridium-based molecular catalysts have also been extensively studied. Brudvig and co-workers studied the iridium molecular precatalyst with pentamethylcyclopentadienyl (Cp*) ligand in great detail,[84] as well as many other iridium complexes with the Cp* ligand.[85]

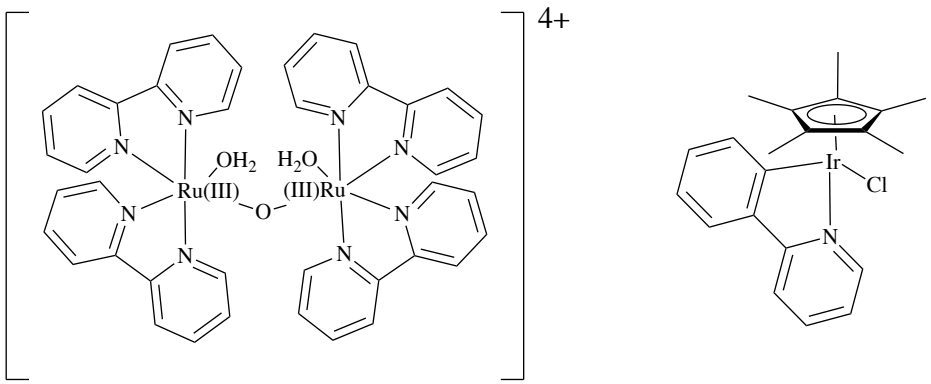

Figure 1.7 Molecular catalysts for water oxidation; (left) the Ru-based "Blue Dimer" and (right) Ir-Cp* complex.

These catalysts and many other organometallic catalytic compounds suffer from organic ligand degradation under turnover conditions of water oxidation. Molecular species based on all-inorganic polyoxometalates has lead to advances in solar fuel research.

1.6 Overview of Polyoxometalate Chemistry for Solar Fuels

Polyoxometalates (POMs) are transition metal oxygen-anion clusters that have been studied for their broad range of properties (chemical, structural, electronic, catalytic, and magnetic) and applications (catalysis, magnetism, antitumor and antiviral, energy storage, etc.).[86-88] Most POMs used for solar fuel production are composed of transition metals in their highest oxidation states. Exchanging the transition metal can modify the electronic properties of POMs. These tunable POMs have become of immense interest in homogenous water oxidation systems.

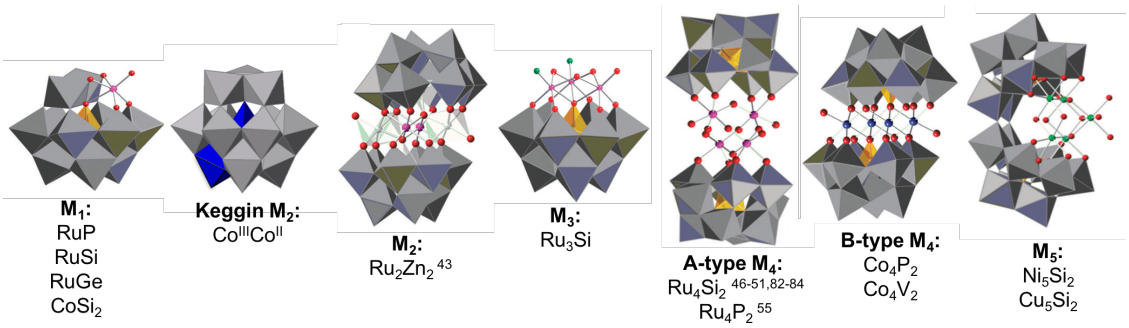

Figure 1.8 X-ray crystal structures of polyoxometalate (POM) water oxidation catalysts (WOCs) from mono-substituted (M_1) to penta-substituted (M_5).

1.6.1 Polyoxometalate Water Reduction Catalysts

In 1987, Kiwi and Grätzel disclosed a system of POM, ($SiW_{12}O_{40}$)-loaded titania for the evolution of hydrogen from water.[89] Upon UV-illumination, the POM removed electrons from the conduction band of the TiO_2 while the resulting reduced POM reduced water to generate H_2.

It wasn't until 2011 when the next POM water reduction catalyst (WRC) was reported. Zhang et al., described a sandwich-type POM, $K_{11}H[Sn_4(SiW_9O_{34})_2]\cdot 25H_2O$ (**Sn_4Si_2**) that was capable of visible-light photocatalytic H_2 evolution with Pt co-catalyst and methanol sacrificial agent.[90] Hydrogen evolution was observed over 5 consecutive runs. A heteropolyoxoniobate, $K_{10}[Nb_2O_2(H_2O)_2][SiNb_{12}O_{40}]\cdot 12H_2O$ (**Nb_2Si**), was reported for photocatalytic water splitting activity with **Nb_2Si** loaded onto Pt co-catalyst in a 20% methanol solution.[91] A TON_{max} of 44 was reported after 7.4 hours. In a separate experiment in pure water with a NiO co-catalyst, overall water splitting as well as an increase in H_2 evolution under UV irradiation was observed.

Liu et al described a visible-light photocatalytic hydrogen evolution catalyst complex. Eosin Y (EY) photosensitizer was combined with POM, α-$K_5[AlSiW_{11}(H_2O)O_{39}]$ $13H_2O$ (**$AlSiW_{11}$**) to create the EY-(**$AlSiW_{11}$**) complex.[92] Hydrogen evolution was observed by this complex in the presence of Pt co-catalyst and triethanolamine (TEOA) electron donor. In this dye-sensitization system, the interaction between **$AlSiW_{11}$** was found to help stabilize the EY-dye by reducing its reactivity. At pH 10, the TON reached 473 after four reaction cycles. The activity decreased after 5 hours of visible light irradiation, indicating instability at longer times.

Similarly, Wu et al., developed the POM WRC $Na_7H_{10}[Co_6(H_2O)_2(PW_9O_{34})_2(PW_6O_{26})]\cdot 30H_2O$ (**Co_6P_2**) sensitized with EY-dye.[93] In the presence of TEOA and visible light irradiation, H_2 generation occurred with an initial turnover frequency of 10 h^{-1}. The impact of dye-sensitizer concentration was investigated to find the critical concentration of EY needed to enhance H_2 evolution. The EY- anions proved to be essential for H_2 evolution.

Artero and co-workers developed a Pt-free WRC composed of covalently linked Ir^{III}-photosensitized POM complex, $[P_2W_{17}O_{61}\{O(SiC_{36}H_{23}N_3O_2Ir)_2\}]^{6-}$ (**Ir-P_2W_{17}**).[94] Under visible light irradiation, this complex was able to generated H_2 with a TON of 41 after 7 days.

Lv et al., synthesized a sandwich-type POM, $Na_{10}[Mn_4(H_2O)_2(VW_9O_{34})_2]$ (**Mn_4V_2**), isostructural to many efficient WOCs, in an effort to create a hydrolytically stable molecular WRC.[95] **Mn_4V_2** showed no activity for water oxidation, yet in the presence of $[Ru(bpy)_3]^{2+}$ photosensitizer and TEOA sacrificial electron donor, **Mn_4V_2** catalyzed hydrogen evolution, yielding a TON of 42 after 5.5 hours of irradiation at pH 9.5. Isotope

labeling confirmed the origin of H_2 (D_2) from H_2O or D_2O. A proposed mechanism for light-driven hydrogen evolution is consistent with quenching of the excited state $[Ru(bpy)_3]^{2+*}$ by $\mathbf{Mn_4V_2}$ through oxidative electron transfer, wherein reduced $\mathbf{Mn_4V_2}$ can reduce water to produce H_2. The resulting $[Ru(bpy)_3]^{3+}$ is reduced by TEOA to regenerate $[Ru(bpy)_3]^{2+}$.

Following the development of $\mathbf{Mn_4V_2}$ WRC, Lv et al., synthesized several other sandwich-type POM WRC including, $Na_6K_4[Ni_4(H_2O)_2(PW_9O_{34})_2]\cdot 32H_2O$ ($\mathbf{Ni_4P_2}$).[96] Using the light absorber $[Ir(ppy)_2(dtbbpy)]^+$ and TEOA sacrificial electron donor, $\mathbf{Ni_4P_2}$ reached a TON for H_2 evolution of nearly 6500 under visible-light irradiation over 1 week. Lv et al., also prepared WRC $Na_3K_7[Cu_4(H_2O)_2(B\text{-}\alpha\text{-}PW_9O_{34})_2]\cdot 30H_2O$ ($\mathbf{Cu_4P_2}$) and studied H_2 production under visible light irradiation in the $[Ir(ppy)_2(dtbbpy)]^+$ and TEOA system .[97] Under optimized conditions, a turnover of ~1270 was measured after 5 hours of irradiation. Without all WRC, photosensitizer and electron donor components, negligible H_2 was generated.

Another Ni-containing POM WRC, $Na_{28}[\{Ni_4(OH)_3AsO_4\}_4(B\text{-}\alpha\text{-}PW_9O_{34})_4]\cdot 120H_2O$ ($\mathbf{Ni_{16}As_4P_4}$) was reported as the POM with the largest number of Ni ions incorporated into a single carbon-free POM cluster.[98] The $\mathbf{Ni_{16}As_4P_4}$ POM was shown to reduce water to generate H_2, but only with a TON_{max} of 580 using TEOA electron donor and $[Ir(ppy)_2(dtbbpy)]^+$ and donor and photosensitizer. More Ni(II) centers did not result in a higher catalytic efficiency relative to $\mathbf{Ni_4P_2}$.

1.6.2 Polyoxometalate Water Oxidation Catalysts

Critical challenges in the development of viable POM multi-electron catalysts for solar fuel production are optimization of activity, selectivity, and stability under water splitting conditions. Water oxidation and reduction catalysts composed of all-inorganic POMs have advanced the field of water splitting over the past decade. The following discussion of current published POM WOCs is organized in terms of the transition metal serving as the active sites in the catalyst.

In 2004, the di-Ru^{III}-substituted POM, $Na_{14}[Ru_2Zn_2(H_2O)_2(ZnW_9O_{34})_2]$, (**$Ru_2Zn_2$**), was investigated for electrochemical O_2 generation measured using a Clark sensor.[99] In contrast, these authors reported that a monosubstituted-Ru POM,[100] $[PW_{11}O_{39}Ru^{III}(H_2O)]^{4-}$, (**RuP**) produced no O_2. Thus, they suggested that the presence of two ruthenium atoms was a key factor for electrocatalytic water oxidation activity. Computational investigations of a similar di-Ru^{III}-substituted POM ($[Ru^{III}_2(OH)_2(\gamma\text{-}SiW_{10}O_{36})^{4-}$) showed high catalytic water oxidation activity but was hydrolytically unstable.[101]

In 2008, the Bonchio group and Hill group simultaneously reported that $[\{Ru_4O_4(OH)_2(H_2O)_4\}(\gamma\text{-}SiW_{10}O_{36})_2^{10-}]$, (**$Ru_4Si_2$**), is a highly active WOC using the strong oxidants Ce^{IV} at pH 0.6[102] and $[Ru(bpy)_3]^{3+}$ at neutral pH, respectively.[103] Since then, **Ru_4Si_2** has been extensively studied by many groups in combination under homogeneous conditions using the visible-light photosensitizer ($[Ru(bpy)_3]^{2+}$) and the sacrificial electron acceptor ($S_2O_8^{2-}$) over a variety of conditions (differing buffers, differing pH values, etc).[41, 104-109] Later, the analogous **Ru_4P_2** POM was synthesized and shown to be a water oxidation catalyst but a somewhat less efficient one (lower O_2 yields under similar photochemical conditions).[110] In 2009, Geletii et al., established the increased reaction rate of the

$[Ru(bpy)_3]^{3+}$ reduction in the presence of **Ru_4Si_2** during O_2 generation reactions.[104] Furthermore, by adding $[Ru(bpy)_3]^{2+}$ to the catalytic system, the overall reaction is completed in a shorter time, but the fast initial step is inhibited. In another method, Orlandi et al., reported the nanosecond flash photolysis kinetics of hole transfer from a photogenerated Ru^{III}-polypyridine complex to **Ru_4Si_2**.[41]

In 2010, the earth-abundant POM, $Na_{10}[Co_4(H_2O)_2(\alpha\text{-}PW_9O_{34})_2]$, (**$Co_4P_2$**) catalyst was recognized as a fast water oxidation catalyst with turnover numbers reaching 1000 in under 3 minutes in the presence of $[Ru(bpy)_3]^{3+}$ at pH 8.[111] In later studies, **Co_4P_2** activity was noted and studied in the $[Ru(bpy)_3]^{2+}/S_2O_8^{2-}$ photochemical systems.[112-114] Under electrochemical water oxidation conditions in pH 8.0 sodium phosphate buffer, and a high concentration (500 μM) of the **Co_4P_2** molecular catalyst were shown to form CoO_x on the glassy carbon working electrode surface.[115] Under similar electrochemical conditions but with low **Co_4P_2** concentrations (2.5 μM), deposited CoO_x did not form, emphasizing the importance of several solution and electrochemical parameters for conducting stability and mechanistic studies on these POM WOCs.[116] Thorough studies of the **Co_4P_2** conducted over the past 5 years have established its stability under oxidant-driven homogenous catalytic water oxidation conditions and the not-so-innocent role of pH and buffer.[117-120] More discussion on POM WOC stability studies is presented in a subsequent section.

In 2014, Lv et al., described the exceptionally fast $Na_{10}[Co_4(H_2O)_2(VW_9O_{34})_2]\cdot 35H_2O$ (**Co_4V_2**) with TOF over 1000 s^{-1} under light driven photochemical conditions.[121] The difference between the geometrically similar structure of **Co_4P_2** was ascribed to differing electronic structures probed by UV-visible spectra, temperature-dependent magnetism measurements, and DFT calculations. Importantly, the

water oxidation activity of **Co_4V_2** was compared directly to equivalent amounts of $Co(NO_3)_2$. The reactions exhibited contrasting kinetic profiles and initial rates, indicating that Co^{2+} leaching from the Co-containing POM under turnover conditions was not a significant competing WOC under these conditions.

Recent studies have combined molecular species with heterogeneous materials, substrates, or electrode systems in order to evaluate the catalyst activity and stability while immobilized.

1.7 Heterogenized Systems with POMs

Investigating the geometrical and electronic structure as well as reactivity of catalysts immobilized on photoelectrode and other surfaces is a core component in the ultimate development of integrated, effective solar water splitting devices. This section focuses on the immobilization techniques for POM multi-electron catalysts. Research on other surface-bound molecular catalysts have been described in review and journal articles elsewhere.[122-126] Recent studies of polyoxometalates incorporated onto the surfaces of photoanodes for water oxidation have addressed the activity and stability of these immobilized catalyst species.[127] Table 1.1 gives a comprehensive list of POMs immobilized for catalytic water oxidation studies.

Table 1.1 Immobilized Polyoxometalate Water Oxidation Catalysts

System (Substrate)	System Characterization (*before* catalysis)	Stability Assessment (*after* catalysis)	Ref
Ru_4Si_2 on MWCNTs/ITO	rRaman, AFM, TGA, SACS, STEM, HRTEM, EDX	-	[128]
Ru_4Si_2 on functionalized SWCNT and MWCNTs/ITO	rRaman, TEM, SEM, TGA	-	[129]
Ru_4Si_2 on Dendron functionalized graphene/ITO	Raman, XPS, HRTEM, AC-TEM, HAADF-STEM, EDX, XPS	O_2 evolution current recorded at 1.1 V *vs*. Ag/AgCl	[130]
Co_4P_2 on mesoporous carbon nitride/ITO	TEM, TGA, FTIR, AFM, XANES, powder-XRD	UV-vis, XRD	[131]
$^{-}Ru_4Si_2$ on graphene/GCE, ITO	CV, SEM, EDX	SEM, EDX	[132]
Co_9 in amorphous carbon paste	FTIR, TGA, EDX, powder XRD	FTIR, EDX, powder XRD	[133]
Ru_4Si_2 LBL assembly with Ru^{II}-metallodendrimer/GCE, ITO	rRaman, CV, XPS, AFM, SEM, EDX,	CV	[134]
Mn_{16} on graphene/ITO	SEM, EDX, XPS, CV, RRDE, Tafel plot	-	[135]
Co_4P_2 on MIL-101/GCE	XRD, FTIR, XPS, XANES, TEM, EDX	XRD, FTIR, XPS, XANES, DLS, catalyst reuse, $THpANO_3$ toluene extraction	[136]
Ru_4Si_2 on $[Ru(bpy)_2(dpbpy)]^{2+}$-sensitized TiO_2, ZrO_2, and SnO_2/FTO	UV-vis, FTIR, ICP-OES, Transient absorption	UV-vis	[137]
Ru_4Si_2 on $[Ru(bpy)_2(H_4dpbpy)]^{2+}$ and $[Ru(5\text{-crownphen})_2(H_2dpbpy)]$-sensitized TiO_2/FTO	UV-vis, Transient absorption	UV-vis	[43]
Ru_4Si_2 and Ru_4P_2 on modified TiO_2/FTO	FTIR, confocal Raman, SEM, TEM, STEM, EDX, UV-vis	FTIR, confocal Raman, SEM, EDX, UV-vis, LSV	[138]

Carbon-based materials have been used for supports in electrochemical studies, because there is substantial adhesion of anionic POM WOCs to the extended π clouds of the graphene-like structures. These materials comprise single-walled or multi-walled carbon nanotubes (SWCNT or MWCNTs), graphene, mesoporous carbon nitride, carbon

paste, and carbon-based polymers (pendant polyamidoamine (PAMAM), protonated polyaniline (PANI), and poly(diallyldimethylammonium chloride) (PDDA)).

Photoelectrochemical reactions for water splitting have been streamlined using light-absorbing metal oxide supports bearing surface-bound water oxidation catalysts. No sacrificial agent is necessary in such photoelectrocatalytic systems.

POM WOC immobilization has been predominantly electrostatic in nature, including anion-π interactions (these also involve dispersion and electron-donor acceptor interactions), pH or point-of-zero-charge (pzc), entrapment through layer-by-layer assembly and vacuum-assisted impregnation. Supports that have been covalently modified to have cationic surfaces rely on electrostatic immobilization of the catalyst species.

Carbon nanotubes (CNTs) with extended three-dimensional electronically conducting large surface areas have been exhaustively studied.[139,140] and chemical functionalization of CNT-based electrodes provides additional features that make immobilization of catalytic species attractive. Toma et al., modified MWCNTs with surface-bound PAMAM units bearing tertiary and primary amino groups that electrostatically bind $\mathbf{Ru_4Si_2}$, at pH values where the amines are protonoated.[128] Compared to amorphous carbon functionalized with $\mathbf{Ru_4Si_2}$, the electrocatalytic activity of $\mathbf{Ru_4Si_2}$ on the derivatized MWCNTs was significantly higher, presumably due to enhanced electron-transfer events in the CNTs. In a similar approach, MWCNTs and single-walled CNTs (SWCNTs) were functionalized with 2-aminoethyltrimethylammonium chloride to which high loadings of electrostatically bound $\mathbf{Ru_4Si_2}$ for water splitting applications could be achieved.[129]

Graphene is believed to be an ideal electrocatalytic surface because of its high stability, conductivity, and extensive π electronic structure suitable for electrostatic and other interactions with various types of molecular catalysts. Graphene is an exceptional charge carrier transport; the electrical communication between the immobilized species and the support is advantageous in electrochemistry. POMs readily adsorb onto graphene and graphene oxide without modification of the surface. Electrochemical water oxidation studies of $\mathbf{Ru_4Si_2}$ on graphene grown on ITO electrodes show excellent catalytic activity and stability.[132] The POM-graphene system displayed higher catalytic activity compared to RuO_2 on graphene, where the amount of RuO_2 is ~200 times more than the amount possible from a complete decomposition of $\mathbf{Ru_4Si_2}$. A new non-noble metal-containing POM, mixed-valent $\mathbf{Mn_{16}}$ polyanion supported on graphene showed comparable electrochemical water oxidation to $\mathbf{Ru_4Si_2}$-graphene system.[135]

Some forms of functionalized graphene have been shown to enhance the binding of anionic POMs; however, chemical reduction methods that enrich the sp^2 connectivity of graphene can result in surface defects. Quintana et al., have functionalized graphene with polyaminoamide (PAMAM) dendrons, whereby protonated tertiary and primary amino groups act as electrostatic anchors for $\mathbf{Ru_4Si_2}$.[141-143] The resulting hybrid materials show high electron transfer rates, enhancing the electrocatalytic performance relative to carbon nanotubes and unmodified graphene.

Wu et al., used a mesoporous carbon nitride (MCN) support with $–NH_2$ and –NH functional group sites for electrostatic binding of the anionic $\mathbf{Co_4P_2}$.[131] Furthermore, this surface provided sufficient electron transfer to the ITO electrode for effective water oxidation from the POM/electrolyte interface. To assemble the system, Wu et al., used a

vacuum-assisted entrapment two-step process. In the first step, the synthesized MCN was vacuum-treated to remove impurities and air trapped in the mesopores followed by soaking in an aqueous **Co_4P_2** solution for 24 hours, allowing the **Co_4P_2** to fill the pores of the MCN by capillary forces. During the process, the $–NH_2$ functional groups were protonated, promoting electrostatic binding within the mesopores of the MCN.

Another entrapment technique to fabricate catalytic electrodes for POM-based WOC-incorporated anionic POMs with organic and inorganic cationic units combined with layer-via by-layer (LBL) assembly driven by electrostatic forces[144] for electrochemical water oxidation.[134] Anwar et al., prepared films by imbedded **Ru_4Si_2** and conducting polypyrrole with a Ru(II)-metalodendrimer photosensitizer onto GCE and ITO electrodes using LBL assembly.

Semiconductor metal oxides are known for their robust properties and charge transfer capacity. Metal oxides with applications as photoelectrodes provide economical and recyclable methods for energy production, but lack the fast and selective qualities of molecular catalysts. Common light absorbing (UV and visible range) oxides, such as TiO_2, ZnO_2, ZrO_2, Fe_2O_3, and SnO_2 have been studied as supports for POM WOCs. Xiang, et al., first constructed a triadic photoanode composed of nanoporous TiO_2, ZrO_2 and SnO_2 films sensitized with $[Ru(bpy)_2(dpbpy)]^{2+}$ (P2). [137] The surface bound cation was used to electrostatically interact with homogeneous **Ru_4Si_2**; however, the catalyst loading remained dependent on the point of zero charge (pzc) for each metal oxide surface. Transient absorption analysis investigated the charge separation dynamics of the system. In the presence of **Ru_4Si_2**, the electron transfer from P2 to TiO_2 was found to be the main pathway with ultrafast electron transfer from **Ru_4Si_2** to the oxidized P2.

Photoelectrochemical measurements of the triad system resulted in a photocurrent enhancement although no oxygen measurements were conducted.

In a following triad study, a novel dye, [Ru(5-crownphen)$_2$(H_2dpbpy)] ($H_2$2) was prepared and bound to TiO_2. This triad afforded a higher O_2 quantum yield compared to the previously reported P2 sensitizer.[43] Furthermore, no catalyst desorption was observed with the $H_2$2 dye when the photoelectrocatalytic experiments were conducted below the pzc of TiO_2. The increased binding affinity of **Ru_4Si_2** to the $H_2$2 dye significantly enhanced the performance of the triad system for water splitting. This research also investigated the difference in optimal pH ranges of homogeneous and TiO_2-bound catalysts.

In order to recover and recycle molecular catalysts, immobilization is necessary; however, supported catalyst systems are not predictable and hence need to be characterized and evaluated for activity. In many cases, POM WOCs adsorb to surfaces in low concentrations, which results in difficult characterization of the active catalyst species under turnover conditions. Extensive investigations of the systems before and after catalysis are necessary to establish the integrity of the heterogenized catalyst species. In more recent immobilized POM studies, exhaustive characterization after turnover conditions has become the convention.

In 2012, Wu et al., characterized **Co_4P_2** on MCN by a combination of TEM, TGA, small angle PXRD, wide-angle PXRD, and FTIR to confirm the encapsulation of **Co_4P_2** in MCN.[131] Along with long-term electrolysis measurements, with a TOF ~ 0.3 s^{-1}, Wu et al., monitored changes in the system through UV-vis spectra and XRD patterns of **Co_4P_2** MCN on ITO before and after electrolysis.

Similarly, Soriano-López et al., investigated the stability of Co_9 in carbon paste after > 8 hours of electrochemistry using FTIR, EDX, and powder XRD before and after this long-term turnover conditions.[133]

1.8 Goal of This Work

Quantitative and qualitative investigations of molecular species immobilized on metal oxide supports during water oxidation are not simple. This thesis explores methods for immobilizing water oxidation catalysts onto metal oxide supports and characterizing the system with multiple complementary physicochemical, spectroscopic and other techniques for a comprehensive assessment of the catalyst stability. To accomplish this, POMs were immobilized onto light absorbing metal oxides and their catalytic properties and stability characterizations were investigated using an assortment of experimental techniques, including photoelectrochemical water oxidation.

In Chapter 2, the method of silyanization of TiO_2 showed to be a powerful immobilization technique for a high coverage of catalyst. The system was investigated to ensure that the immobilized POM species retained catalytic properties while remaining intact. In chapter 3, TiO_2 was replaced with a visible-light absorbing metal oxide, α-Fe_2O_3. An additional stabilizing exterior layer was added by atomic layer deposition (ALD) in order to protect the POM catalyst on the surface during turnover conditions. Chapter 4 examines stability of several POM systems, namely the ultra-fast $\mathbf{Co_4V_2}$ POM for water oxidation. This set of techniques provides insight into the true active catalyst in a complex reaction like water oxidation.

1.9 References

1. Princen, T., *Ending the Fossil Fuel Era*. Cambridge : The MIT Press: Cambridge, 2015.

2. Dresselhaus, M. S.; Thomas, I. L., Alternative energy technologies. *Nature* **2001,** *414* (6861), 332-337.

3. Agency, I. E., *World Energy Outlook 2016*. 2016.

4. Kim, K.-J.; Pan, C.; Bansal, S.; Malhotra, R.; Kim, D.-H.; Chang, C.-H., Scalably synthesized environmentally benign, aqueous-based binary nanoparticle inks for Cu2ZnSn(S,Se)4 photovoltaic cells achieving over 9% efficiency. *Sustainable Energy Fuels* **2017**.

5. Swanson, R. M., Photovoltaics Power UP. *Science* **2009,** *324* (5929), 891-892.

6. Schlapbach, L.; Zuttel, A., Hydrogen-storage materials for mobile applications. *Nature* **2001,** *414* (6861), 353-358.

7. Maeda, K.; Teramura, K.; Domen, K., Effect of post-calcination on photocatalytic activity of (Ga1−xZnx)(N1−xOx) solid solution for overall water splitting under visible light. *Journal of Catalysis* **2008,** *254* (2), 198-204.

8. Mills, A.; Le Hunte, S., An overview of semiconductor photocatalysis. *Journal of Photochemistry and Photobiology A: Chemistry* **1997,** *108* (1), 1-35.

9. Sze, S. M.; Ng, K. K., *Physics of Semiconductor Devices*. Third ed.; Wiley, 2007.

10. Tan, M. X.; Laibinis, P. E.; Nguyen, S. T.; Kesselman, J. M.; Stanton, C. E.; Lewis, N. S., Principles and Applications of Semiconductor Photoelectrochemistry. In *Prog. Inorg. Chem.*, Karlin, K. D., Ed. John Wiley & Sons, Inc.: 1994; Vol. 41, pp 21-144.

11. Asahi, R.; Morikawa, T.; Ohwaki, T.; Aoki, K.; Taga, Y., Visible-Light Photocatalysis in Nitrogen-Doped Titanium Oxides. *Science* **2001,** *293* (5528), 269-271.

12. Dong, S. J.; Liu, M. J., Preparation and Properties of Polypyrrole Film Doped with a Dawson-Type Heteropolyanion. *Electrochim. Acta* **1994,** *39* (7), 947-951.

13. Green, M.; Harries, J.; Wakefield, G.; Taylor, R., The Synthesis of Silica Nanospheres Doped with Polyoxometalates. *J. Am. Chem. Soc.* **2005,** *127*, 12812-12813.

14. Ling, Y.; Wang, G.; Wheeler, D. A.; Zhang, J. Z.; Li, Y., Sn-Doped Hematite Nanostructures for Photoelectrochemical Water Splitting. *Nano Lett.* **2011,** *11* (5), 2119-2125

15. Marshall, A. T.; Haverkamp, R. G., Electrocatalytic activity of IrO_2–RuO_2 supported on Sb-doped SnO_2 nanoparticles *Electrochim. Acta* **2010,** *55* (6), 1978-1984.

16. Yu, X.; Marks, T. J.; Facchetti, A., Metal oxides for optoelectronic applications. *Nature Materials* **2016,** *15*, 383-396.

17. Bard, A. J.; Bocarsly, A. B.; Fan, F. R. F.; Walton, E. G.; Wrighton, M. S., The concept of Fermi level pinning at semiconductor/liquid junctions. Consequences for energy conversion efficiency and selection of useful solution redox couples in solar devices. *Journal of the American Chemical Society* **1980,** *102* (11), 3671-3677.

18. Wrighton, M. S.; Austin, R. G.; Bocarsly, A. B.; Bolts, J. M.; Haas, O.; Legg, K. D.; Nadjo, L.; Palazzoto, M. C., Design and study of a photosensitive interface: a derivatized n-type silicon photoelectrode. *Journal of the American Chemical Society* **1978,** *100* (5), 1602-1603.

19. Bolts, J. M.; Wrighton, M. S., Chemically derivatized n-type semiconducting germanium photoelectrodes. Persistent attachment and photoelectrochemical activity of

ferrocene derivatives. *Journal of the American Chemical Society* **1978,** *100* (17), 5257-5262.

20. Bolts, J. M.; Bocarsly, A. B.; Palazzotto, M. C.; Walton, E. G.; Lewis, N. S.; Wrighton, M. S., Chemically derivatized n-type silicon photoelectrodes. Stabilization to surface corrosion in aqueous electrolyte solutions and mediation of oxidation reactions by surface-attached electroactive ferrocene reagents. *Journal of the American Chemical Society* **1979,** *101* (6), 1378-1385.

21. Gores, H. J.; Barthel, J. M. G., Nonaqueous electrolyte solutions: New materials for devices and processes based on recent applied research. *Pure and Applied Chemistry* **1995,** *67* (6), 919-930.

22. Salzmann, I.; Heimel, G., Toward a comprehensive understanding of molecular doping organic semiconductors (review). *Journal of Electron Spectroscopy and Related Phenomena* **2015,** *204, Part A*, 208-222.

23. Parkinson, B. A.; Furtak, T. E.; Canfield, D.; Kam, K.-K.; Kline, G., *Faraday Discussions of the Chemical Society* **1980,** *70*, 233.

24. Parkinson, B. A., *Langmuir* **1986,** *2*, 549.

25. Spitler, M. T., *J. Electroanaol. Chem. Interfacial Electrochem.* **1987,** *228*, 69.

26. Eichberger, R.; Willig, F., *Chem. Phys.* **1990,** *141*, 159.

27. O'Regan, B.; Gratzel, M., *Nature (London)* **1991,** *141*, 159.

28. Delgadillo, A.; Arias, M.; Leiva, A. M.; Loeb, B.; Meyer, G. J., Interfacial Charge-Transfer Switch: Ruthenium-dppz Compounds Anchored to Nanocrystalline TiO_2. *Inorg. Chem.* **2006,** *45*, 5721-5723.

29. Grätzel, M., Conversion of sunlight to electric power by nanocrystalline dye-sensitized solar cells. *J. Photochem. Photobiol. A: Chem.* **2004,** *164*, 3-14.

30. Pechy, P.; Rotzinger, F. P.; Nazeeruddin, M. K.; Kohle, O.; Zakeeruddin, S. M.; Humphry-Baker, R.; Gratzel, M., Preparation of phosphonated polypyridyl ligands to anchor transition-metal complexes on oxide surfaces: application for the conversion of light to electricity with nanocrystalline TiO2 films. *Journal of the Chemical Society, Chemical Communications* **1995,** (1), 65-66.

31. Ruile, S.; Kohle, O.; Péchy, P.; Grätzel, M., Novel sensitisers for photovoltaic cells. Structural variations of Ru(II) complexes containing 2,6-bis(1-methylbenzimidazol-2-yl)pyridine. *Inorganica Chimica Acta* **1997,** *261* (2), 129-140.

32. Zakeeruddin, S. M.; Nazeeruddin, M. K.; Pechy, P.; Rotzinger, F. P.; Humphry-Baker, R.; Kalyanasundaram, K.; Grätzel, M.; Shklover, V.; Haibach, T., Molecular Engineering of Photosensitizers for Nanocrystalline Solar Cells: Synthesis and Characterization of Ru Dyes Based on Phosphonated Terpyridines. *Inorganic Chemistry* **1997,** *36* (25), 5937-5946.

33. Yan, S. G.; Hupp, J. T., Semiconductor-Based Interfacial Electron-Transfer Reactivity: Decoupling Kinetics from pH-Dependent Band Energetics in a Dye-Sensitized Titanium Dioxide/Aqueous Solution System. *The Journal of Physical Chemistry* **1996,** *100* (17), 6867-6870.

34. Yan, S. G.; Prieskorn, J. S.; Kim, Y.; Hupp, J. T., In Search of the Inverted Region: Chromophore-Based Driving Force Dependence of Interfacial Electron Transfer Reactivity at the Nanocrystalline Titanium Dioxide Semiconductor/Solution Interface. *The Journal of Physical Chemistry B* **2000,** *104* (46), 10871-10877.

35. Trammell, S. A.; Wimbish, J. C.; Odobel, F.; Gallagher, L. A.; Narula, P. M.; Meyer, T. J., Mechanisms of Surface Electron Transfer. Proton-Coupled Electron Transfer. *Journal of the American Chemical Society* **1998,** *120* (50), 13248-13249.

36. Trammell, S. A.; Moss, J. A.; Yang, J. C.; Nakhle, B. M.; Slate, C. A.; Odobel, F.; Sykora, M.; Erickson, B. W.; Meyer, T. J., Sensitization of TiO2 by Phosphonate-Derivatized Proline Assemblies. *Inorganic Chemistry* **1999,** *38* (16), 3665-3669.

37. Zimmermann, C.; Willig, F.; Ramakrishna, S.; Burfeindt, B.; Pettinger, B.; Eichberger, R.; Storck, W., Experimental Fingerprints of Vibrational Wave-Packet Motion during Ultrafast Heterogeneous Electron Transfer. *The Journal of Physical Chemistry B* **2001,** *105* (38), 9245-9253.

38. Gillaizeau-Gauthier, I.; Odobel, F.; Alebbi, M.; Argazzi, R.; Costa, E.; Bignozzi, C. A.; Qu, P.; Meyer, G. J., Phosphonate-Based Bipyridine Dyes for Stable Photovoltaic Devices. *Inorganic Chemistry* **2001,** *40* (23), 6073-6079.

39. Zabri, H.; Gillaizeau, I.; Bignozzi, C. A.; Caramori, S.; Charlot, M.-F.; Cano-Boquera, J.; Odobel, F., Synthesis and Comprehensive Characterizations of New cis-RuL2X2 (X = Cl, CN, and NCS) Sensitizers for Nanocrystalline TiO2 Solar Cell Using Bis-Phosphonated Bipyridine Ligands (L). *Inorganic Chemistry* **2003,** *42* (21), 6655-6666.

40. Wang, P.; Klein, C.; Moser, J.-E.; Humphry-Baker, R.; Cevey-Ha, N.-L.; Charvet, R.; Comte, P.; Zakeeruddin, S. M.; Grätzel, M., Amphiphilic Ruthenium Sensitizer with 4,4‘-Diphosphonic Acid-2,2‘-bipyridine as Anchoring Ligand for Nanocrystalline Dye Sensitized Solar Cells. *The Journal of Physical Chemistry B* **2004,** *108* (45), 17553-17559.

41. Orlandi, M.; Argazzi, R.; Sartorel, A.; Carraro, M.; Scorrano, G.; Bonchio, M.; Scandola, F., Ruthenium polyoxometalate water splitting catalyst: very fast hole scavenging from photogenerated oxidants. *Chem. Commun.* **2010,** *46*, 3152-3154.

42. Xiang, X.; Fielden, J.; Rodríguez-Córdoba, W.; Huang, Z.; Zhang, N.; Luo, Z.; Musaev, D. G.; Lian, T.; Hill, C. L., Electron Transfer Dynamics in Semiconductor–Chromophore–Polyoxometalate Catalyst Photoanodes. *J. Phys. Chem. C* **2013,** *117* (2), 918-926.

43. Fielden, J.; Sumliner, J. M.; Han, N.; Geletii, Y. V.; Xiang, X.; Musaev, D. G.; Lian, T.; Hill, C. L., Water Splitting with Polyoxometalate-Treated Photoanodes: Enhancing Performance through Sensitizer Design. *Chem. Sci.* **2015,** *6*, 5531-5543.

44. McKone, J. R.; Lewis, N. S.; Gray, H. B., Will Solar-Driven Water-Splitting Devices See the Light of Day? *Chem. Mater.* **2014,** *26*, 407-414.

45. Zou, Z.; Ye, J.; Sayama, K.; Arakawa, H., Direct splitting of water under visible light irradiation with an oxide semiconductor photocatalyst. *Nature* **2001,** *414* (6864), 625-627.

46. Green, M. J.; Hill, H., Chemistry of Dioxygen. *Methods in Enzymology* **1984**, 3-22.

47. Grigoriev, S. A.; Porembsky, V. I.; Fateev, V. N., Pure hydrogen production by PEM electrolysis for hydrogen energy. *International Journal of Hydrogen Energy* **2006,** *31* (2), 171-175.

48. Jaramillo, T. F.; Jorgensen, K. P.; Bonde, J.; Nielsen, J. H.; Horch, S.; Chorkendorff, I., Identification of Active Edge Sites for Electrochemical H2 Evolution from MoS2 Nanocatalysts. *Science* **2007,** *317* (5834), 100-102.

49. Chang, Y.-H.; Lin, C.-T.; Chen, T.-Y.; Hsu, C.-L.; Lee, Y.-H.; Zhang, W.; Wei, K.-H.; Li, L.-J., Highly Efficient Electrocatalytic Hydrogen Production by MoSx Grown on Graphene-Protected 3D Ni Foams. *Advanced Materials* **2013,** *25* (5), 756-760.

50. Greiner, M. T.; Helander, M. G.; Tang, W.-M.; Wang, Z.-B.; Qiu, J.; Lu, Z.-H., Universal energy-level alignment of molecules on metal oxides. *Nat Mater* **2012,** *11* (1), 76-81.

51. Laursen, A. B.; Kegnaes, S.; Dahl, S.; Chorkendorff, I., Molybdenum sulfides-efficient and viable materials for electro - and photoelectrocatalytic hydrogen evolution. *Energy & Environmental Science* **2012,** *5* (2), 5577-5591.

52. Merki, D.; Hu, X., Recent developments of molybdenum and tungsten sulfides as hydrogen evolution catalysts. *Energy & Environmental Science* **2011,** *4* (10), 3878-3888.

53. Chen, W.-F.; Iyer, S.; Iyer, S.; Sasaki, K.; Wang, C.-H.; Zhu, Y.; Muckerman, J. T.; Fujita, E., Biomass-derived electrocatalytic composites for hydrogen evolution. *Energy & Environmental Science* **2013,** *6* (6), 1818-1826.

54. Chen, W. F.; Wang, C. H.; Sasaki, K.; Marinkovic, N.; Xu, W.; Muckerman, J. T.; Zhu, Y.; Adzic, R. R., Highly active and durable nanostructured molybdenum carbide electrocatalysts for hydrogen production. *Energy & Environmental Science* **2013,** *6* (3), 943-951.

55. Chen, W.-F.; Sasaki, K.; Ma, C.; Frenkel, A. I.; Marinkovic, N.; Muckerman, J. T.; Zhu, Y.; Adzic, R. R., Hydrogen-Evolution Catalysts Based on Non-Noble Metal Nickel–Molybdenum Nitride Nanosheets. *Angewandte Chemie International Edition* **2012,** *51* (25), 6131-6135.

56. Vrubel, H.; Hu, X., Molybdenum Boride and Carbide Catalyze Hydrogen Evolution in both Acidic and Basic Solutions. *Angewandte Chemie International Edition* **2012,** *51* (51), 12703-12706.

57. Brown, D. E.; Mahmood, M. N.; Man, M. C. M.; K., T. A., Preparation and characterization of low overvoltage transition metal alloy electrocatalysts for hydrogen evolution in alkaline solutions. *Electrochimica Acta* **1984,** *29* (11), 1551-1556.

58. Stachurski, J. Z. O.; Pouli, D.; Ripa, J. A.; Pokrzyk, G. F. Low overvoltage hydrogen cathodes. 1982.

59. Brown, D. E.; Mahmood, M. N. Method of preparing active electrodes. 1982.

60. Dincă, M.; Surendranath, Y.; Nocera, D. G., Nickel-borate oxygen-evolving catalyst that functions under benign conditions. *Proc. Natl. Acad. Sci.* **2010,** *107(23)* (June 8), 10337-10341.

61. Kanan, M. W.; Nocera, D. G., In Situ Formation of an Oxygen-Evolving Catalyst in Neutral Water Containing Phosphate and Co^{2+}. *Science* **2008,** *321*, 1072-1075.

62. Kanan, M. W.; Surendranath, Y.; Nocera, D. G., Cobalt–phosphate oxygen-evolving compound. *Chem. Soc. Rev.* **2009,** *38*, 109-114.

63. McAlpin, J. G.; Surendranath, Y.; Dinca, M.; Stich, T. A.; Stoian, S. A.; Casey, W. H.; Nocera, D. G.; Britt, R. D., EPR Evidence for Co(IV) Species Produced During Water Oxidation at Neutral pH. *J. Am. Chem. Soc.* **2010,** *132*, 6882-6883.

64. Surendranath, Y.; Kanan, M. W.; Nocera, D. G., Mechanistic Studies of the Oxygen Evolution Reaction by a Cobalt-Phosphate Catalyst at Neutral pH. *J. Am. Chem. Soc.* **2010,** *132*, 16501-16509.

65. Esswein, A. J.; Surendranath, Y.; Reece, S. Y.; Nocera, D. G., Highly active cobalt phosphate and borate based oxygen evolving catalysts operating in neutral and natural waters. *Energy & Environmental Science* **2011,** *4* (2), 499-504.

66. Fujishima, A.; Honda, K., Electrochemical photolysis of water at a semiconductor electrode. *Nature* **1972,** *238* (5358), 37-38.

67. Mi, Q.; Zhanaidarova, A.; Brunschwig, B. S.; Gray, H. B.; Lewis, N. S., A quantitative assessment of the competition between water and anion oxidation at WO3 photoanodes in acidic aqueous electrolytes. *Energy & Environmental Science* **2012,** *5* (2), 5694-5700.

68. Miseki, Y.; Sayama, K., High-efficiency water oxidation and energy storage utilizing various reversible redox mediators under visible light over surface-modified WO3. *RSC Advances* **2014,** *4* (16), 8308-8316.

69. Liu, M.; Nam, C.-Y.; Black, C. T.; Kamcev, J.; Zhang, L., Enhancing Water Splitting Activity and Chemical Stability of Zinc Oxide Nanowire Photoanodes with Ultrathin Titania Shells. *The Journal of Physical Chemistry C* **2013,** *117* (26), 13396-13402.

70. Joly, A. G.; Williams, J. R.; Chambers, S. A.; Xiong, G.; Hess, W. P.; Laman, D. M., Carrier dynamics in α-Fe2O3 (0001) thin films and single crystals probed by femtosecond transient absorption and reflectivity *Journal of Applied Physics* **2006,** *99* (5), 053521.

71. Smith, R. D. L.; Prévot, M. S.; Fagan, R. D.; Zhang, Z.; Sedach, P. A.; Siu, M. K. J.; Trudel, S.; Berlinguette, C. P., Photochemical Route for Accessing Amorphous Metal Oxide Materials for Water Oxidation Catalysis. *Science* **2013,** *340*, 60-63.

72. Cesar, I.; Kay, A.; Martinez, J. A. G.; Grätzel, M., Translucent Thin Film Fe_2O_3 Photoanodes for Efficient Water Splitting by Sunlight: Nanostructure-Directing Effect of Si-Doping. *J. Am. Chem. Soc.* **2006,** *128*, 4582-4583.

73. Park, Y.; McDonald, K. J.; Choi, K.-S., Progress in bismuth vanadate photoanodes for use in solar water oxidation. *Chemical Society Reviews* **2013,** *42* (6), 2321-2337.

74. Risch, M.; Klingan, K.; Ringleb, F.; Chernev, P.; Zaharieva, I.; Fischer, A.; Dau, H., Water Oxidation by Electrodeposited Cobalt Oxides—Role of Anions and Redox-Inert Cations in Structure and Function of the Amorphous Catalyst. *ChemSusChem* **2012,** *5*, 542-549.

75. Dangwal Pandey, A.; Jia, C.; Schmidt, W.; Leoni, M.; Schwickardi, M.; Schüth, F.; Weidenthaler, C., Size-Controlled Synthesis and Microstructure Investigation of Co3O4 Nanoparticles for Low-Temperature CO Oxidation. *The Journal of Physical Chemistry C* **2012,** *116* (36), 19405-19412.

76. Gardner, G. P.; Go, Y. B.; Robinson, D. M.; Smith, P. F.; Hadermann, J.; Abakumov, A.; Greenblatt, M.; Dismukes, G. C., Structural Requirements in Lithium Cobalt Oxides for the Catalytic Oxidation of Water. *Angewandte Chemie International Edition* **2012,** *51* (7), 1616-1619.

77. Grzelczak, M.; Zhang, J.; Pfrommer, J.; Hartmann, J.; Driess, M.; Antonietti, M.; Wang, X., Electro- and Photochemical Water Oxidation on Ligand-free Co3O4 Nanoparticles with Tunable Sizes. *ACS Catalysis* **2013,** *3* (3), 383-388.

78. Gersten, S. W.; Samuels, G. J.; Meyer, T. J., Catalytic Oxidation of Water by an Oxo-Bridged Ruthenium Dimer. *J. Am. Chem. Soc.* **1982,** *104*, 4029-4030.

79. Norris, M. R.; Concepcion, J. J.; Harrison, D. P.; Binstead, R. A.; Ashford, D. L.; Fang, Z.; Templeton, J. L.; Meyer, T. J., Redox Mediator Effect on Water Oxidation in a Ruthenium-Based Chromophore–Catalyst Assembly. *J. Am. Chem. Soc.* **2013,** *135* (6), 2080-2083.

80. Concepcion, J. J.; Jurss, J. W.; Templeton, J. L.; Meyer, T. J., Mediator-assisted water oxidation by the ruthenium ''blue dimer'' cis,cis-$[(bpy)_2(H_2O)RuORu(OH_2)(bpy)_2]^{4+}$. *Proc. Natl. Acad. Sci.* **2008,** *105* (46), 17632-17635.

81. Wada, T.; Tsuge, K.; Tanaka, K., Electrochemical Oxidation of Water to Dioxygen Catalyzed by the Oxidized Form of the Bis(ruthenium-hydroxo) Complex in H_2O. *Angew. Chem. Int. Ed.* **2000,** *39* (8), 1479-1482.

82. Liao, Y. H.; Moss, J. R., Ruthenium-containing organometallic dendrimers. *J. Chem. Soc., Chem. Commun.* **1993,** *23*, 1774-1777.

83. Wada, T.; Muckerman, J. T.; Fujita, E.; Tanaka, K., Substituents dependent capability of bis(ruthenium-dioxolene-terpyridine) complexes toward water oxidation. *Dalton Trans.* **2011,** *40*, 2225-2233.

84. McDaniel, N. D.; Coughlin, F. J.; Tinker, L. L.; Bernhard, S., Cyclometalated Iridium(III) Aquo Complexes: Efficient and Tunable Catalysts for the Homogeneous Oxidation of Water. *J. Am. Chem. Soc.* **2008,** *130* (1), 210-217.

85. Blakemore, J. D.; Schley, N. D.; Balcells, D.; Hull, J. F.; Olack, G. W.; Incarvito, C. D.; Eisenstein, O.; Brudvig, G. W.; Crabtree, R. H., Half-Sandwich Iridium Complexes for Homogeneous Water-Oxidation Catalysis. *Journal of the American Chemical Society* **2010,** *132* (45), 16017-16029.

86. Pope, M. T.; Müller, A., Chemistry of polyoxometallates. Actual variation on an old theme with interdisciplinary references. *Angew. Chem.* **1991,** *103* (1), 56-70.

87. Hill, C. L., *Special Thematic Issue on Polyoxometalates*. 1998; Vol. 98, No. 1, p 1-390.

88. Pope, M. T.; Müller, A., *Polyoxometalate Chemistry From Topology via Self-Assembly to Applications*. Kluwer Academic Publishers: Dordrecht, 2001.

89. Kiwi, J.; Grätzel, M., Characterization of tungstosilicate ((SiW12O40)4-)/titania suspensions and their activity in the evolution of hydrogen from water. *J. Phys. Chem.* **1987,** *91* (27), 6673-6677.

90. Zhang, Z.; Lin, Q.; Zheng, S.-T.; Bu, X.; Feng, P., A novel sandwich-type polyoxometalate compound with visible-light photocatalytic H_2 evolution activity. *Chem. Commun.* **2011,** *47*, 3918-3920.

91. Zhang, Z.; Lin, Q.; Kurunthu, D.; Wu, T.; Zuo, F.; Zheng, S.-T.; Bardeen, C. J.; Bu, X.; Feng, P., Synthesis and Photocatalytic Properties of a New Heteropolyoxoniobate Compound: $K_{10}[Nb_2O_2(H_2O)_2][SiNb_{12}O_{40}] \cdot 12H_2O$. *J. Am. Chem. Soc.* **2011,** *133*, 6934-6937.

92. Liu, X.; Li, Y.; Peng, S.; Lu, G.; Li, S., Photocatalytic hydrogen evolution under visible light irradiation by the polyoxometalate α-[AlSiW11(H2O)O39]5− -Eosin Y system. *Int. J. Hydrogen Energy* **2012,** *37* (17), 12150-12157.

93. Wu, W.; Teng, T.; Wu, X.-Y.; Dui, X.; Zhang, L.; Xiong, J.; Wu, L.; Lua, C.-Z., A cobalt-based polyoxometalate catalyst for efficient visible-light-driven H2 evolution from water splitting. *Catalysis Communications* **2015,** *64*, 44-47.

94. Matt, B.; Fize, J.; Moussa, J.; Amouri, H.; Pereira, A.; Artero, V.; Izzet, G.; Proust, A., Charge photo-accumulation and photocatalytic hydrogen evolution under visible light at an iridium(III)-photosensitized polyoxotungstate. *Energy Environ. Sci* **2013,** *6*, 1504-1508.

95. Lv, H.; Song, J.; Zhu, H.; Geletii, Y. V.; Bacsa, J.; Zhao, C.; Lian, T.; Musaev, D. G.; Hill, C. L., Visible-light-driven hydrogen evolution from water using a noble-metal-free polyoxometalate catalyst. *J. Catal.* **2013,** *307*, 48-54.

96. Lv, H.; Guo, W.; Wu, K.; Chen, Z.; Bacsa, J.; Musaev, D. G.; Geletii, Y. V.; Lauinger, S. M.; Lian, T.; Hill, C. L., A Noble-Metal-Free, Tetra-nickel Polyoxotungstate Catalyst for Efficient Photocatalytic Hydrogen Evolution. *J. Am. Chem. Soc.* **2014,** *136* (40), 14015-14018.

97. Lv, H.; Gao, Y.; Guo, W.; Lauinger, S. M.; Chi, Y.; Bacsa, J.; Sullivan, K. P.; Wieliczko, M.; Musaev, D. G.; Hill, C. L., Cu-based Polyoxometalate Catalyst for Efficient Catalytic Hydrogen Evolution. *Inorganic Chemistry* **2016,** *55*, 6750-6758.

98. Lv, H.; Chi, Y.; Leusen, J. v.; Kögerler, P.; Chen, Z.; Bacsa, J.; Guo, W.; Lian, T.; Hill, C. L., $[\{Ni_4(OH)_3AsO_4\}_4(B\text{-}\alpha\text{-}PW_9O_{34})_4]^{28-}$ a New Polyoxometalate Structural Family with Catalytic Hydrogen Evolution Activity. *Chem. Eur. J.* **2015,** *21* (48), 17363 - 17370.

99. Howells, A. R.; Sankarraj, A.; Shannon, C., A Diruthenium-Substituted Polyoxometalate as an Electrocatalyst for Oxygen Generation. *J. Am. Chem. Soc.* **2004,** *126*, 12258-12259.

100. Rong, C.; Pope, M. T., Lacunary Polyoxometalate Anions Are π-Acceptor Ligands. Characterization of Some Tungstoruthenate(II,III,IV,V) Heteropolyanions and Their Atom-Transfer Reactivity. *J. Am. Chem. Soc.* **1992,** *114*, 2932-2938.

101. Quiñonero, D.; Wang, Y.; Morokuma, K.; Khavrutskii, L. A.; Botar, B.; Geletii, Y. V.; Hill, C. L.; Musaev, D. G., The Role of the Central Atom in Structure and Reactivity of Polyoxometalates with Adjacent d-Electron Metal Sites. Computational and Experimental Studies of γ-$[(X^{n+}O_4)Ru^{III2}(OH)_2(M_{FM})_{10}O_{32}]^{(8-n)-}$ for M_{FM} = Mo and W, and X = Al^{III}, Si^{IV}, P^{V}, and S^{VI}. *J. Phys. Chem.* **2006,** *110*, 170-173.

102. Sartorel, A.; Carraro, M.; Scorrano, G.; Zorzi, R. D.; Geremia, S.; McDaniel, N. D.; Bernhard, S.; Bonchio, M., Polyoxometalate Embedding of a Tetraruthenium(IV)-oxo-core by Template-Directed Metalation of $[\gamma\text{-}SiW_{10}O_{36}]^{8-}$: A Totally Inorganic Oxygen-Evolving Catalyst. *J. Am. Chem. Soc.* **2008,** *130* (15), 5006-5007.

103. Geletii, Y. V.; Botar, B.; Kögerler, P.; Hillesheim, D. A.; Musaev, D. G.; Hill, C. L., An All-Inorganic, Stable, and Highly Active Tetraruthenium Homogeneous Catalyst for Water Oxidation. Selected as the VIP Article by the reviewers and editor. *Angew. Chem. Int. Ed.* **2008,** *47*, 3896-3899.

104. Geletii, Y. V.; Besson, C.; Hou, Y.; Yin, Q.; Musaev, D. G.; Quinonero, D.; Cao, R.; Hardcastle, K. I.; Proust, A.; Kögerler, P.; Hill, C. L., Structural, Physicochemical and Reactivity Properties of an All-Inorganic, Highly Active Tetraruthenium Homogeneous Catalyst for Water Oxidation. *J. Am. Chem. Soc.* **2009,** *131* (47), 17360-17370.

105. Kuznetsov, A. E.; Geletii, Y. V.; Hill, C. L.; Morokuma, K.; Musaev, D. G., Dioxygen and Water Activation Processes on Multi-Ru-Substituted Polyoxometalates:

Comparison with the "Blue-Dimer" Water Oxidation Catalyst. *J. Am. Chem. Soc.* **2009,** *131*, 6844-6854.

106. Natali, M.; Orlandi, M.; Berardi, S.; Campagna, S.; Bonchio, M.; Sartorel, A.; Scandola, F., Photoinduced Water Oxidation by a Tetraruthenium Polyoxometalate Catalyst: Ion-pairing and Primary Processes with $Ru(bpy)_3^{2+}$ Photosensitizer. *Inorg. Chem.* **2012,** *51*, 7324-7331.

107. Sartorel, A.; Bonchio, M.; Campagna, S.; Scandola, F., Tetrametallic molecular catalysts for photochemical water oxidation. *Chem. Soc. Rev.* **2013,** *42*, 2262-2280.

108. Dau, H.; Limberg, C.; Reier, T.; Risch, M.; Roggan, S.; Strasser, P., The Mechanism of Water Oxidation: From Electrolysis via Homogeneous to Biological Catalysis. *Chem. Cat. Chem.* **2010,** *2*, 724-761.

109. Sartorel, A.; Miro, P.; Salvadori, E.; Romain, S.; Carraro, M.; Scorrano, G.; Valentin, M. D.; Llobet, A.; Bo, C.; Bonchio, M., Water Oxidation at a Tetraruthenate Core Stabilized by Polyoxometalate Ligands: Experimental and Computational Evidence To Trace the Competent Intermediates. *J. Am. Chem. Soc.* **2009,** *131*, 16051-16053.

110. Besson, C.; Huang, Z.; Geletii, Y. V.; Lense, S.; Hardcastle, K. I.; Musaev, D. G.; Lian, T.; Proust, A.; Hill, C. L., $Cs_9[(\Upsilon\text{-}PW_{10}O_{36})_2Ru_4O_5(OH)(H_2O)_4]$, a new all-inorganic, soluble catalyst for the efficient visible-light-driven oxidation of water. *Chem. Commun.* **2010**, 2784-2786.

111. Yin, Q.; Tan, J. M.; Besson, C.; Geletii, Y. V.; Musaev, D. G.; Kuznetsov, A. E.; Luo, Z.; Hardcastle, K. I.; Hill, C. L., A fast soluble carbon-free molecular water oxidation catalyst based on abundant metals. *Science* **2010,** *328*, 342-345.

112. Huang, Z.; Luo, Z.; Geletii, Y. V.; Vickers, J.; Yin, Q.; Wu, D.; Hou, Y.; Ding, Y.; Song, J.; Musaev, D. G.; Hill, C. L.; Lian, T., Efficient Light-Driven Carbon-Free Cobalt-Based Molecular Catalyst for Water Oxidation. *J. Am. Chem. Soc.* **2011,** *133*, 2068-2071.

113. Vickers, J. W.; Lv, H.; Sumliner, J. M.; Zhu, G.; Luo, Z.; Musaev, D. G.; Geletii, Y. V.; Hill, C. L., Differentiating Homogeneous and Heterogeneous Water Oxidation Catalysis: Confirmation that $[Co_4(H_2O)_2(\alpha\text{-}PW_9O_{34})_2]^{10-}$ Is a Molecular Water Oxidation Catalyst. *J. Am. Chem. Soc.* **2013,** *135* (38), 14110-14118.

114. Lv, H.; Rudd, J. A.; Zhuk, P. F.; Lee, J. Y.; Constable, E. C.; Housecroft, C. E.; Hill, C. L.; Musaev, D. G.; Geletii, Y. V., Bis(4'-(4-pyridyl)-2,2':6',2''-terpyridine)ruthenium(II) complexes and their N-alkylated derivatives in catalytic light-driven water oxidation. *RSC Adv.* **2013,** *3*, 20647-20654.

115. Stracke, J. J.; Finke, R. G., Electrocatalytic Water Oxidation Beginning with the Cobalt Polyoxometalate $[Co_4(H_2O)_2(PW_9O_{34})_2]^{10-}$: Identification of Heterogeneous CoO_x as the Dominant Catalyst. *J. Am. Chem. Soc.* **2011,** *133*, 14872-14875.

116. Stracke, J. J.; Finke, R. G., Water Oxidation Catalysis Beginning with 2.5 μM [Co4(H2O)2(PW9O34)2]10–: Investigation of the True Electrochemically Driven Catalyst at ≥600 mV Overpotential at a Glassy Carbon Electrode. *ACS Catal.* **2013,** *3* (6), 1209-1219.

117. Schiwon, R.; Klingan, K.; Dau, H.; Limberg, C., Shining light on integrity of a tetracobalt-polyoxometalate water oxidation catalyst by X-ray spectroscopy before and after catalysis. *Chem. Commun.* **2014,** *50*, 100-102.

118. Natali, M.; Berardi, S.; Sartorel, A.; Bonchio, M.; Campagna, S.; Scandola, F., Is [Co4(H2O)2([small alpha]-PW9O34)2]10- a genuine molecular catalyst in photochemical water oxidation? Answers from time-resolved hole scavenging experiments. *Chem. Commun.* **2012,** *48* (70), 8808-8810.

119. Ohlin, C. A.; Harley, S. J.; McAlpin, J. G.; Hocking, R. K.; Mercado, B. Q.; Johnson, R. L.; Villa, E. M.; Fidler, M. K.; Olmstead, M. M.; Spiccia, L.; Britt, R. D.; Casey, W. H., Rates of Water Exchange for Two Cobalt(II) Heteropolyoxotungstate Compounds in Aqueous Solution. *Chem. Eur. J.* **2011,** *17*, 4408-4417.

120. Lieb, D.; Zahl, A.; Wilson, E. F.; Streb, C.; Nye, L. C.; Meyer, K.; Ivanović-Burmazović, I., Water Exchange Reactivity and Stability of Cobalt Polyoxometalates under Catalytically Relevant pH Conditions: Insight into Water Oxidation Catalysis. *Inorg. Chem.* **2011,** *50* (18), 9053-9058.

121. Lv, H.; Song, J.; Geletii, Y. V.; Vickers, J. W.; Sumliner, J. M.; Musaev, D. G.; Kögerler, P.; Zhuk, P. F.; Bacsa, J.; Zhu, G.; Hill, C. L., An Exceptionally Fast Homogeneous Carbon-free Cobalt-based Water Oxidation Catalyst. *J. Am. Chem. Soc.* **2014,** *136* (26), 9268-9271.

122. Li, F.; Li, L.; Tong, L.; Daniel, Q.; Göthelid, M.; Sun, L., Immobilization of a molecular catalyst on carbon nanotubes for highly efficient electro-catalytic water oxidation. *Chem. Commun.* **2014,** *50*, 13948-13951.

123. Blakemore, J. D.; Crabtree, R. H.; Brudvig, G. W., Molecular Catalysis for Water Oxidation. *Chem. Rev.* **2015,** *115*, 12974-13005.

124. Xue, L.-X.; Meng, T.-T.; Yang, W.; Wang, K.-Z., Recent advances in ruthenium complex-based light-driven water oxidation catalysts. *J. Photochem. Photobiol. B: Biology* **2015,** *152, Part A* (Special Issue on Artificial Photosynthesis), 95-105.

125. Alibabaei, L.; Brennaman, M. K.; Norris, M. R.; Kalanyan, B.; Song, W.; Losego, M. D.; Concepcion, J. J.; Binstead, R. A.; Parsons, G. N.; Meyer, T. J., Solar water splitting in a molecular photoelectrochemical cell. *Proc. Natl. Acad. Sci.* **2013,** *110* (50), 20008-20013.

126. Stevens, M. B.; Enman, L. J.; Batchellor, A. S.; Cosby, M. R.; Vise, A. E.; Trang, C. D. M.; Boettcher, S. W., Measurement Techniques for the Study of Thin Film Heterogeneous Water Oxidation Electrocatalysts. *Chemistry of Materials* **2016**.

127. Li, W.; He, D.; Sheehan, S. W.; He, Y.; Thorne, J. E.; Yao, X.; Brudvig, G. W.; Wang, D., Comparison of heterogenized molecular and heterogeneous oxide catalysts for photoelectrochemical water oxidation. *Energy & Environ. Sci.* **2016,** *9*, 1794-1802.

128. Toma, F. M.; Sartorel, A.; Iurlo, M.; Carraro, M.; Parisse, P.; Maccato, C.; Rapino, S.; Gonzalez, B. R.; Amenitsch, H.; Ros, T. D.; Casalis, L.; Goldoni, A.; Marcaccio, M.; Scorrano, G.; Scoles, G.; Paolucci, F.; Prato, M.; Bonchio, M., Efficient water oxidation at carbon nanotube–polyoxometalate electrocatalytic interfaces. *Nat. Chem.* **2010,** *2*, 826-831.

129. Toma, F. M.; Sartorel, A.; Iurlo, M.; Carraro, M.; Rapino, S.; Hoober-Burkhardt, L.; Ros, T. D.; Marcaccio, M.; Scorrano, G.; Paolucci, F.; Bonchio, M.; Prato, M., Tailored Functionalization of Carbon Nanotubes for Electrocatalytic Water Splitting and Sustainable Energy Applications

. *ChemSusChem* **2011,** *4*, 1447-1451.

130. Quintana, M.; Lopez, A. M.; Rapino, S.; Toma, F. M.; Iurlo, M.; Carraro, M.; Sartorel, A.; Maccato, C.; Ke, X.; Bittencourt, C.; Ros, T. D.; Tendeloo, G. V.; Marcaccio, M.; Paolucci, F.; Prato, M.; Bonchio, M., Knitting the Catalytic Pattern of Artificial Photosynthesis to a Hybrid Graphene Nanotexture. *ACS Nano* **2012,** *7*, 811-817.

131. Wu, J.; Liao, L.; Yan, W.; Xue, Y.; Sun, Y.; Yan, X.; Chen, Y.; Xie, Y., Polyoxometalates Immobilized in Ordered Mesoporous Carbon Nitride as Highly Efficient Water Oxidation Catalysts. *ChemSusChem* **2012,** *5* (7), 1207-1212.

132. Guo, S.-X.; Liu, Y.; Lee, C.-Y.; Bond, A. M.; Zhang, J.; Geletii, Y. V.; Hill, C. L., Graphene-supported [{$Ru_4O_4(OH)_2(H_2O)_4$}([gamma]-$SiW1_0O_{36})_2$]$^{10-}$ for highly efficient electrocatalytic water oxidation. *Energy Environ. Sci.* **2013,** *6* (9), 2654-2663.

133. Soriano-López, J.; Goberna-Ferrón, S.; Vigara, L.; Carbó, J. J.; Poblet, J. M.; Galán-Mascarós, J. R., Cobalt Polyoxometalates as Heterogeneous Water Oxidation Catalysts. *Inorg. Chem.* **2013,** *52* (9), 4753-4755.

134. Anwar, N.; Sartorel, A.; Yaqub, M.; Wearen, K.; Laffir, F.; Armstrong, G.; Dickinson, C.; Bonchio, M.; McCormac, T., Surface Immobilization of a Tetra-Ruthenium Substituted Polyoxometalate Water Oxidation Catalyst Through the Employment of Conducting Polypyrrole and the Layer-by-Layer (LBL) Technique. *ACS Appl. Mater. & Interfaces* **2014,** *6*, 8022-8031.

135. Xing, X.; Wang, M.; Liu, R.; Zhang, S.; Zhangc, K.; Li, B.; Zhang, G., Highly efficient electrochemically driven water oxidation by graphene-supported mixed-valent Mn_{16}-containing polyoxometalate. *Green Energy & Environ.* **2016**, Available online 19 April 2016.

136. Hana, J.; Wang, D.; Du, Y.; Xi, S.; Chen, Z.; Yin, S.; Zhou, T.; Xu, R., Polyoxometalate immobilized in MIL-101(Cr) as an efficient catalyst for water oxidation. *Appl. Catal A: Gen.* **2016,** *521*, 83-89.

137. Xiang, X.; Fielden, J.; Rodriguez-Cordoba, W.; Huang, Z.; Zhang, N.; Luo, Z.; Musaev, D. G.; Lian, T.; Hill, C. L., Electron Transfer Dynamics in Semiconductor-Chromophore-Polyoxometalate Catalyst Photoanodes. *J. Phys. Chem. C* **2013,** *117* (Copyright (C) 2013 American Chemical Society (ACS). All Rights Reserved.), 918-926.

138. Lauinger, S. M.; Sumliner, J. M.; Yin, Q.; Xu, Z.; Liang, G.; Glass, E. N.; Lian, T.; Hill, C. L., High Stability of Immobilized Polyoxometalates on TiO_2 Nanoparticles and Nanoporous Films for Robust, Light-Induced Water Oxidation. *Chem. Mater.* **2015,** *27* (17), 5886-5891.

139. Volder, M. F. L. D.; Tawfick, S. H.; Baughman, R. H.; Hart, A. J., Carbon Nanotubes: Present and Future Commercial Applications. *Science* **2013,** *339* (6119), 535-539.

140. Srivastava, S., Sorption of divalent metal ions from aqueous solution by oxidized carbon nanotubes and nanocages: A review. *Adv. Mat. Lett.* **2013,** *4* (1), 2-8.

141. Quintana, M.; López, A. M.; Rapino, S.; Toma, F. M.; Iurlo, M.; Carraro, M.; Sartorel, A.; Maccato, C.; Ke, X.; Bittencourt, C.; Da Ros, T.; Van Tendeloo, G.; Marcaccio, M.; Paolucci, F.; Prato, M.; Bonchio, M., Knitting the Catalytic Pattern of Artificial Photosynthesis to a Hybrid Graphene Nanotexture. *ACS Nano* **2013,** *7* (1), 811-817.

142. Ke, X.; Turner, S.; Quintana, M.; Hadad, C.; Montellano-López, A.; Carraro, M.; Sartorel, A.; Bonchio, M.; Prato, M.; Bittencourt, C.; Tendeloo, G. V., Dynamic Motion

of Ru-Polyoxometalate Ions (POMs) on Functionalized Few-Layer Graphene. *Small* **2013,** *9* (23), 3922-2927.

143. Ma, C.; Piccinin, S.; Fabris, S., Interface structure and reactivity of water-oxidation Ru–polyoxometalate catalysts on functionalized graphene electrodes. *Phys. Chem. Chem. Phys* **2014,** *16*, 5333-5341.

144. Ma, H.; Shi, S.; Zhang, Z.; Pang, H.; Zhang, Y., An thin film of the di-decatungstosilicate with a tetra-ruthenium(IV)-oxo core and its electrochemical properties. *J. Electroanal. Chem.* **2010,** *648* (2), 128-133.

IMMOBILIZATION METHODS FOR BINDING POLYOXOMETALATES ONTO SURFACES FOR WATER SPLITTING APPLICATIONS

CHAPTER 2

Immobilization of Polyoxometalate Water Oxidation Catalysts onto Titanium Dioxide

with Jordan M. Sumliner, Qiushi Yin, Zihao Xu, Guijie Liang, Elliot N. Glass, Tianquan Lian and Craig L. Hill

Published in part in: Lauinger S. M., Sumliner, J. M., Yin, Q., Xu, Z., Liang, G., Glass, E. N. Lian, T., Hill, C. L. "High Stability of Immobilized Polyoxometalates on TiO_2 Nanoparticles and Nanoporous Films for Robust, Light-Induced Water Oxidation," *Chemistry of Materials*. **2015**, *27*, 5886-5891.

2.1 Abstract

Immobilization methods of molecular water oxidation catalysts (WOCs) on photoelectrode surfaces were investigated to increase the concentration of the semiconductor-immobilized WOCs. The increase in the surface loading using this straightforward electrostatic method allows for easy spectroscopic characterization. The polyoxometalate WOCs, $[Ru^{IV}_4O_5(OH)(H_2O)_4(\gamma\text{-}PW_{10}O_{36})_2]^{9-}$ (**Ru_4P_2**), and $[\{Ru^{IV}_4(OH)_2(H_2O)_4\}(\gamma\text{-}SiW_{10}O_{34})_2]^{10-}$ (**Ru_4Si_2**) have been immobilized by silanization on TiO_2 nanoparticles and nanoporous electrodes and found to retain catalytic water oxidation activity. In photoelectrochemical experiments, increased and sustained current density of WOC-TiO_2 films on FTO electrodes is consistent with water oxidation occurring on the derivatized, modified semiconductor surface. Using nanoparticles in place of bulk materials allows for increased surface area and sufficient concentrations of immobilized POM WOC species to enable easier characterization methods and increased water oxidation activity. Multiple techniques have been used to observe the effectiveness of silanization for POM WOC immobilization on nanoparticle surfaces as well as TiO_2/FTO electrodes before and after catalysis.

2.2 Introduction

As solar fuels diminish, research into renewable energy sources is growing in high demand. At the same time, global population and energy demands are climbing.[1,3] Towards the generation of fuel from water, water oxidation systems and devices with high efficiency and stability remains a key challenge.[4-5]

To date, molecular WOCs such as those based on oxidatively stable POMs, provide high turnover numbers under conditions driven chemically by $Ce^{IV}(NH_4)_2(NO_3)_6$,[6-7] photochemically by light, photosensitizer, and sacrificial oxidant,[8] and electrochemically.[9] The use of homogeneous WOCs requires their immobilization on appropriate surfaces with retention of catalytic activity for long periods under operating conditions.[10, 12] In this context, the use of POM derivatives as WOCs is attractive because POMs[13, 15] exhibit the advantages of both heterogeneous catalysts (recoverability, robustness, etc.) and homogeneous catalysts (readily characterized by spectroscopic and other methods).[16, 19]

POM catalysts have recently been supported on a variety of materials,[20] including porous carbons[21-23] and cationic silica nanoparticles.[15,20, 24-27] To date, the principle applications of supported POM catalysts are for organic substrate oxidations.[20] Water splitting research has been conducted on dye-sensitized cells incorporating metal oxides such as TiO_2 and IrO_2 catalysts.[3,28-33] There are fewer reports of POM immobilization chemistry for the catalysis of multi-electron reactions associated with solar fuel generation in aqueous media. In this area, the tetra-ruthenium POM WOC, $[\{Ru_4O_4(OH)_2(H_2O)_4\}(\gamma\text{-}SiW_{10}O_{36})_2]^{10-}$ (**Ru_4Si_2**) has been immobilized by a layer-by-layer technique involving conducting polypyrrole, and a Ru(II) metallodendrimer.[34] This layered system was found to be stable from pH 2-5; however, major leaching of **Ru_4Si_2** was observed during catalysis at pH 7. In another study, the hydrophobic salt, $[Ru^{II}(bpy)_3]_5[Ru^{III}{}_4Si_2]$, has been supported as a thin film on glassy carbon electrodes and shown to facilitate electrocatalytic water oxidation with a TOF of 0.35 s-1 at an overpotential of 0.49 V at pH 7.[35] More immobilization of POM WOC techniques are shown in table 1.1.

POM-containing dyad and triad systems have been reported on a variety of support systems.[36] Multiple groups have reported the immobilization of POM WOCs on TiO_2-[$Ru(bpy)_3$] dyadic systems to make TiO_2-[$Ru(bpy)_3$]-POM triads[37] or on semiconductor metal oxides (SMOs) to make SMO-POM dyads.[38] The resulting photoelectrocatalytic water oxidizing electrodes enable study of POM association with the surface, the electron transfer dynamics and some aspects of water oxidation involving these discrete surface-bound molecular WOCs.[37-38] However, the concentrations of these surface-bound POM WOCs are too low in the case of conventional SMO photoelectrodes to facilitate satisfactory characterization of the these catalysts and in most cases to even assess if the catalyst remains intact or decomposes to another catalytic competent species (usually a metal oxide film on the surface) under turnover conditions. This fundamental lack of certainty regarding the nature of the catalysts on electrode and photoelectrode surfaces starting with adsorbed molecular catalysts greatly hampers the study and thus comprehension of the photocatalytic dyadic and triadic systems noted above.

To address these major limitations of immobilized molecular WOCs, we report here a general and simple method to strongly bind POM catalysts to SMO surfaces involving initial treatment of these surfaces with a reactive silyl derivative containing a quaternary ammonium side chain. The resulting silanized cationic surface then quickly binds the POM catalyst when immersed in a solution of the POM. Although the resulting POM-Me_3N-O_3Si-SMO linkages are primarily electrostatic in nature, the very high charges on the POM WOCs (typically ~10 minus) render these catalyst-surface linkages very robust. Secondly, the SMO support is in the form of high-surface-area NPs and these are silylated with pendant cations, then treated with POMs, that the resulting greatly increased concentration

of surface-bound catalyst, is now sufficient to facilitate assessment by some forms of spectroscopy and other methods. For this study, **Ru_4Si_2**[39-40] and $[Ru^{IV}_4O_5(OH)(H_2O)_4(\gamma\text{-}PW_{10}O_{36})_2]^{9-}$ (**Ru_4P_2**)[41] have been immobilized on TiO_2 nanoparticles and nanoporous electrodes via the above silanization-cationization process and the resulting multicomponent photoelectrodes characterized by FT-IR, confocal Raman, and EDX before and after water oxidation to assess stability. The photon-to-current efficiency (IPCE) of the system was investigated using photoelectrochemical methods.

2.3 Experimental

2.3.1 General

Materials and solvents were purchased as ACS analytical or reagent grade and used as received. $Cs_9[Ru^{IV}_4O_5(OH)(H_2O)_4(\gamma\text{-}PW_{10}O_{36})_2]$, (**$Ru_4P_2$**),[41] and $Rb_8K_2[\{Ru^{IV}_4(OH)_2(H_2O)_4\}(\gamma\text{-}SiW_{10}O_{34})_2]$, (**$Ru_4Si_2$**),[39] were prepared based on published procedures. The potassium γ-decatungstosilcate precursor ($K_8[\gamma\text{-}SiW_{10}O_{36}]\cdot 12H_2O$ was mixed with 2.67 mmol $RuCl_2\cdot H_2O$ and dissolved in water. The pH was adjusted to 2.6 with 6 M HCl and allowed to mix for 5 minutes. A solution of 20 mmol RbCl was added to precipitate the product.

2.3.2 Synthesis of TiO_2 nanoparticles coated with the molecular WOC, Ru_4P_2

The silylating agent, 3-aminopropyltrimethoxysilane (APS), was mixed with an anhydrous toluene suspension of Degussa P25 TiO_2, previously dried in an oven at 200 °C for 1 hour. After washing with ethanol and water three times, the POM WOC, either **Ru_4P_2** or **Ru_4Si_2**, was added as an aqueous solution at varying concentrations. Decolorization of

the homogeneous **Ru_4P_2** solution as the modified TiO_2 nanoparticles (NPs) gained color provided direct evidence for POM binding to the NP surfaces (Figures 2.1 and 2.2). The product was collected by centrifugation and washed three times with deionized water.

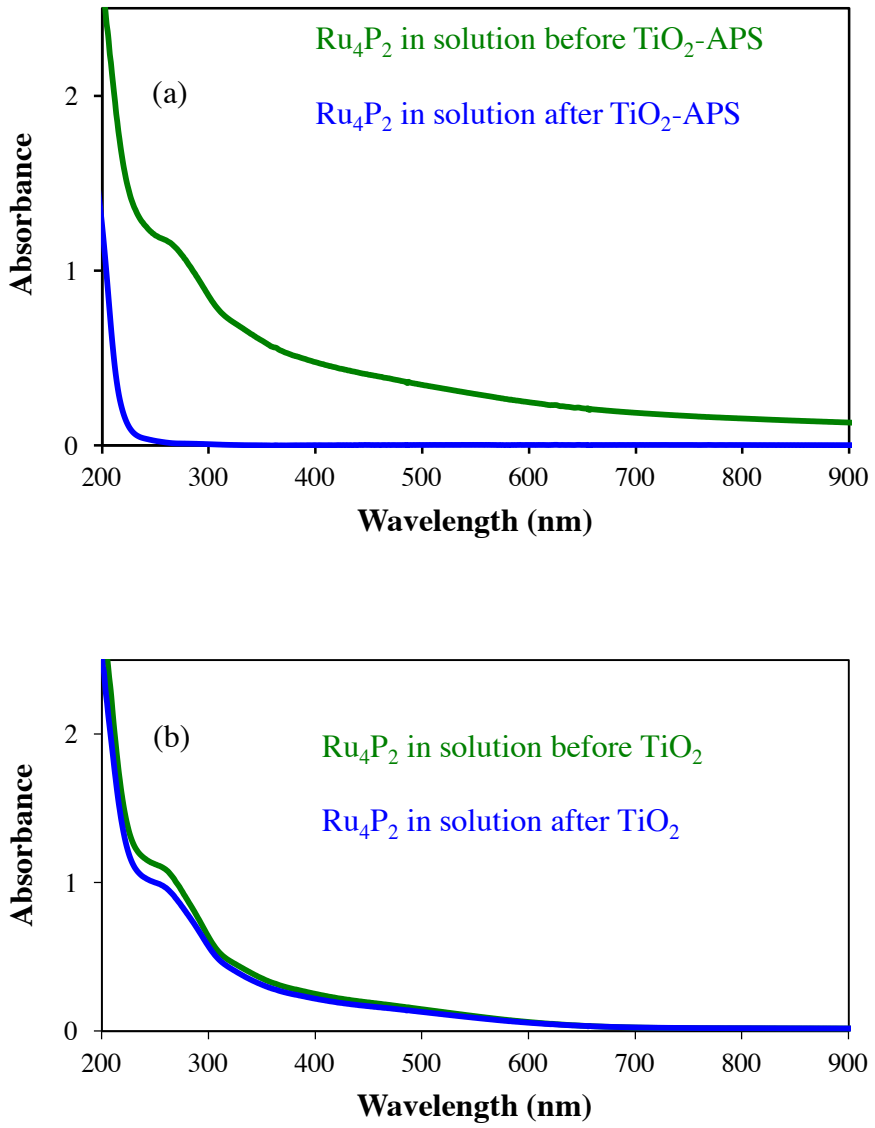

Figure 2.1 UV-vis of aqueous **Ru_4P_2** before and after immobilizing **Ru_4P_2** on TiO_2 nanoparticles (a) with silanization (treatment with APS) and (b) without silanization.

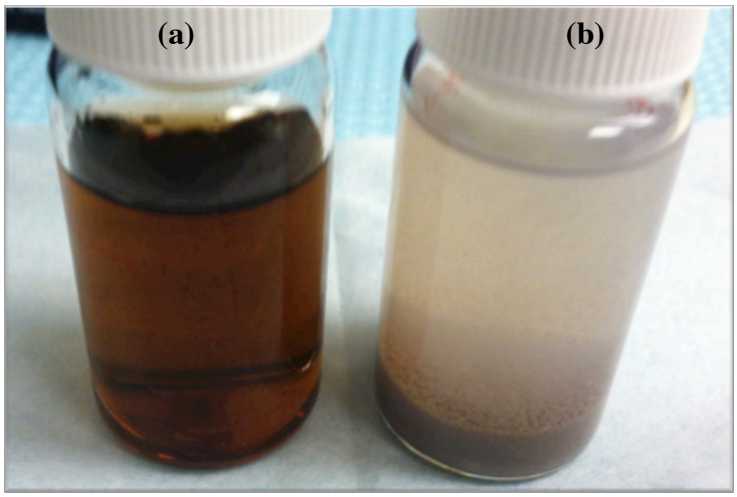

Figure 2.2 Decolorization of (a) aqueous $\mathbf{Ru_4P_2}$ to (b) $\mathbf{Ru_4P_2}$ on TiO_2 nanoparticles.

The POM covered *ca*. 25-30% of the surfaces of the resulting NPs as determined from EDX of $\mathbf{Ru_4P_2}$ on TiO_2. The EDX results for $\mathbf{Ru_4P_2}$ on modified TiO_2 show that the average weight ratio of 2.1 for Ru/P and 0.9 for Ru/W equates to 4 Ru atoms vs 2 P atoms and 4 Ru atoms vs 20 W atoms, respectively, indicating that $\mathbf{Ru_4P_2}$ is intact on the surface. The EDX data when the SMO (TiO_2) surfaces were not modified by silyl cations led to undetectable amounts of Ru and P on the TiO_2, indicating that without APS-modification, the POM is not retained on the TiO_2 surface (Figure 2.3).

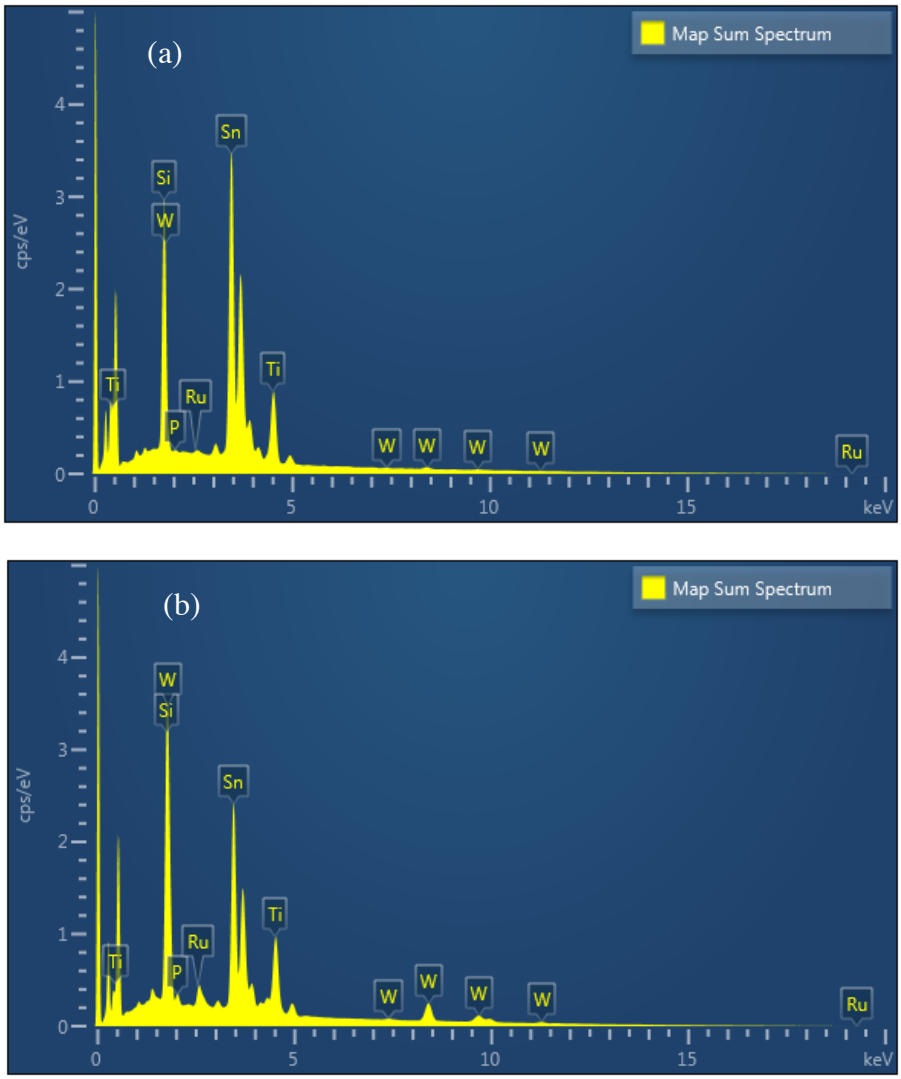

Figure 2.3 EDX spectra of $\mathbf{Ru_4P_2}$ on TiO_2 nanoparticles (a) without APS silanization and (b) with APS silanization.

2.3.3 Preparation of TiO_2/FTO electrodes coated with the molecular WOC, Ru_4P_2

The fluorine-doped tin oxide substrates, FTO, (Pilkington TEC15, ~15Ω/sq resistance) were cleaned by sonicating sequentially in acetone, ethanol and deionized water for 20 min each time, followed by blowing dry with nitrogen gas. Before coating, the top area of substrate was covered by tape to provide a non-coated area for electrical

conductance for the final electrode. A ~50 nm-thick compact layer of TiO_2 was deposited onto the FTO by spin coating at 3000 rpm for 50 s, using a solution of titanium diisopropoxide bis(acetylacetonate) (75% in 2-propanol) (Sigma-Aldrich) diluted in ethanol (1:40, v/v). Subsequently, the substrates were annealed at 450 °C for 1 h. For the TiO_2 mesoporous layer, ~10 mg of ethyl cellulose (Sigma-Aldrich) and ~0.05 mL of acetylacetone (Sigma-Aldrich) was added to 3.75 mL of terpineol. A solution of 1.25 mL of 20-nm-sized paste (Dyesol, 90-T) was diluted in the terpineol (1:3, v/v). A uniform TiO_2 colloid was obtained with this method. The single-layered substrate was lined up in the middle of two substrates with the same thickness, each of which has two layers of adhesive tape (40 μm thickness per layer) to control the thickness of the TiO_2 film. A similar tape cover for the electrical conductance was applied before the second layer was coated. The TiO_2 colloid was applied in the center of the substrate and distributed with a glass rod sliding over the tape-covered substrates on the side. The substrates were sintered at 500 ºC for 1-2 h, yielding a ~10-20 μm thick nanostructured double layer TiO_2 film. The TiO_2 electrodes were suspended in an anhydrous toluene mixture of 6% APS overnight at 70 ºC. The resulting films were washed with toluene, acetone and ethanol before being suspended in the aqueous solution of the POM. The electrodes were rinsed with 5 mL of water three times and dried in air. The concentration of $\mathbf{Ru_4Si_2}$ and $\mathbf{Ru_4P_2}$ retained on the surface was monitored by UV-visible spectroscopy of the washing water.

2.3.4 Vibrational Spectroscopic and Electron Microscopic Studies

Infrared spectra were recorded using a Nicolet 6700 FTIR spectrometer with 2-3% sample in KBr pellet. Raman spectra of $\mathbf{Ru_4P_2}$ and $\mathbf{Ru_4Si_2}$ on TiO_2 nanoparticles were

collected utilizing an argon ion spectra-physics, 514 nm laser. The powdered samples were illuminated at a 45-degree angle in an NMR tube. Scattered light was collected by an Olympus plan N 20x objective; the excitation light was passed through a holographic notch Kyser optical systems filter. The transmitted light was dispersed in a Halo Spec VIT system and imaged by a 1340x400 pixel CCD PIXIS 400 Princeton Instrumental camera. The confocal Raman spectra of the Ru_4P_2-TiO_2 and Ru_4Si_2-TiO_2 electrodes were collected using an Alpa-Witek confocal Raman microscope with high resolution mapping (xy < 250 nm; z < 0.7 micron) capability and 514-nm excitation laser. Scanning electron microscopy and energy dispersive X-ray spectroscopy (SEM/EDX) data were gathered at the Clemson University Advanced Materials Center using three Hitachi transmission electron microscopes (STEM HD2000, TEM H7600T, and TEM 9500) and scanning electron microscopes (SEM 3400, SU-6600, and S4800) equipped with EDX.

2.3.5 Light-driven water oxidation reactions

Reactions were carried out in a cylindrical cuvette containing 2 mL of liquid with a rubber stopper. A magnetic bar was stirred at a rate of 5000 rpm on the flat side of the cuvette. After purging the system of N_2 and O_2 using Ar gas, the solution was then exposed to light for the desired length of time. A 250-μL gastight syringe replaced 100 μL of Ar with 100 μL of headspace from the cuvette, of which 50 μL was injected into the GC. Calibrations of the cuvette for the moles of O_2 produced were conducted by injecting known amounts of O_2 gas into a purged cuvette of water and generating a calibration curve from the resulting GC peak area for O_2.[42] An Agilent 7890A gas chromatography (GC) system comprising a HP-MOLESIEVE capillary column (30m x 0.535 mm x 25.00 μm)

and thermal conductivity detector with Ar carrier gas was used to quantify O_2 before and during catalytic light-driven water oxidation experiments.

2.3.6 Photoelectrochemical studies

Photoelectrochemical reactions were carried out using standard three-electrode measurements on a Pine Research Instrument WaveDriver 20 bipotentiostat. All potentials were measured against a 1M KCl Ag/AgCl reference electrodes (+0.237 V vs RHE) purchased from Bioanalytical Systems, Inc. Platinum wire was used as the counter electrode. Working electrodes were fabricated from the films discussed above. A copper wire was fixed to the exposed FTO surface using conductive silver adhesive 503 (Electron Microscopy Sciences). The copper wire was fitted through a glass tube and the FTO/copper wire was insulated and attached to the glass tube with Epoxy adhesive (Henkel Loctite Hysol 1C Epoxi). Electrodes were dried overnight before testing. Bulk electrolysis and linear scan voltammetry were conducted in a custom rounded 50 mL PEC cell with a flat quartz window and four arms equipped with airtight adaptors for electrodes and headspace access (Tudor Scientific Glass). The cell was purged with Ar gas prior to use. A 150-W Xe light source was focused on the flat quartz window with and without a 400 nm cutoff filter (130 mW power at the quartz window). The configuration without the cutoff filter allowed the incident UV light to pass through to the working electrode. (Figure 2.4) Chronoamperometry measurements and linear sweep voltammetric studies were conducted in 160 mM sodium borate buffer pH 8, with 0.1 M KNO_3 electrolyte and 10 mV/s scan rate. Bulk electrolysis stability tests were conducted in 0.050 M sodium borate buffer, pH 9.6 with 0.1 M KNO_3. The potential was held at 1.24 V vs RHE for 24 hours

under UV illumination, gentle stirring and argon gas (Figure 2.5). The pH dependence linear sweep voltammetry was conducted in 0.1 M KNO_3 electrolyte and adjusted to desired pH with KOH and HNO_3 with a 100 mV/s scan rate.

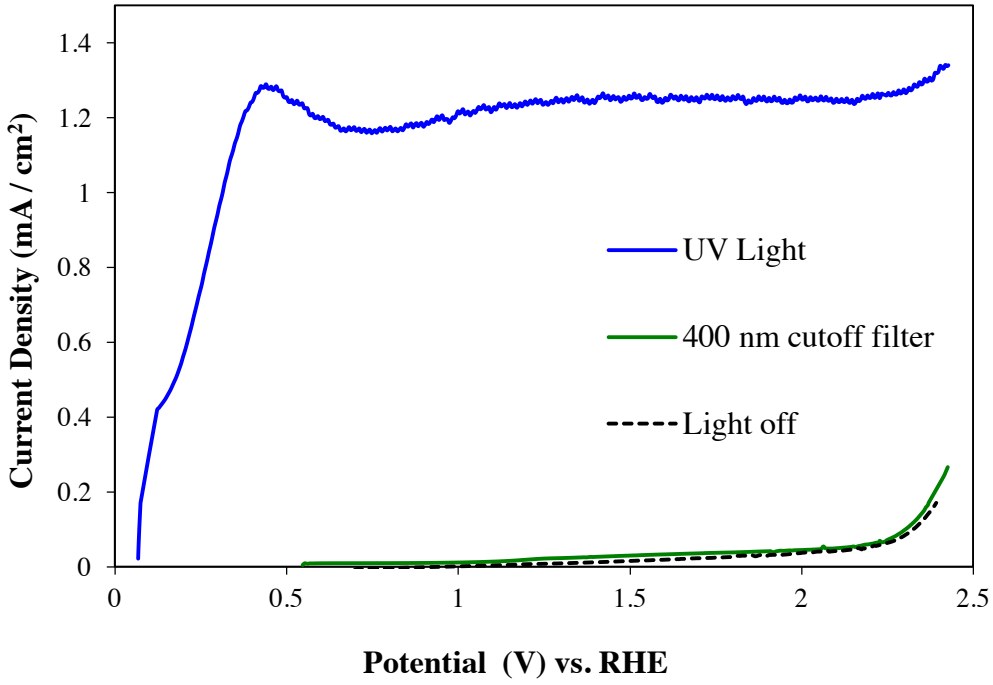

Figure 2.4 Linear scan voltammetry of **Ru_4P_2**-TiO_2 electrodes with UV light illumination, 400 nm cutoff filter, and light off. Conditions: 160 mM sodium borate buffer pH 10, with 0.1 M KNO_3 electrolyte, 100 mV/s scan rate, 0.15 mW/cm^2 UV light power density, 0.25 mW/cm^2, 400 nm cutoff filter power density.

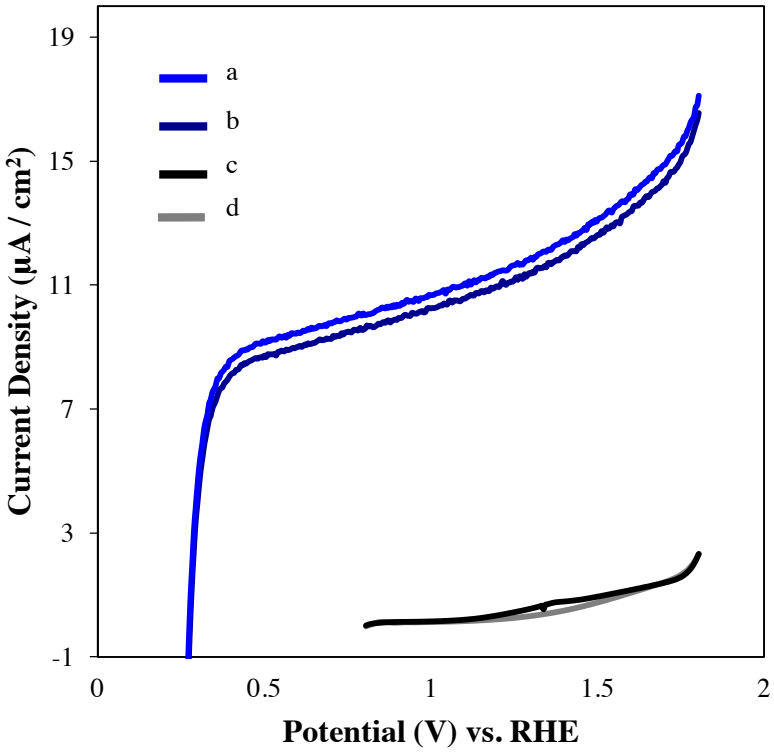

Figure 2.5 Linear sweep voltammograms of $\mathbf{Ru_4P_2}$-TiO_2 (a) before chronoamperometry with UV illumination, (b) after chronoamperometry with UV illumination, (c) before chronoamperometry with light off, and (d) after chronoamperometry with light off. Conditions: 160 mM sodium borate buffer pH 9.6, with 0.1 M KNO_3 electrolyte, 10 mV/s scan rate, 0.15 mW/cm^2 UV light power density.

2.4 Results and Discussion

The POM-coated TiO_2 nanoparticles were prepared as described in the Experimental Section. In this study, FTIR and Raman spectroscopy were carried out to observe the presence of $\mathbf{Ru_4P_2}$ and $\mathbf{Ru_4Si_2}$ on TiO_2-APS. Figure 2.6 shows the FTIR spectra of pure $\mathbf{Ru_4P_2}$ and immobilized $\mathbf{Ru_4P_2}$. The TiO_2 spectrum has a broad feature centered at

500-600 cm^{-1} due to the Ti—O vibrations. The characteristic W—O_x group frequencies in Ru_4P_2 are strong in the IR spectra of both **Ru_4P_2** alone (1123 ν_{as}(P—O_a), 1070 ν_s(W—O_d), 1044 ν_{as}(W—O_b—W), 1032 ν_{as}(W—O_c—W), and 943 cm^{-1} ν_s(P—O_a))[43] and the TiO_2-immobilized **Ru_4P_2** (1122, 1072, 1043, and 946 cm^{-1}), where O_a is bound to three tungsten atoms and the central heteroatom, O_b and O_c are bridging oxygens, and O_d is a terminal oxygen.

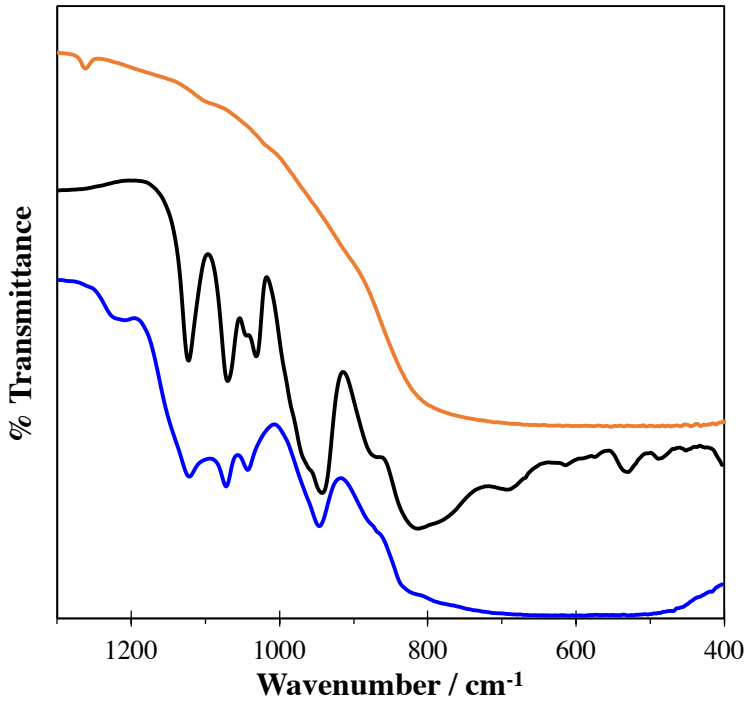

Figure 2.6 FTIR spectra of 30 nm TiO_2 nanoparticles (orange), **Ru_4P_2** alone (black), and TiO_2 nanoparticles with surface-immobilized **Ru_4P_2** (blue).

Electron microscopy coupled with EDX strongly suggests that the **Ru_4P_2** WOC molecules are intact on the surface of TiO_2 based on the atomic ratios of ruthenium, phosphorus, and tungsten in both free nanoparticles and FTO films (Figure 2.7). The ratio

of ruthenium to phosphorus agrees within 4% of the theoretical ratio expected with the **Ru_4P_2** POM and within 2% deviation in the ruthenium to tungsten ratio. Analysis of **Ru_4Si_2** presents a silicon overlap with the silyl binding agent; however, the tungsten to ruthenium ratio agrees within 2% deviation. We thus suspect that both **Ru_4P_2** and **Ru_4Si_2** WOC molecules are intact on the surface within the ~0.1 atom % detection limit of EDX.

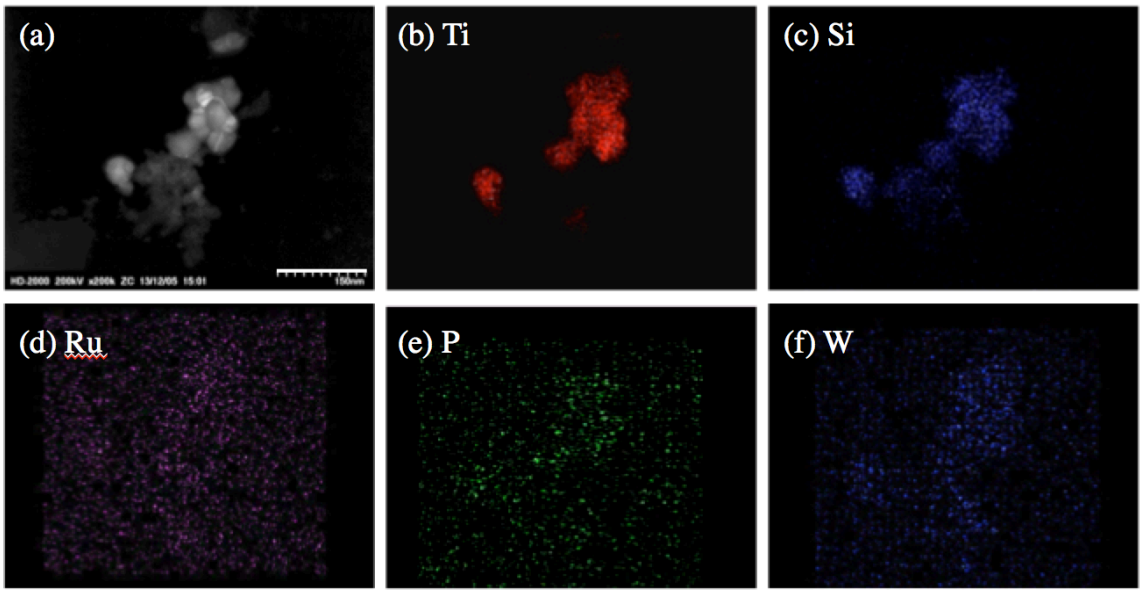

Figure 2.7 STEM/EDX of (a) **Ru_4P_2** immobilized on TiO_2 nanoparticles (30 nm) after catalysis with elemental mapping of Ti (34.09 at%) of TiO_2 support (b), Si (0.07 at%) of the silylating agent, APS (c), Ru (0.86 at%), P (0.43 at%), and W (5.35 at%) of **Ru_4P_2** (d, e, and f, respectively). The scale bar is 150 nm.

The heterogenized particles were initially assessed for WOC properties on the TiO_2 surface and for **Ru_4P_2** and **Ru_4Si_2** leaching in a light-driven water oxidation system described elsewhere,[44-46] using photosensitizer and sacrificial oxidant. When the particles

are removed from the solution mid-reaction, the O_2 yield of the resulting solution is diminished, indicating negligible **Ru_4P_2** leaching occurs (Figure 2.8).

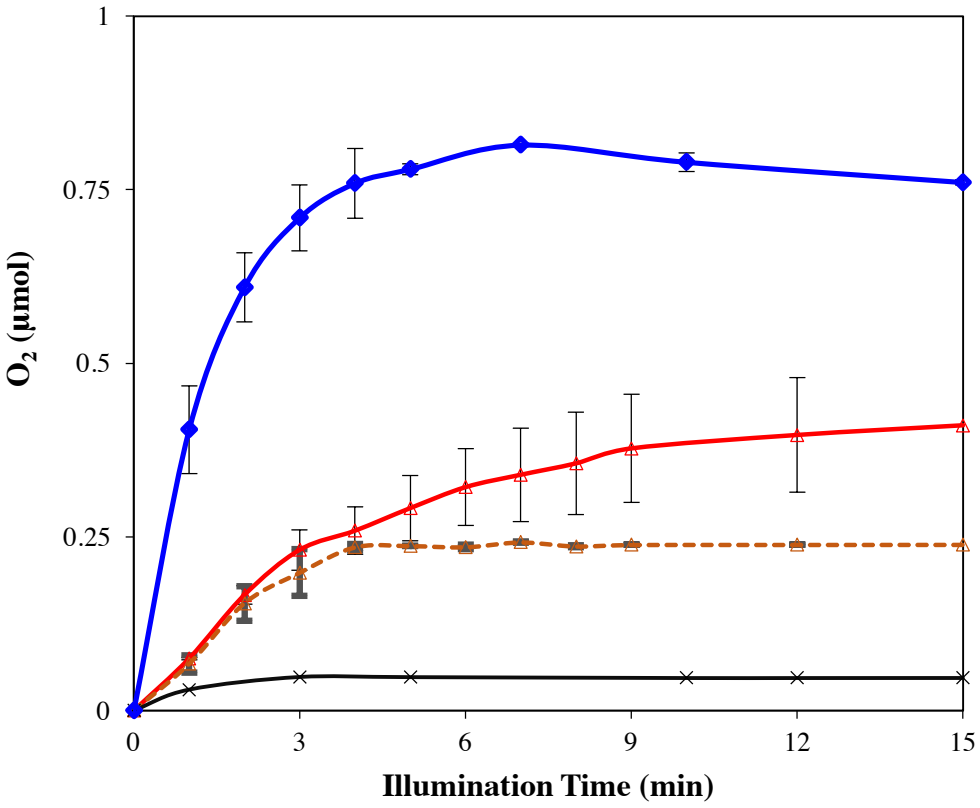

Figure 2.8 Moles of O_2 product versus illumination time during visible-light-driven water oxidation in the presence of **Ru_4Si_2**-TiO_2 (blue diamonds) **Ru_4P_2**-TiO_2 (red triangles), and with **Ru_4P_2**-TiO_2 particles removed at four minutes (dashed line, dark red triangles), and TiO_2 alone (black). Error bars represent the standard deviation of experiments done in triplicate. Conditions: 440 nm LED, 20 mW, 1.0 mM $[Ru(bpy)_3]Cl_2$, 5.0 mM $Na_2S_2O_8$, 80 mM sodium borate buffer pH 8.0, 0.4 µM catalyst.

The electrochemical process of water oxidation is expected to show a strong pH dependence.[47] Figure 2.9 shows the electrode **Ru_4P_2**-TiO_2 pH dependence under UV illumination, with the catalytic photocurrent increasing with pH. **Ru_4Si_2**-TiO_2 electrodes

show the same trend, suggesting electrochemical water oxidation is occurring on the electrodes upon UV illumination.

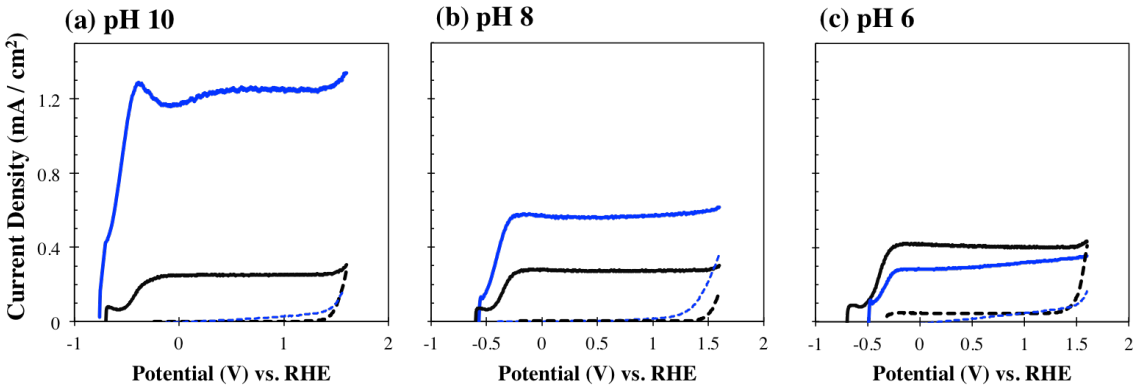

Figure 2.9 pH dependence of $\mathbf{Ru_4P_2}$-TiO_2 electrodes under UV illumination (solid blue) and dark (dotted red) and TiO_2/FTO electrodes under UV illumination (solid black) and dark (dotted black) at (a-c) pH 10, 8, and 6, respectively.

Chronoamperometry measurements were performed on $\mathbf{Ru_4P_2}$-TiO_2 and $\mathbf{Ru_4Si_2}$-TiO_2 electrodes under dark and UV illumination intervals (Figure 2.10). The photocurrent of the immobilized POM remained steady as the TiO_2-APS electrode photocurrent declined over time. The physical integrity of the immobilized POM and evidence for stability of the films after photoelectrochemical measurements were shown by linear sweep voltammetry, UV-vis, and Raman spectroscopy (Figure 2.11). Film surface analysis by EDX suggests that the POM is intact with a W:Ru ratio within 6% of the theoretical ratio before and after photoelectrochemical studies (Figure 2.12).

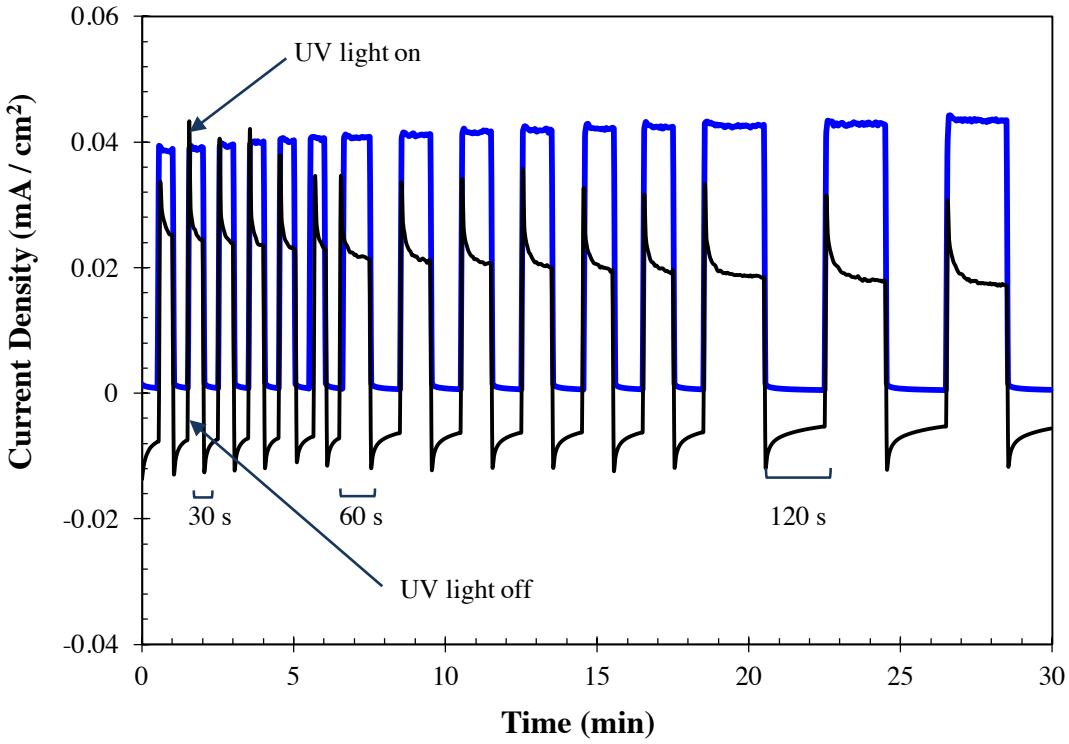

Figure 2.10 Chronoamperometry of **Ru_4P_2**-TiO_2 (blue) and TiO_2-APS (black) with UV light illumination and the light blocked at varying time intervals (30s, 60s, and 120s). Conditions: 160 mM sodium borate buffer pH 8, with 0.1 M KNO_3 electrolyte, 0.15 mW/cm^2 UV light power density, potential held at 0.521 V *vs*. Ag/AgCl, 1.23 V *vs*. RHE ($\Phi_{RHE} = E_{Ag/AgCl} + 0.237 + (0.059*pH)$).

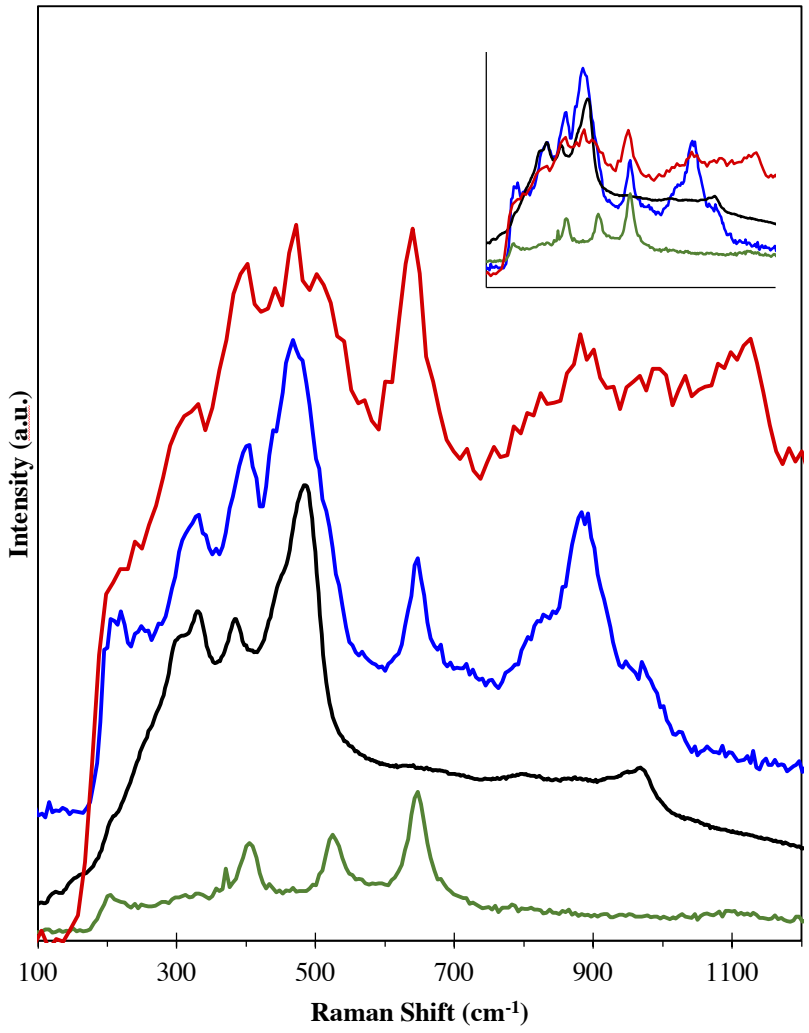

Figure 2.11 Confocal Raman spectra of nanoporous TiO_2 electrodes (orange), **Ru_4Si_2** alone (black), and **Ru_4Si_2**-TiO_2 electrode before (blue) and after 24 hour bulk electrolysis (red). Inset shows real intensities.

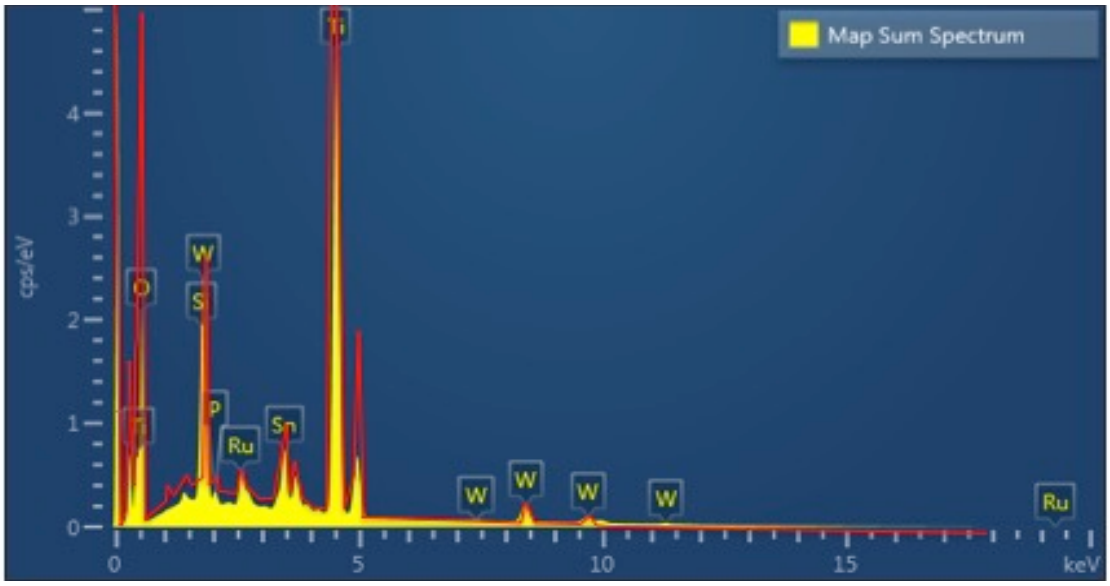

Figure 2.12 EDX spectra of $\mathbf{Ru_4P_2}$-TiO_2 films before (red) and after (yellow) photoelectrochemical measurements.

2.5 Conclusions

Immobilizing homogenous WOCs onto inert surface supports such as active carbon or silica frequently results in loosely bound catalyst molecules with attendant leaching problems under catalytic turnover conditions. Treatment of TiO_2 nanoparticle surfaces and nanoporous films with the cationic silylating agent, APS, greatly enhances the stability of the POM WOCs on the surface. Although the current density of these POM-bound electrodes is extremely low and no oxygen was measured during this study, the concept of immobilization via silylation provides insight into the POM WOC activity on a surface.

FT-IR, Raman, and EDX demonstrate that the POM remains intact on the nanoparticle surfaces after photo-driven catalytic water oxidation. The system also exhibits increased and sustained photocurrent density in TiO_2/FTO films upon illumination. A similar POM WOC immobilization technique will be used to prepare POM WOC-

semiconductor metal oxide (SMO) dyad materials with better overlap of the SMO with the terrestrial solar spectrum, as discussed in chapter 3.

2.6 References

1. Lewis, N. S., Powering the Planet. *MRS Bull*. **2007,** *32*, 208-820.

2. Yapsaklı, K.; Can, Z. S., Interaction of Ozone with Formic Acid: A System which Supresses the Scavenging Effect of HCO_3-/$CO3^{2-}$. *Water Qual. Res. J. Canada* **2004,** *39* (2), 140-148.

3. Gust, D.; Moore, T. A.; Moore, A. L., Solar Fuels via Artificial Photosynthesis. *Acc. Chem. Res*. **2009,** *42* (12), 1890-1898.

4. Hisatomi, T.; Kubota, J.; Domen, K., Recent advances in semiconductors for photocatalytic and potoelectrochemical water splitting. *Chem. Soc. Rev*. **2014,** *43*, 7520-7535.

5. Thomas, J. M., Designing Catalysts for Tomorrow's Environmentally Benign Processes. *Top. Catal*. **2014,** *57*, 1115-1123.

6. Cao, R.; Lai, W.; Du, P., Catalytic water oxidation at single metal sites. *Energy Environ. Sci*. **2012,** *5* (8), 8134-8157.

7. Lv, H.; Song, J.; Geletii, Y. V.; Vickers, J. W.; Sumliner, J. M.; Musaev, D. G.; Kögerler, P.; Zhuk, P. F.; Bacsa, J.; Zhu, G.; Hill, C. L., An Exceptionally Fast Homogeneous Carbon-free Cobalt-based Water Oxidation Catalyst. *J. Am. Chem. Soc*. **2014,** *136* (26), 9268-9271.

8. Duan, L. L.; Tong, L. P.; Xu, Y. H.; Sun, L. C., Visible light-driven water oxidation-from molecular catalysts to photoelectrochemical cells. *Energy Environ. Sci.* **2011,** *4* (9), 3296-3313.

9. Soriano-López, J.; Goberna-Ferrón, S.; Vigara, L.; Carbó, J. J.; Poblet, J. M.; Galán-Mascarós, J. R., Cobalt Polyoxometalates as Heterogeneous Water Oxidation Catalysts. *Inorg. Chem.* **2013,** *52* (9), 4753-4755.

10. Li, F.; Zhang, B.; Li, X.; Jiang, Y.; Chen, L.; Li, Y.; Sun, L., Highly Efficient Oxidation of Water by a Molecular Catalyst Immobilized on Carbon Nanotubes. *Angew. Chem. Int. Ed.* **2011,** *50*, 12276-12279.

11. Song, W.; Chen, Z.; Glasson, C. R. K.; Hanson, K.; Luo, H.; Norris, M. R.; Ashford, D. L.; Concepcion, J. J.; Brennaman, M. K.; Meyer, T. J., Interfacial Dynamics and Solar Fuel Formation in Dye-Sensitized Photoelectrosynthesis Cells. *ChemPhysChem* **2012,** *13* (12), 2882-2890.

12. Vannucci, A. K.; Alibabaei, L.; Losego, M. D.; Concepcion, J. J.; Kalanyan, B.; Parsons, G. N.; Meyer, T. J., Crossing the divide between homogeneous and heterogeneous catalysis in water oxidation. *Proc. Natl. Acad. Sci.* **2013,** *110* (52), 20918-20922.

13. Sartorel, A.; Bonchio, M.; Campagna, S.; Scandola, F., Tetrametallic molecular catalysts for photochemical water oxidation. *Chem. Soc. Rev.* **2013,** *42*, 2262-2280.

14. Pope, M. T.; Müller, A., Chemistry of polyoxometallates. Actual variation on an old theme with interdisciplinary references. *Angew. Chem.* **1991,** *103* (1), 56-70.

15. Hill, C. L., Introduction: Polyoxometalates--Multicomponent Molecular Vehicles To Probe Fundamental Issues and Practical Problems. *Chem. Rev.* **1998,** *98* (1), 1-2.

16. Miras, H. N.; Yan, J.; Long, D.-L.; Cronin, L., Engineering polyoxometalates with emergent properties. *Chem. Soc. Rev.* **2012,** *41*, 7403-7430.

17. Misono, M., Heterogeneous Catalysis by Heteropoly Compounds of Molybdenum and Tungsten. *Catal. Rev. Sci. Eng.* **1987,** *29*, 269-321.

18. Hill, C. L.; Prosser-McCartha, C. M., Homogeneous catalysis by transition metal oxygen anion clusters. *Coord. Chem. Rev.* **1995,** *143*, 407-455.

19. Neumann, R., Polyoxometalate Complexes in Organic Oxidation Chemistry. *Prog. Inorg. Chem.* **1998,** *47*, 317-370.

20. Hill, C. L.; Kholdeeva, O. A., Selective Liquid Phase Oxidations in the Presence of Supported Polyoxometalates. In *Liquid Phase Oxidation via Heterogeneous Catalysis*, Clerici, M. G.; Kholdeeva, O. A., Eds. John Wiley & Sons, Inc.: Hoboken, New Jersey, 2013; pp 263-319.

21. Guo, S.-X.; Liu, Y.; Lee, C.-Y.; Bond, A. M.; Zhang, J.; Geletii, Y. V.; Hill, C. L., Graphene-supported [{$Ru_4O_4(OH)_2(H_2O)_4$}([gamma]-$SiW1_0O_{36})_2$]$^{10-}$ for highly efficient electrocatalytic water oxidation. *Energy Environ. Sci.* **2013,** *6* (9), 2654-2663.

22. Gall, R. D.; Hill, C. L.; Walker, J. E., Selective oxidation of thioether mustard (HD) analogs by *tert*-butylhydroperoxide catalyzed by $H_5PV_2Mo_{10}O_{40}$ supported on porous carbon materials. *J. Catal.* **1996,** *159* (2), 473-478.

23. Gall, R. D.; Hill, C. L.; Walker, J. E., Carbon Powder and Fiber-Supported Polyoxometalate Catalytic Materials. Preparation, Characterization, and Catalytic Oxidation of Dialkyl Sulfides as Mustard (HD) Analogues. *Chem. Mater.* **1996,** *8* (10), 2523-2527.

24. Okun, N. M.; Anderson, T. M.; Hill, C. L., $[(Fe^{III}(OH_2)_2)_3(A\text{-}\alpha\text{-}PW_9O_{34})_2]^{9-}$ on Cationic Silica Nanoparticles, a New Type of Material and Efficient Heterogeneous Catalyst for Aerobic Oxidations. *J. Am. Chem. Soc.* **2003,** *125* (11), 3194-3195.

25. Okun, N. M.; Anderson, T. M.; Hill, C. L., Polyoxometalates on Cationic Silica. Highly Selective and Efficient O_2/Air-Based Oxidation of 2-Chloroethyl Ethyl Sulfide at Ambient Temperature. *J. Mol. Catal. A: Chem.* **2003,** *197* (1-2), 283-290.

26. Okun, N. M.; Ritorto, M. D.; Anderson, T. M.; Apkarian, R. P.; Hill, C. L., Polyoxometalates on Cationic Silica Nanoparticles. Physicochemical Properties of an Electrostatically Bound Multi-Iron Catalyst. *Chem. Mater.* **2004,** *16*, 2551-2558.

27. Maldotti, A.; Molinari; Bigi, F., Selective photooxidation of diols with silica bound $W_{10}O^{4-}_{32}$. *J. Catal.* **2008,** *253*, 312-317.

28. Song, W.; Brennaman, M. K.; Concepcion, J. J.; Jurss, J. W.; Hoertz, P. G.; Luo, H.; Chen, C.; Hanson, K.; Meyer, T. J., Interfacial Electron Transfer Dynamics for $[Ru(bpy)_2((4,4'\text{-}PO_3H_2)_2bpy)]^{2+}$ Sensitized TiO_2 in a Dye-Sensitized Photoelectrosynthesis Cell: Factors Influencing Efficiency and Dynamics. *J. Phys. Chem. C* **2011,** *115*, 7081-7091.

29. Youngblood, W. J.; Lee, S.-H. A.; Kobayashi, Y.; Hernandez-Pagan, E. A.; Hoertz, P. G.; Moore, T. A.; Moore, A. L.; Gust, D.; Mallouk, T. E., Photoassisted Overall Water Splitting in a Visible Light-Absorbing Dye-Sensitized Photoelectrochemical Cell. *J. Am. Chem. Soc.* **2009,** *131* (3), 926-927.

30. Youngblood, W. J.; Lee, S.-H. A.; Maeda, K.; Mallouk, T. E., Visible Light Water Splitting Using Dye-Sensitized Oxide Semiconductors. *Acc. Chem. Res.* **2009,** *42* (12), 1966-1973.

31. Moore, G. F.; Blakemore, J. D.; Milot, R. L.; Hull, J. F.; Song, H.-e.; Cai, L.; Schmuttenmaer, C. A.; Crabtree, R. H.; Brudvig, G. W., A visible light water-splitting cell with a photoanode formed by codeposition of a high-potential porphyrin and an iridium water-oxidation catalyst. *Energy Environ. Sci.* **2011,** *4*, 2389-2392.

32. Alibabaei, L.; Brennaman, M. K.; Norris, M. R.; Kalanyan, B.; Song, W.; Losego, M. D.; Concepcion, J. J.; Binstead, R. A.; Parsons, G. N.; Meyer, T. J., Solar water splitting in a molecular photoelectrochemical cell. *Proc. Natl. Acad. Sci.* **2013,** *110* (50), 20008-20013.

33. Ardo, S.; Meyer, G. J., Photodriven heterogeneous charge transfer with transition-metal compounds anchored to TiO_2 semiconductor surfaces. *Chem. Soc. Rev.* **2009,** *38*, 115-164.

34. Song, W.; Vannucci, A. K.; Farnum, B. H.; Lapides, A. M.; Brennaman, M. K.; Kalanyan, B.; Alibabaei, L.; Concepcion, J. J.; Losego, M. D.; Parsons, G. N.; Meyer, T. J., Visible Light Driven Benzyl Alcohol Dehydrogenation in a Dye Sensitized Photoelectrosynthesis Cell. *J. Am. Chem. Soc.* **2014,** *136*, 9773-9779.

35. Guo, S.-X.; Lee, C.-Y.; Zhang, J.; Bond, A. M.; Geletii, Y. V.; Hill, C. L., Mediator Enhanced Water Oxidation Using $Rb_4[Ru^{II}(bipy)_3]_5$ [$\{Ru^{III}_4O_4(OH)_2(H_2O)_4\}$ (γ-$SiW_{10}O_{36})_2$] Film Modified Electrodes. *Inorg. Chem.* **2014,** *53* (14), 7561-7570.

36. Odobel, F.; Séverac, M.; Pellegrin, Y.; Blart, E.; Fosse, C.; Cannizzo, C.; Mayer, C. R.; Elliott, K. J.; Harriman, A., Coupled Sensitizer–Catalyst Dyads: Electron-Transfer Reactions in a Perylene–Polyoxometalate Conjugate. *Chem. Eur. J.* **2009,** *15*, 3130-3138.

37. Xiang, X.; Fielden, J.; Rodríguez-Córdoba, W.; Huang, Z.; Zhang, N.; Luo, Z.; Musaev, D. G.; Lian, T.; Hill, C. L., Electron Transfer Dynamics in Semiconductor–

Chromophore–Polyoxometalate Catalyst Photoanodes. *J. Phys. Chem. C* **2013,** *117* (2), 918-926.

38. Orlandi, M.; Argazzi, R.; Sartorel, A.; Carraro, M.; Scorrano, G.; Bonchio, M.; Scandola, F., Ruthenium polyoxometalate water splitting catalyst: very fast hole scavenging from photogenerated oxidants. *Chem. Commun.* **2010,** *46*, 3152-3154.

39. Geletii, Y. V.; Botar, B.; Kögerler, P.; Hillesheim, D. A.; Musaev, D. G.; Hill, C. L., An All-Inorganic, Stable, and Highly Active Tetraruthenium Homogeneous Catalyst for Water Oxidation. Selected as the VIP Article by the reviewers and editor. *Angew. Chem. Int. Ed.* **2008,** *47*, 3896-3899.

40. Sartorel, A.; Carraro, M.; Scorrano, G.; Zorzi, R. D.; Geremia, S.; McDaniel, N. D.; Bernhard, S.; Bonchio, M., Polyoxometalate Embedding of a Tetraruthenium(IV)-oxo-core by Template-Directed Metalation of $[\gamma\text{-}SiW_{10}O_{36}]^{8-}$: A Totally Inorganic Oxygen-Evolving Catalyst. *J. Am. Chem. Soc.* **2008,** *130* (15), 5006-5007.

41. Besson, C.; Huang, Z.; Geletii, Y. V.; Lense, S.; Hardcastle, K. I.; Musaev, D. G.; Lian, T.; Proust, A.; Hill, C. L., $Cs_9[(\Upsilon\text{-}PW_{10}O_{36})_2Ru_4O_5(OH)(H_2O)_4]$, a new all-inorganic, soluble catalyst for the efficient visible-light-driven oxidation of water. *Chem. Commun.* **2010**, 2784-2786.

42. Huang, Z.; Luo, Z.; Geletii, Y. V.; Vickers, J.; Yin, Q.; Wu, D.; Hou, Y.; Ding, Y.; Song, J.; Musaev, D. G.; Hill, C. L.; Lian, T., Efficient Light-Driven Carbon-Free Cobalt-Based Molecular Catalyst for Water Oxidation. *J. Am. Chem. Soc.* **2011,** *133*, 2068-2071.

43. Thouvenot, R.; Fournier, M.; Franck, R.; Rocchiccioli-Deltcheff, C., Vibrational Investigations of Polyoxometalates. 3. Isomerism in Molybdenum (VI) and Tungsten(VI) Compounds Related to the Keggin Structure. *Inorg. Chem.* **1984,** *23*, 598-605.

44. Geletii, Y. V.; Huang, Z.; Hou, Y.; Musaev, D. G.; Lian, T.; Hill, C. L., Homogeneous Light-Driven Water Oxidation Catalyzed by a Tetraruthenium Complex with All Inorganic Ligands. *J. Am. Chem. Soc.* **2009,** *131*, 7522-7523.

45. Geletii, Y. V.; Besson, C.; Hou, Y.; Yin, Q.; Musaev, D. G.; Quinonero, D.; Cao, R.; Hardcastle, K. I.; Proust, A.; Kögerler, P.; Hill, C. L., Structural, Physicochemical and Reactivity Properties of an All-Inorganic, Highly Active Tetraruthenium Homogeneous Catalyst for Water Oxidation. *J. Am. Chem. Soc.* **2009,** *131* (47), 17360-17370.

46. Yin, Q.; Tan, J. M.; Besson, C.; Geletii, Y. V.; Musaev, D. G.; Kuznetsov, A. E.; Luo, Z.; Hardcastle, K. I.; Hill, C. L., A fast soluble carbon-free molecular water oxidation catalyst based on abundant metals. *Science* **2010,** *328*, 342-345.

47. Tsunashima, R.; Long, D.-L.; Endo, T.; Noro, S.-i.; Akutagawa, T.; Nakamura, T.; Cabrera, R. Q.; McMillan, P. F.; Kögerler, P.; Cronin, L., Exploring the thermochromism of sulfite-embedded polyoxometalate capsules. *Phys. Chem. Chem. Phys.* **2011,** *13*, 7295-7297.

IMMOBILIZATION METHODS FOR BINDING POLYOXOMETALATES ONTO SURFACES FOR WATER SPLITTING APPLICATIONS

CHAPTER 3

Stabilization of Polyoxometalate Water Oxidation Catalysts onto Hematite Using Atomic Layer Deposition

with Brandon Piercy, Wei Li, Qiushi Yin, Daniel L. Collins-Wildman, Elliot N. Glass, Mark Losego, Dunwei Wang, Yurii V. Geletii, and Craig L. Hill

Published in part in: Lauinger S. M., Piercy, B. D., Li, W., Yin Q., Collins-Wildman D. L., Glass, E. N., Losego M., Wang D., Geletii, Y. V., and Hill C. L. "Stabilization of Polyoxometalate Water Oxidation Catalysts on Hematite by Atomic Layer Deposition" *ACS Applied Materials & Interfaces*. **2017**, in review.

3.1 Abstract

Fast and selective polyoxometalate (POM) water oxidation catalysts (WOC) have been previously shown to interact with metal oxide surfaces with cationic surface properties. The system with TiO_2 nanoporous films and **Ru_4Si_2** has elucidated evidence of a strongly bound catalyst that retains water oxidation properties under UV-illumination. In this work, we have enhanced the stability of **Ru_4Si_2** under turnover conditions using atomic layer deposition (ALD) while increasing the photocurrent density of the system with visible light absorbing hematite thin films. Characterization techniques including FTIR, XPS, EDX and voltammetric studies indicate that **Ru_4Si_2** remains intact on the hematite surface with 4 nm of ALD protection.

3.2 Introduction

The increase in population and energy demand has resulted in harmful environmental impacts as fossil fuel reserves dramatically plummet while steadily increasing CO_2 emissions rise. The drive for renewable sources of energy has led many research groups to investigate solar fuel production through water splitting; generating energy-dense H_2 from H_2O using the solar spectrum. Because the oxidation of water is the more demanding half reaction of water splitting, efficient catalysts must be incorporated into photoanodes in order to develop a sufficient water splitting device.

Polyoxometalates have been widely studied as both water oxidation and reduction catalysts.[1] These transition metal oxide clusters have previously been immobilized onto and into many types of surfaces for water oxidation.[1-8] Previously, **Ru_4Si_2** had been incorporated into a triad system with Ru-based chromophore covalently bound to TiO_2

support.[9] In the presence of **Ru_4Si_2** in the triadic system, the electron transfer between the TiO_2 film and the chromophore was the main pathway instead of electron recombination and the transfer between **Ru_4Si_2** and the oxidized chromophore was ultrafast; however, no oxygen measurements were conducted to confirm water oxidation was occurring. In another study, **Ru_4Si_2** was immobilized onto TiO_2 and studied for UV illumination water oxidation activity without the use of a chromophore.[10] Under oxidative conditions, the system proved to be sufficient but also lost ~15% of the overall potential over 24 hours of photoelectrochemical experiments.

Methods of immobilizing molecular catalyst species has become a distinct field of research in context with solar fuel generation. Among various immobilization techniques explored, covalent and electrostatic interactions have been widely used for attaching catalyst and chromophore species onto semiconductor surfaces. Although these techniques have shown to be advantageous in many systems,[9, 11] either the molecular catalyst, especially organometallic compounds,[12] or the organic-based covalent bonding is susceptible to corrosion and decomposition over long-term use under oxidative conditions.

Atomic layer deposition (ALD) is a useful technique for many energy conversion applications including nanostructured photovoltaics[13] and energy storage.[14] ALD growth is a process with four steps: introduction of reactants, purging with inert gas to remove excess reactants, introduction of counter-reactants, and final purging with inert gas to remove excess counter-reactants and by-products.[13, 15] ALD offers form-fitting layers on a substrate and provides excellent control of deposition thickness due to its sequential, self-limiting vapor-phase precursors binding and reacting on the substrate in one atomic layer (figure 3.1).[16] Much solar fuels research applying ALD techniques has incorporated catalyst

growth via ALD on a surface.[17-25]

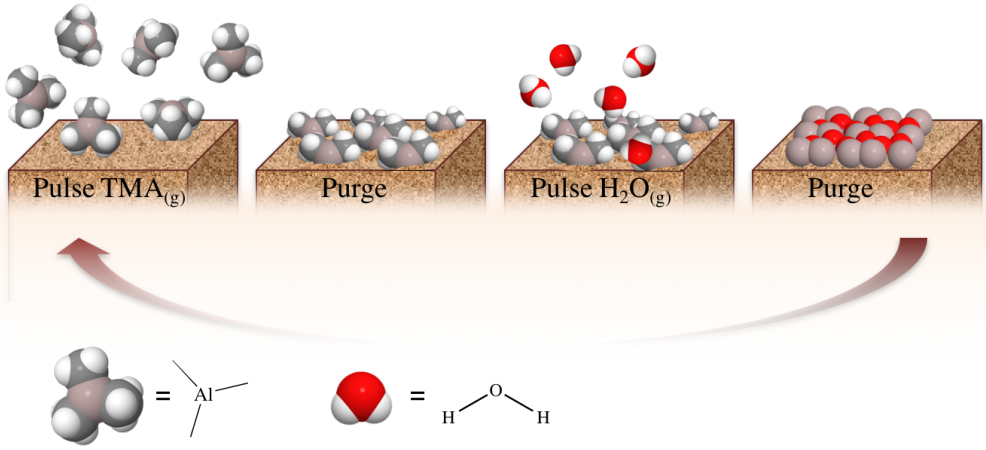

Figure 3.1 Schematic of atomic layer deposition (ALD) process. Steps: (1) Precursor A (trimethylaluminium [TMA] for Al_2O_3) is pulsed and reacts with substrate surface. (2) Precursor A and by-products removed by purging with inert gas. (3) Reactant B (water for Al_2O_3) is pulsed and reacts with precursor A on surface to form Al_2O_3. (4) Inert gas purged again to remove reaction by-products and excess reactant B. (5) Steps 1-4 are repeated until desired thickness is achieved.

To the best of our knowledge, the use of ALD overlayers protecting catalysts on the surface has only been utilized in a chromophore-catalyst assembly.[26] In this research, the Ru(II) polypyridyl chromophore was embedded onto TiO_2 with 10 layers of Al_2O_3 ALD. This exterior oxide was then used to bind a molecular Ru-based catalyst ([Ru(2,6-bis(1-methyl-1*H*-benzo[*d*]imidazole-2-yl)pyridine)(4,4'-$((OH)_2(O)P\text{-}CH_2)_2$-2,2'-bipyridine)$(OH_2)]^{2+}$) followed by another 10 layer ALD deposition to stabilize the catalyst. This system was studied for electocatalytic water oxidation and light-assisted photoelectrochemical water oxidation but displayed low activity due to slow electron

transfer throughout the ALD surfaces. However, the ALD overlayers did enhance stability of the catalyst and chromophore binding over 6 hours of photoelectrochemistry, reaching a 16.8% Faradaic efficiency.

Hematite has been a highly studied metal oxide support due to its wide-range pH stability, worldwide abundance, and suitable band gap (2.0-2.2 eV) that allows for visible light absorbing properties. One of the downsides of hematite is the fast recombination of the photon-generated electron-hole pairs. Much research has been conducted to enhance the efficiency of this substrate for solar water splitting. Hematite has been studied as an efficient photoanode for water oxidation in extremely alkaline(refs) or acidic[12] conditions; however, very few WOCs are stable under these conditions.

In this research, a POM WOC has been protected on the surface of hematite by ALD. In order to assess the stabilization of surface-bound POMs on hematite, layers up to 6 nm of amorphous Al_2O_3 have been added to cover the surface. Protective thin films show promise for use in photoelectrochemical systems.

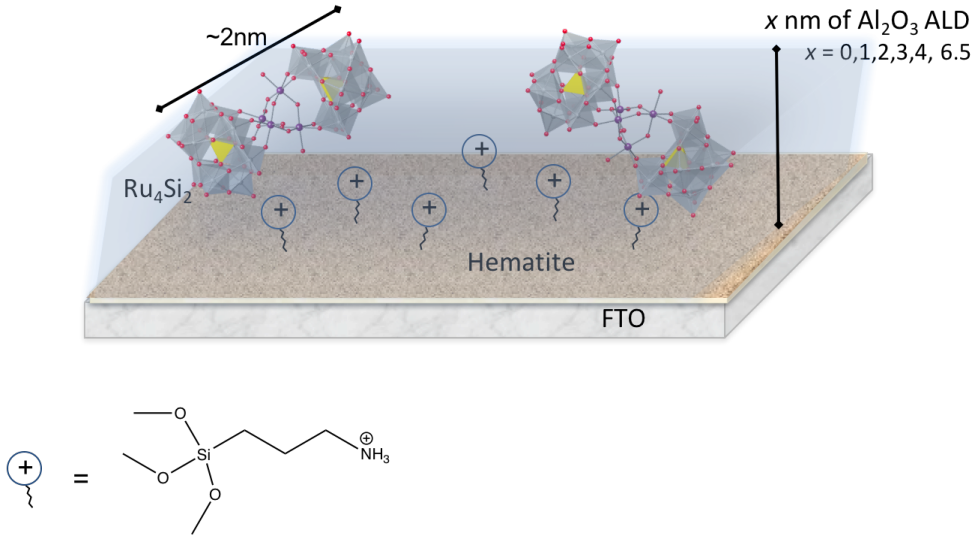

Figure 3.2 Schematic of hematite-APS-**Ru_4Si_2**-ALD system for water oxidation.

3.3 Experimental

3.3.1 General

Materials and solvents were purchased as ACS analytical or reagent grade and used as received. $Rb_8K_2[\{Ru^{IV}_4(OH)_2(H_2O)_4\}(\gamma\text{-}SiW_{10}O_{34})_2]$, (**$Ru_4Si_2$**), were prepared as previously described.[27] The potassium γ-decatungstosilcate precursor ($K_8[\gamma\text{-}SiW_{10}O_{36}]\cdot 12H_2O$ was mixed with 2.67 mmol $RuCl_2\cdot H_2O$ and dissolved in water. The pH was adjusted to 2.6 with 6 M HCl and allowed to mix for 5 minutes. A solution of 20 mmol RbCl was added to precipitate the product.

3.3.2 Synthesis of hematite films

Fluorine-doped tin oxide (FTO) substrates (~7 $\Omega.sq^{-1}$, Sigma) were cleaned with acetone, methanol and isopropanol. Following cleaning, FTO substrates were soaked in a solution consisting of 0.15 M iron(III) chloride hexahydrate ($FeCl_3.6H_2O$) and 1 M sodium nitrate ($NaNO_3$) in an oven at 100 °C for 1 h. The backside of the FTO substrates were protected by Kapton tape to prevent growth during the synthesis. Afterwards, the tape was removed and the substrate was rinsed with deionized (DI) water and dried with N_2 gas. Films were then annealed at 800 °C for 5 min to convert the resulting FeOOH to hematite. All hematite photoelectrodes labeled as hematite in this manuscript refer to samples subjected to the growth-annealing cycles three times.

3.3.3 Atomic layer deposition

Al_2O_3 ALD was conducted using a custom-built, hot wall flow-tube style reactor with a 1.5-inch diameter tube. The reactor was operated at approximately 1.5 Torr, using

ultra-high purity nitrogen (99.999%, Airgas) as the process gas with a downstream O_2 purifier (SAES MicroTorr). Trimethylaluminum (TMA, 99%, Strem) was used as the aluminum precursor, with deionized water as the coreactant. The deposition zone was maintained at 120 °C for all depositions, while the process gas lines were fixed at 110 °C to prevent precursor condensation. The ALD recipe used was: 0.2 s TMA/30 s purge/0.2 s H_2O/30 s purge, with process gas constantly flowing. Deposition was controlled by a LabVIEW sequencer. Film thicknesses were measured using spectroscopic ellipsometry on witness Si wafer chips, using a Cauchy model for the Al_2O_3 layer.

3.3.4 Characterization

All UV-Vis spectroscopy was performed with an Agilent 8453 spectrometer at room temperature. The Fourier transform infrared spectroscopy (FTIR) spectra were measured on a Nicolet 6700 FT-IR spectrometer with a diamond HATR smart accessory in the range of 4000 – 550 cm^{-1}. Scanning electron microscopy coupled with energy dispersive X-ray spectroscopy (SEM/EDX) were collected from the Clemson University Advanced Materials Center with the Hitachi SEM 3400.

3.3.5 Preparation of hematite/FTO electrodes coated with Ru_4Si_2 and varying layers of ALD

The working electrodes were fabricated from the films prepared as discussed above. A sharp blade was used to scrape off the exterior ALD, **Ru_4Si_2**, and hematite to expose the conductive FTO. A copper wire or copper tape was fixed to the exposed FTO surface using conductive silver adhesive 503 (Electron Microscopy Sciences). The copper wire or copper

tape was insulated using Epoxy adhesive (Henkel Loctite Hysol 1C Epoxi). Electrodes were then dried in an oven at 60 ºC for 1 hour prior to use.

3.3.6 Photoelectrochemical measurements

Photoelectrochemical reactions were carried out using a standard three-electrode cell for measurements on a Pine Research Instrument WaveDriver 20 bipotentiostat. All potentials were measured against a 1 M KCl Ag/AgCl reference electrode (+0.237 V vs. RHE) purchased from Bioanalytical Systems, Inc. A platinum wire was used as the counter electrode and working electrodes were fabricated as discussed earlier. Bulk photoelectrolysis and linear scan voltammetry with a 10 mV/s scan rate were conducted in a custom rounded 50 mL PEC cell with a flat quartz window and four arms equipped with airtight adapters for electrodes and headspace access (Tudor Scientific Glass). The cell was purged with Ar gas prior to use and a blanket of Ar gas was provided during measurements unless otherwise mentioned. A 150 W Xe light source was focused on the flat quartz window with and without a 400nm cutoff filter with 160 mW/cm^2 power at the film. In other photoelectrochemical experiments, a 455 nm LED, 9.5 mW/cm^2 power at the film, was used. Measurements were conducted in 240 mM sodium borate buffer, pH 8.25 with 0.1 M KNO_3 electrolyte. For bulk photoelectrolysis, the potential was held at 1.24 V vs. RHE for multiple hours under either visible or white light with gentle stirring and argon gas.

3.3.7 Oxygen Measurements

Oxygen measurements were performed in a 40mm x 10 mm quartz cuvette (Science Outlet) with a custom-fitted Teflon lid with holes for counter, reference, and working electrodes and FOXY Forspor oxygen probe. Solutions of 240 mM borate buffer, pH 8.25 and 0.1 M KNO_3 were purged with Ar gas for 30 minutes before use. The 1.0 M KCl Ag/AgCl reference electrode, Pt wire within a tube with a Nafion proton membrane tip, and working electrodes were fit into the Teflon lid and secured with paraffin and vacuum grease. The Ar-purged solution was added into the cell through an open hole in the lid until the solution overflowed and the last open hole was sealed with grease. The closed cell was placed into an airtight box with constant Ar flow with a quartz window for light passage and septa for the potentiostat electrode clips. The potential was held at 1.24 V vs. RHE during oxygen measurements with visible and white light illumination. The oxygen probe was placed directly in front of the working electrode and the initial oxygen level dissolved in solution served as the baseline for the experiment. With an airtight box with argon flow, all oxygen sensed was due to the oxygen generation at the electrode. Faradaic yields were calculated from the current passed through the working electrode during bulk photoelectrolysis.

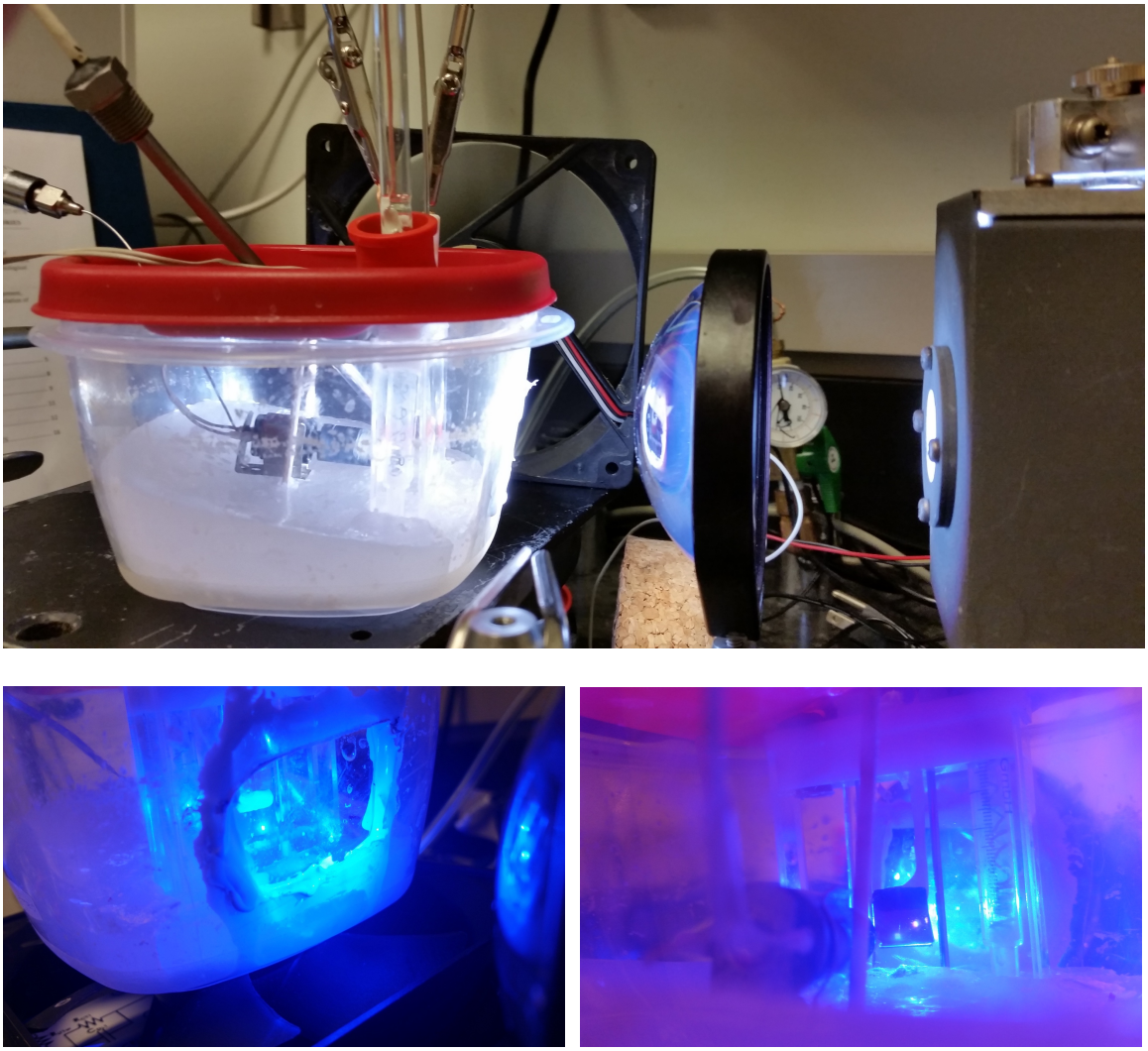

Figure 3.3 Homemade "argon box" for oxygen measurements to maintain an air-free atmosphere.

3.4 Results and Discussion

The POM-coated hematite using 3-aminopropyltrimethoxysilane (APS) silylating techniques applied in an earlier study[10] was characterized by ATR-FTIR, XPS, EDX and electrochemical techniques. The FTIR and XPS show the presence of **Ru_4Si_2** on the

hematite-APS surface in figure 1(a). The characteristic POM W-O stretches are present, albeit slightly shifted, between 876 and 945 cm^{-1}.

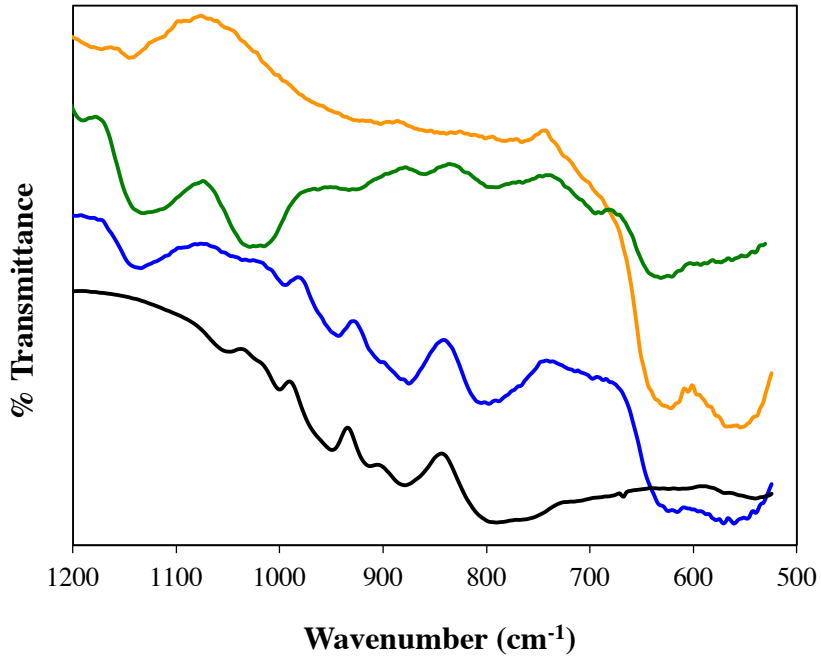

Figure 3.4 FTIR-ATR of hematite (orange), hematite with APS (green), hematite-APS-**Ru_4Si_2** (blue), and **Ru_4Si_2** on FTO (black).

The photocurrent density of POM-bound hematite was slightly enhanced compared to bare hematite photoanodes. Under long-term bulk electrolysis, the surface catalyst is susceptible to degradation and this enhancement is not sustained after multiple linear scans with the catalyst on the exterior surface of the electrode (figure 3.4(a)). For this reason, ALD of amorphous Al_2O_3 was added on the surface of the films as a protecting layer. Figure 3.4(b) shows the stabilization after 3 hours of bulk electrolysis compared to hematite-**Ru_4Si_2** films with no ALD protection.

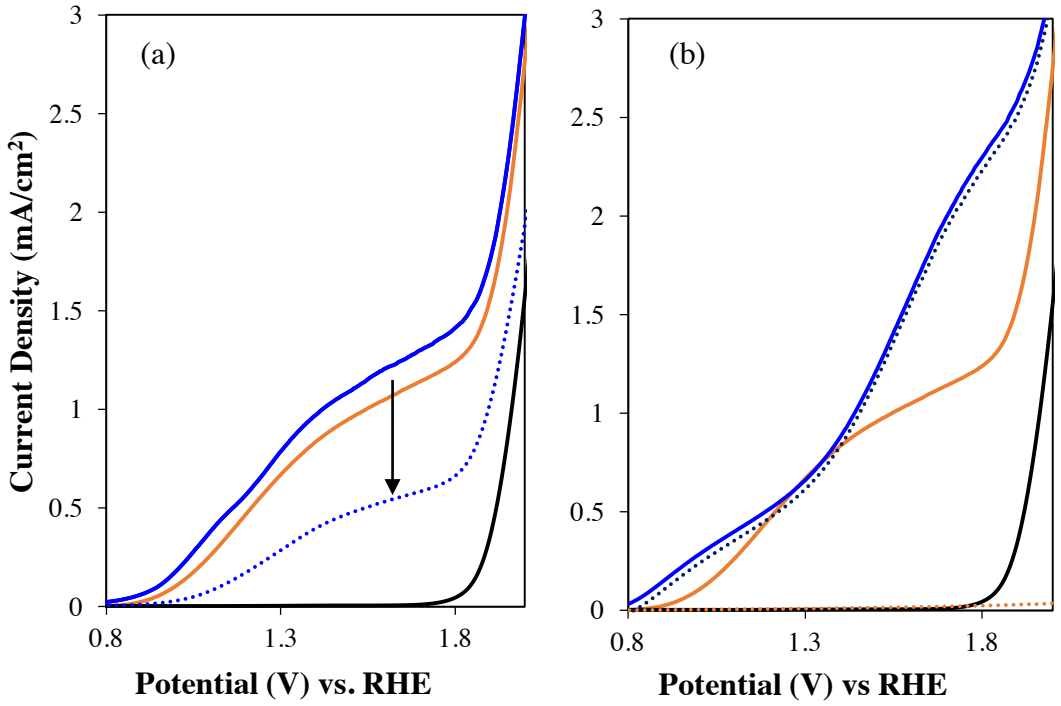

Figure 3.5 Linear scan voltammetry, in mA/cm^2, of photoanodes in the dark (black line) and under white light illumination (Xe light source, 160 mW/cm^2) of (a) hematite (orange line), hematite-APS-**Ru_4Si_2** before (solid blue line) and after 3 hour bulk electrolysis (dotted blue line). (b) hematite (solid orange line), hematite-1nm ALD (dotted orange line), hematite-APS-**Ru_4Si_2**-4nm ALD before (solid blue line) and after 3 hour bulk electrolysis (dotted blue line). Conditions: 0.1 M KNO_3, 240 mM sodium borate buffer, pH 8.3.

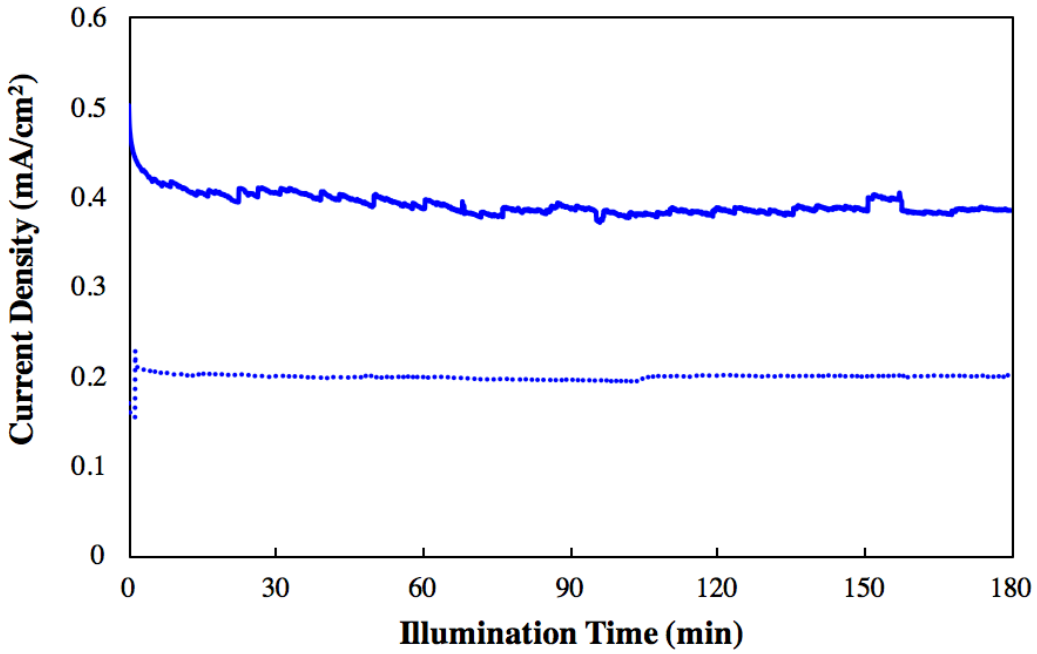

Figure 3.6 3 hour bulk electrolysis stability experiments for hematite-APS-**Ru_4Si_2**-4nm ALD (solid blue line) and hematite-APS-**Ru_4Si_2** with no ALD (dotted blue line). Conditions: 0.1 M KNO_3, 240 mM sodium borate buffer, pH 8.3, potential held at 1.24 V vs. RHE.

UV/vis spectra in figure 3.6 show a negligible change in absorbance when **Ru_4Si_2** is bound to the surface of hematite; therefore, a difference in light absorbance is not the cause of the enhanced photocurrent density. Using 1-6 nm thickness of Al_2O_3 ALD ensures an optically transparent protective surface.

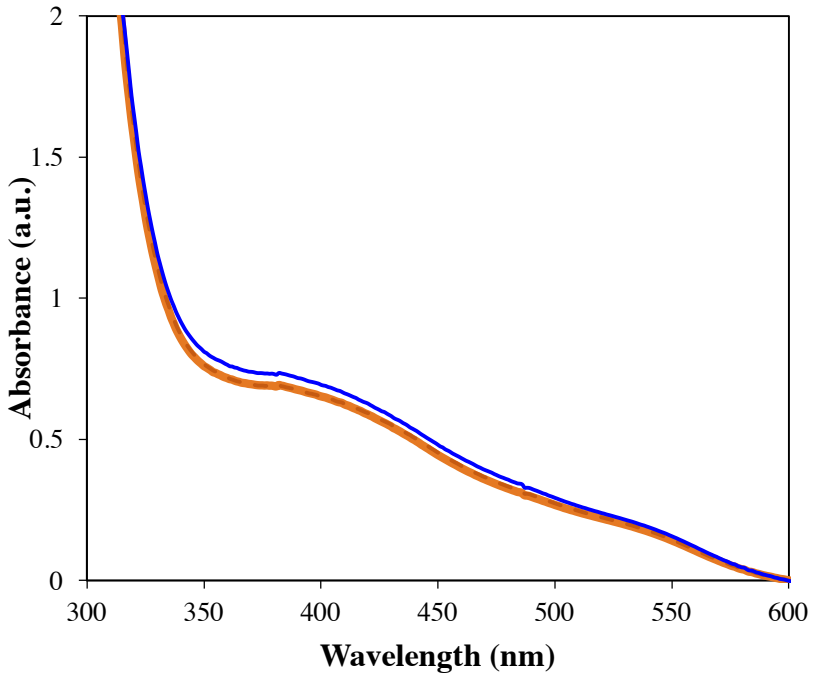

Figure 3.7 UV-visible spectra of hematite, preannealed (orange), and hematite after annealing at 650 C (dashed red line) and immobilized hematite-**Ru_4Si_2** (blue line), normalized at 700 nm.

It has already been shown that more layers of Al_2O_3 ALD on hematite films results in passivation of the photoanode and destroys the photocurrent density.[28] This decrease in photocurrent is described to be related to the elevated disorder in the amorphous Al_2O_3 ALD on the surface of hematite, preventing hole injection between the hematite surface and electrolyte. Le Formal et al., fixed this recombination hurdle by annealing the films at 300 or 400 °C, resulting in regeneration of hematite's photocurrent densities.

We have confirmed this phenomenon (figure 3.7), but have discovered throughout this process that the Al_2O_3 over layers protecting the surface-bound catalyst does not result in the same extreme passivation of hematite. Instead, the Al_2O_3 serves as a protecting layer

over the catalyst that results in an increased and sustained photocurrent density during long-term bulk electrolysis (figure 3.8).

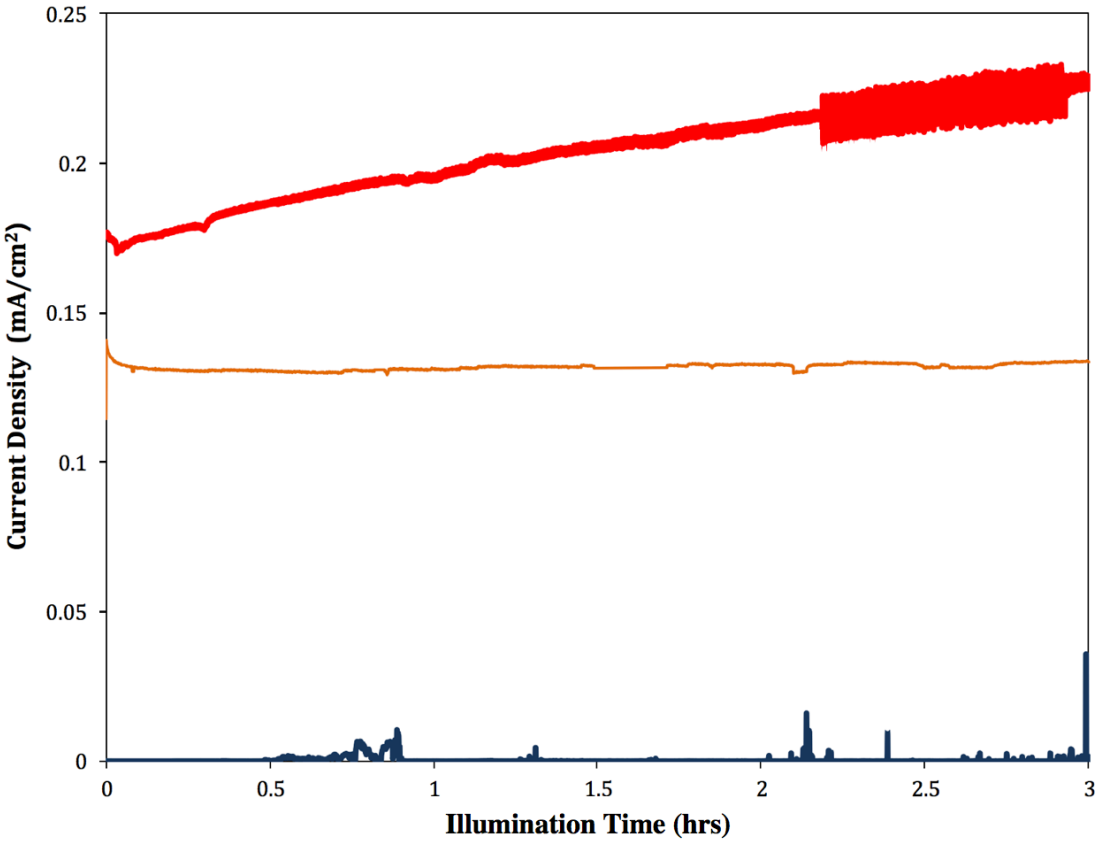

Figure 3.8 3 hour bulk electrolysis of hematite (orange line), hematite-4nm ALD (black line), and hematite-4nm ALD, annealed at 300 °C (red line). Conditions: 0.1 M KNO_3, 240 mM sodium borate buffer, pH 8.3, visible light illumination, Xe light source, 160 mW/cm^2, applied potential 1.24 V vs. RHE.

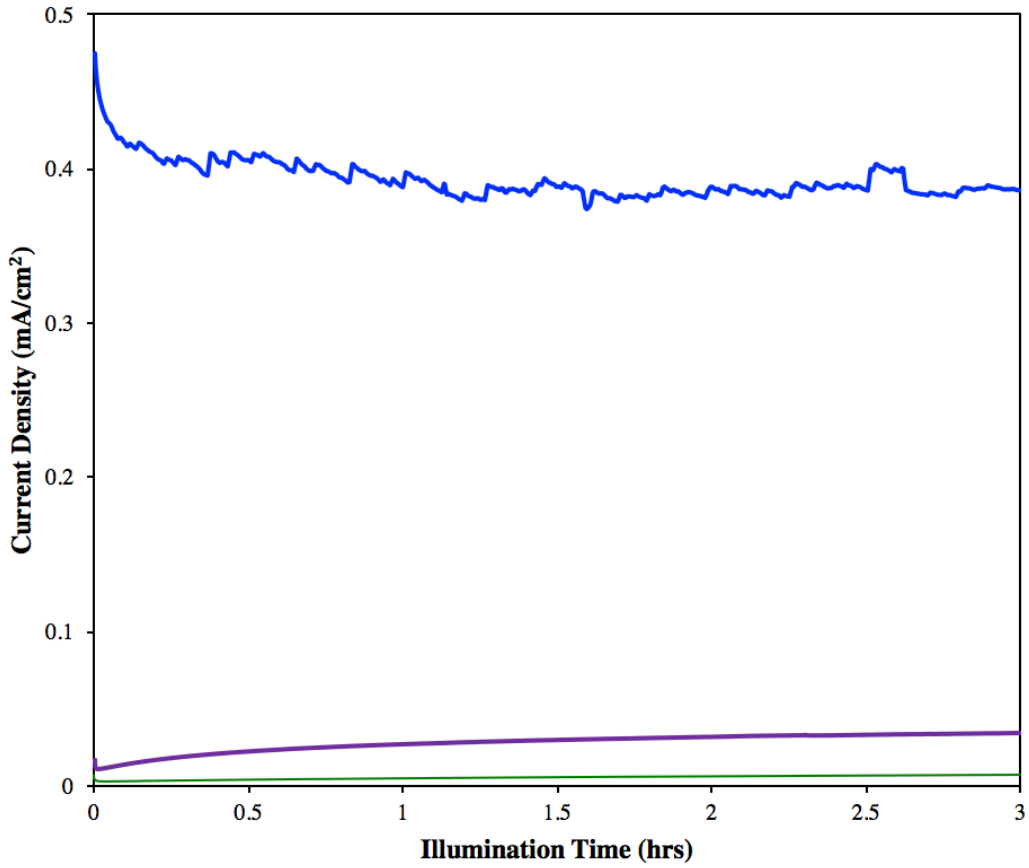

Figure 3.9 3 hour bulk electrolysis measurements of hematite-**Ru_4Si_2**-4nm ALD (blue line), hematite-**Ru_4Si_2**-6.5nm ALD (green line), and hematite-**Ru_4Si_2**-4nm ALD annealed at 300 °C/RuO_x (purple line). Conditions: 0.1 M KNO_3, 240 mM sodium borate buffer, pH 8.3, visible light illumination, Xe light source, 160 mW/cm^2, applied potential 1.24 V vs. RHE.

Longer-term bulk electrolysis experiments help assess the stability of the hematite-APS-**Ru_4Si_2**-ALD system. Figure 3.9 shows 8 hour stability measurements under white light illumination.

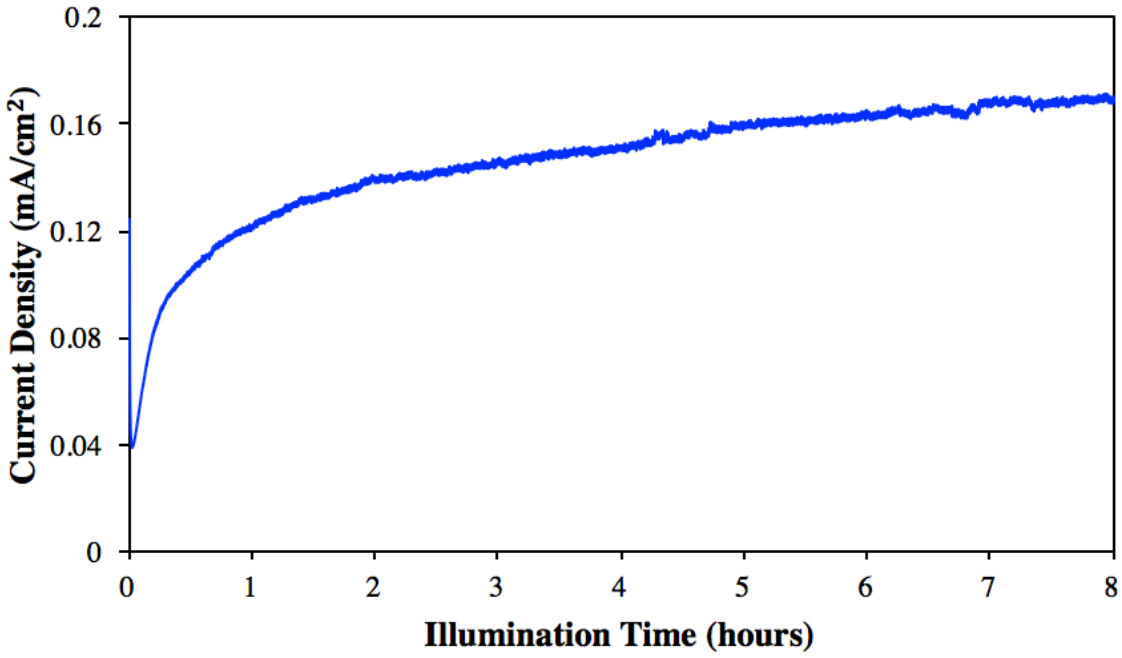

Figure 3.10 Long term bulk electrolysis of hematite-APS-$\mathbf{Ru_4Si_2}$-4nm ALD. Conditions: 0.1 M KNO_3, 240 mM sodium borate buffer, pH 8.3, visible light illumination, Xe light source, 160 mW/cm^2, applied potential 1.24 V vs. RHE.

The elemental analysis for hematite-$\mathbf{Ru_4Si_2}$ with varying depths of Al_2O_3 ALD over layers is shown in table 3.1. Although silicon is present in the glass of the FTO, the APS silylating agent on the surface of hematite, and the heteroatom of the POM there is a trend of increased Si as more protecting layers of ALD are applied. More importantly, the presence of $\mathbf{Ru_4Si_2W_{20}}$ is only still present when 4 nm of ALD had been administered, regardless of the length of photoelectrochemical experiments. Furthermore, the ratio of W:R in these films after bulk electrolysis remains ~5:1, as would be expected for the $\mathbf{Ru_4Si_2W_{20}}$ POM structure.

Table 3.1 Elemental composition of films of varying Al_2O_3 ALD depth measured by SEM/EDX.

	After 3 Hours Photoelectrochemistry					After 12 Hrs
ELEMENT	**0 nm**	**1 nm**	**2 nm**	**3 nm**	**4 nm**	**4 nm**
Fe	9.20	10.11	8.92	7.42	8.60	8.75
Si	0.86	0.68	0.84	0.98	0.96	1.15
W	0	0	0	0	0.71	0.30
Ru	0	0	0	0	0.14	0.06
Al	0	0.04	0.09	0.30	0.34	0.36
***Note elements O, Sn, C, and the POM counter ions have been omitted for clarity**						

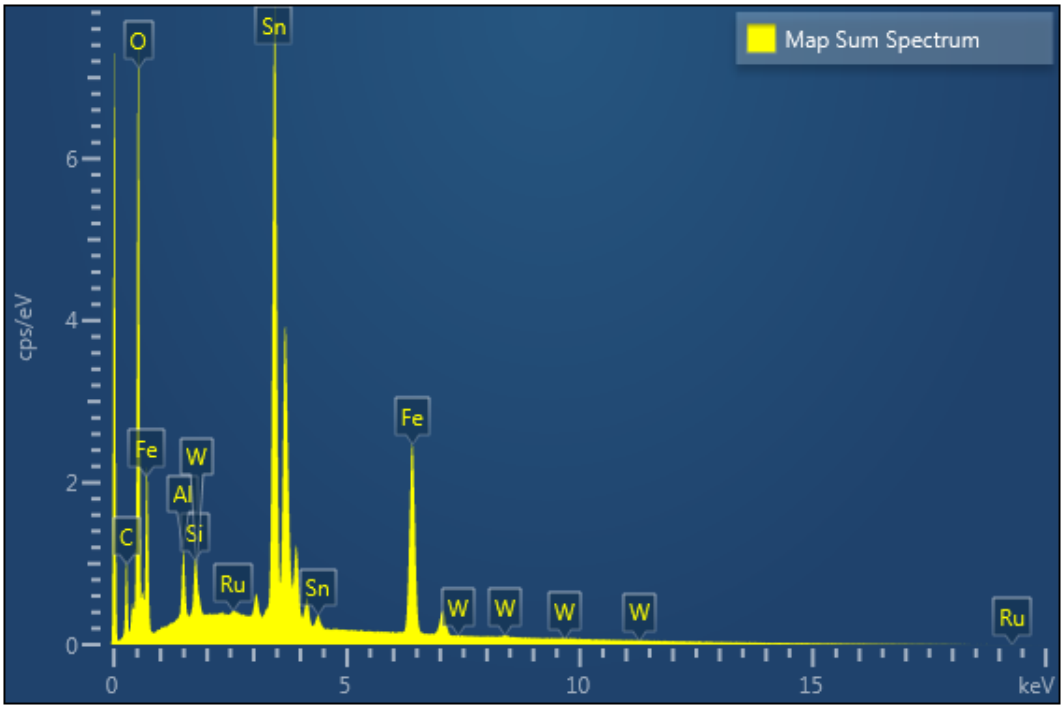

Figure 3.11 EDX spectra of hematite-APS-$\mathbf{Ru_4Si_2}$-4nm ALD.

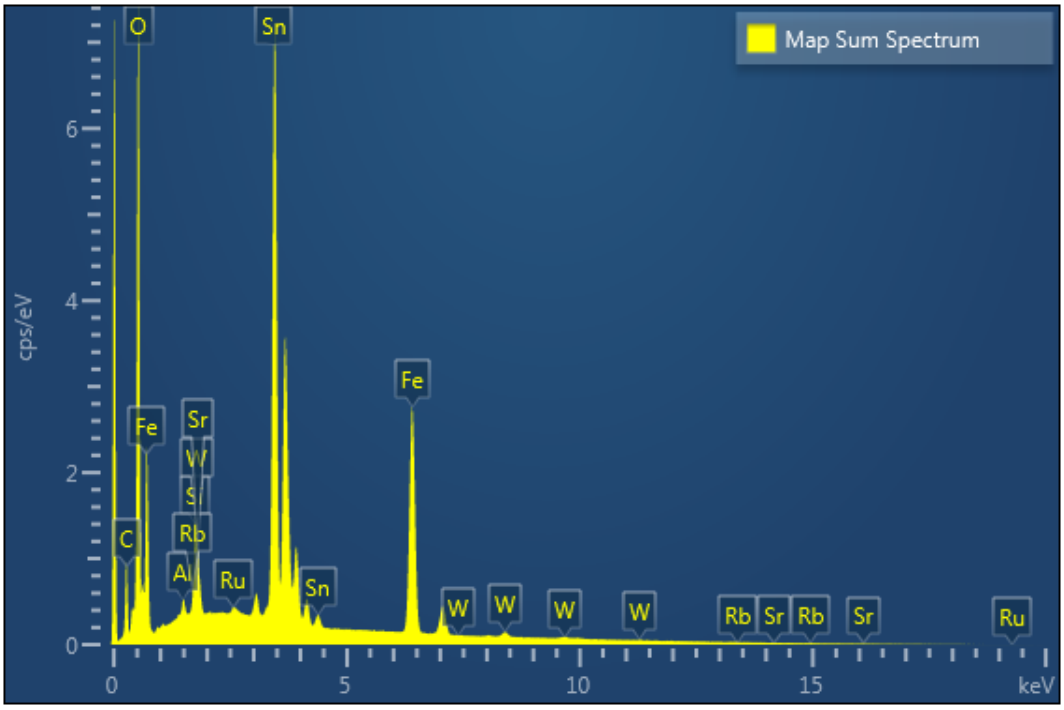

Figure 3.12 EDX spectra of hematite-APS-**Ru_4Si_2**-4nm ALD after 12 hours bulk photoelectrolysis.

In the XPS spectra in figure 3.13, the presence of Ru and W before and after 12 hour bulk photoelectrolysis further supports the catalyst loading and protection with ALD. The binding energies of Ru $3d^{5/2}$ peaks at 282 eV, and W $4f^{7/2}$ peak at 35.2 eV corresponds to Ru(IV) and W(VI), respectively, as expected. The Al 2p signal overlaps with the Ru 4s and W 5s peaks and may be too weak to be observed in XPS. While it is difficult to obtain quantitative elemental composition data with XPS, the relevant stoichiometry of W:Ru both before and after bulk photoelectrochemical reactions. Figure 3.11 indicates the presence of not only ruthenium and tungsten, but also that W:Ru maintains close to the expected 5:1 ratio after 12 hours. This is good evidence that **Ru_4Si_2** remains intact on the surface of hematite.

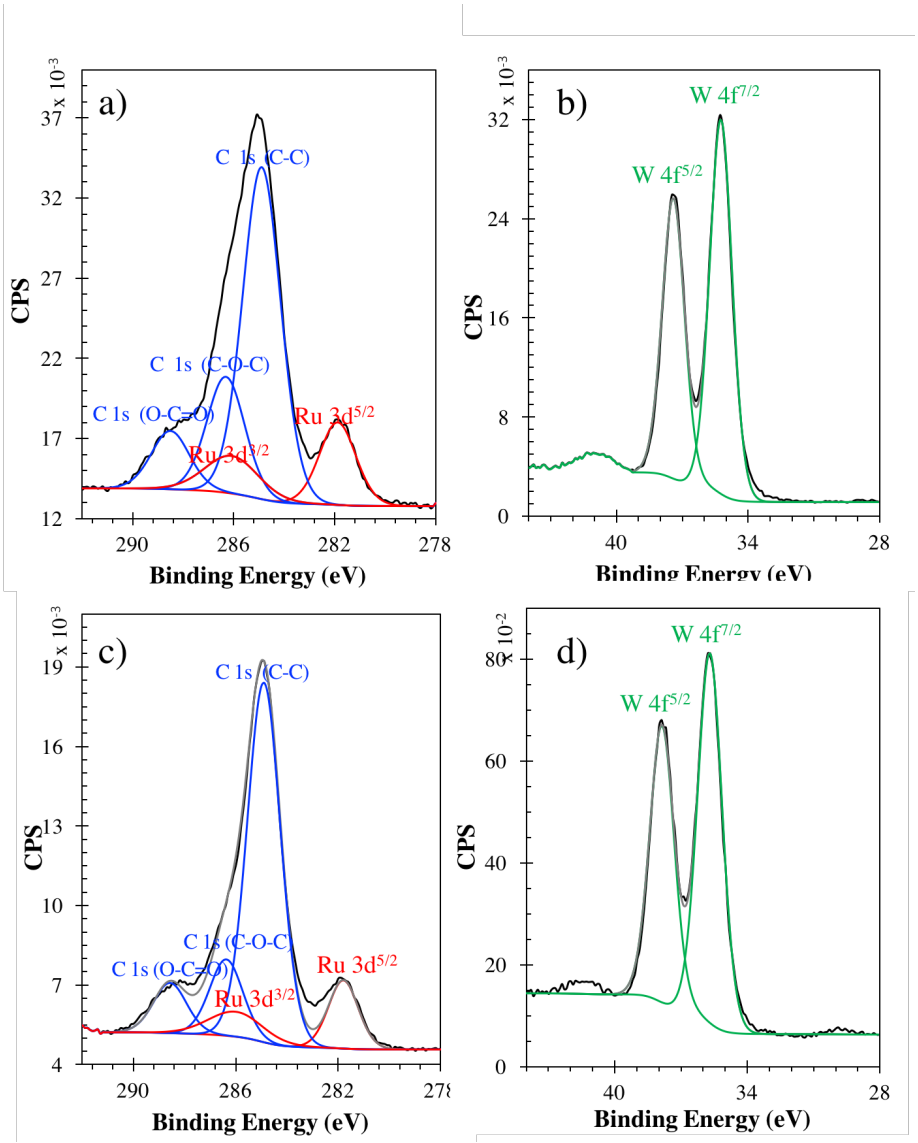

Figure 3.13 High resolution XPS spectra with fitted peaks of hematite-APS-**Ru_4Si_2**-4nm ALD of (a) Ru 3d and C 1s region and (b) W 4f before bulk photoelectrolysis; and (c) Ru 3d and C 1s region and (b) W 4f after bulk photoelectrolysis.

Oxygen measurements were collected for hematite films and hematite-**Ru_4Si_2**-4nm ALD. Figures 3.14 - 3.17 show the oxygen yield and the Faradaic yield based on the

current passed through the electrode. Under a biased potential and illumination, hematite electrodes generate an oxygen, but the Faradaic yield is not 100% as compared to the hematite-4nm ALD film (figure 3.13(b)). The high photocurrent density of the hematite with less than 100% Faradaic yields suggests electron recombination. In figure 3.14, the hematite-4nm ALD electrodes undergoes passivation of the surface due to Al_2O_3 results in no water oxidation occurring. This is not the case for hematite-**Ru_4Si_2**-4nm ALD. In the film with protected **Ru_4Si_2**, the Faradaic yield is 100% under 455nm LED and white light illumination. Table 3.2 lists the electrodes and the resulting oxygen yield and Faradaic efficiency under 455 nm LED illumination. More importantly, when there is 0 V vs RHE applied potential on the electrode, both bare hematite and hematite-APS-**Ru_4Si_2**-4nm ALD electrodes oxygen generation and Faradaic efficiency drop by almost half. But when comparing the oxygen generation of the two films with no biased potential, the hematite film's oxygen levels begin to plateau after the first hour, as shown in figure 3.15(c). Bare hematite can no longer oxidize water due to the recombination of electrons on the surface.

Further oxygen measurement studies using a non-water oxidation catalyst sandwich-type POM, $[Zn_4(H_2O)_2(PW_9O_{34})_2]^{10-}$, **$Zn_4P_2$**, replaced the **$Ru_4Si_2$** on the hematite surface. In this system, the lack of oxygen generated shown in figure 3.17 supports the enhanced activity of the hematite-**Ru_4Si_2**-4nm ALD system.

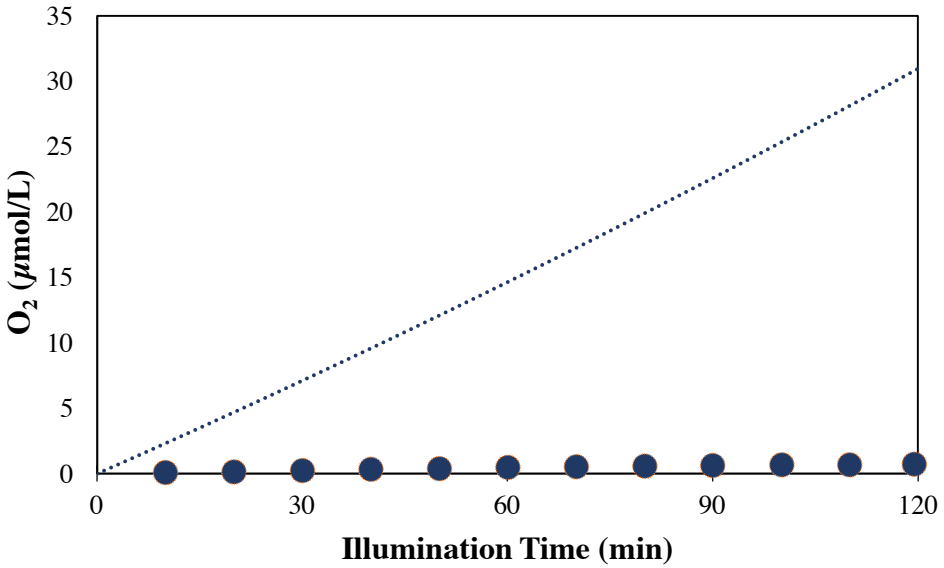

Figure 3.14 Oxygen measurements (circles) and Faradiac yield (dotted line) of hematite-4nm ALD under 455 nm LED (9.5 mW/cm^2). Conditions: 0.1 M KNO_3, 240 mM sodium borate buffer, pH 8.3, potential held at 1.24 V vs. RHE.

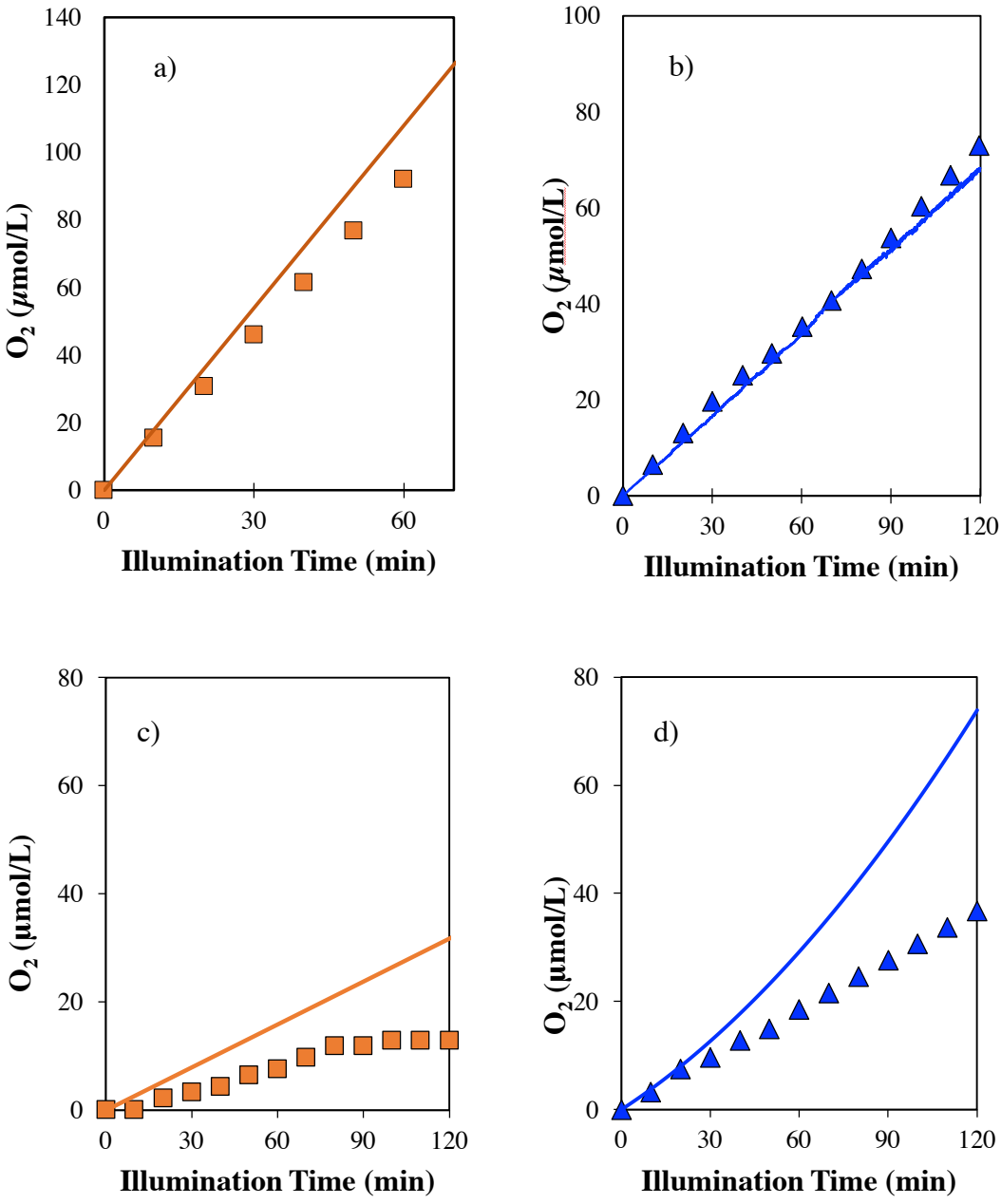

Figure 3.15 Oxygen measurements (markers) and Faradiac yield (lines) of (a) hematite (orange), 1.24 V vs RHE applied potential and (b) hematite-APS-**Ru_4Si_2**-4nm ALD (blue) 1.24 V vs RHE applied potential; (c) hematite (orange), 0 V vs. RHE applied potential and (d) hematite-APS-**Ru_4Si_2**-4nm ALD (blue), 0 V vs. RHE applied potential. Conditions: 0.1 M KNO_3, 240 mM sodium borate buffer, pH 8.3, 455 nm LED (9.5 mW/cm^2) illumination.

When using white light illumination from a Xenon light source, the Faradaic yield is near 100%, but when blocking the UV wavelengths with a 400nm cutoff filter, the power of the light source drops significantly and the Faradaic yield for oxygen is decreased as shown in Figure 3.16.

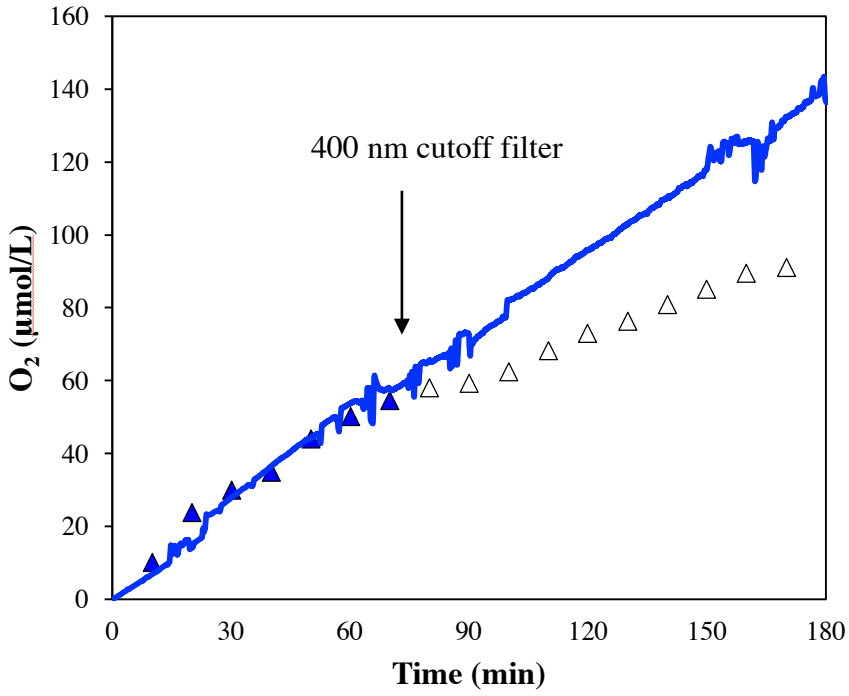

Figure 3.16 Oxygen measurements (triangles) and Faradiac yield (solid line) of hematite-**Ru_4Si_2**-4nm ALD under white light illumination. Arrow and open triangles represents oxygen measurements with visible light via the 400 nm cutoff filter. Conditions: 0.1 M KNO_3, 240 mM sodium borate buffer, pH 8.3, potential held at 1.24 V vs. RHE.

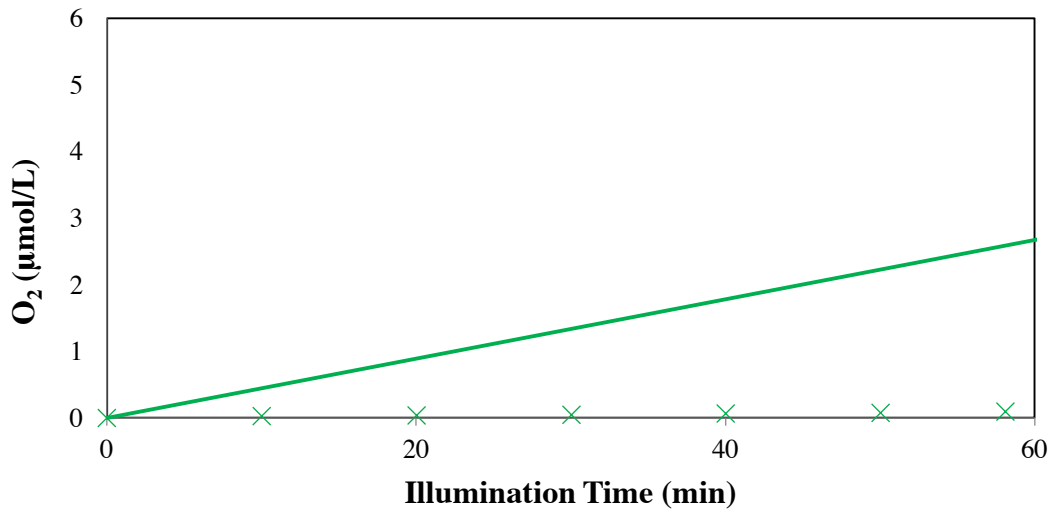

Figure 3.17 Oxygen measurements (markers) and Faradiac yield (solid line) of hematite-**Zn_4P_2**-4nm ALD under 455 nm LED (9.5 mW/cm^2). Conditions: 0.1 M KNO_3, 240 mM sodium borate buffer, pH 8.3, potential held at 1.24 V vs. RHE.

Table 3.2 Oxygen yield and Faradaic efficiency of electrodes after 2 hours of 455 nm LED illumination under 0 V and 1.24 V applied potential.

Electrode	**Applied Potential**	**Moles O_2 (µmol)**	**Faradaic Efficiency**
Hematite	0 V	12.85	43.9%
	1.24 V	107.37	84.8%
Hematite-APS-**Ru_4Si_2**-4nm ALD	0 V	36.76	49.8%
	1.24 V	70.02	99.9%
Hematite-APS-**Ru_4Si_2**-no ALD	1.24 V	0.54	7.7%
Hematite-4nm ALD	1.24 V	0.74	2.4%
Hematite-APS-**Zn_4P_2**-4nm ALD	1.24 V	0.18	3.4%

3.5 Conclusion

Catalyst immobilization is a significant new area of water oxidation research in context with solar fuels. Using a visible-light-absorbing hematite support facilitates water oxidation without the need of an attached, adjacent chromophore. Fast and selective polyoxometalate water oxidation catalysts are stabilized and protected by 4 nm of Al_2O_3 ALD while still capable of efficient water oxidation. Although the activity of this system is lower than many other immobilized water oxidation species,[12] when the most efficient homogenous catalysts are deposited on efficient light absorbers, the most efficient photoelectrodes are not always the result.[29] The concept of protecting efficient water oxidation catalysts on light-absorbing supports using ALD has proven to be effective in this system. In future work, the protection of a more active POM WOC may result in a more attractive system for water splitting.

3.6 References

1. Guo, S.-X.; Liu, Y.; Lee, C.-Y.; Bond, A. M.; Zhang, J.; Geletii, Y. V.; Hill, C. L., Graphene-supported [{$Ru_4O_4(OH)_2(H_2O)_4$}([gamma]-$SiW1_0O_{36})_2$]$^{10-}$ for highly efficient electrocatalytic water oxidation. *Energy Environ. Sci.* **2013,** *6* (9), 2654-2663.

2. Soriano-López, J.; Goberna-Ferrón, S.; Vigara, L.; Carbó, J. J.; Poblet, J. M.; Galán-Mascarós, J. R., Cobalt Polyoxometalates as Heterogeneous Water Oxidation Catalysts. *Inorg. Chem.* **2013,** *52* (9), 4753-4755.

3. Toma, F. M.; Sartorel, A.; Iurlo, M.; Carraro, M.; Parisse, P.; Maccato, C.; Rapino, S.; Gonzalez, B. R.; Amenitsch, H.; Ros, T. D.; Casalis, L.; Goldoni, A.; Marcaccio, M.; Scorrano, G.; Scoles, G.; Paolucci, F.; Prato, M.; Bonchio, M., Efficient

water oxidation at carbon nanotube–polyoxometalate electrocatalytic interfaces. *Nat. Chem.* **2010,** *2*, 826-831.

4. Xing, X.; Wang, M.; Liu, R.; Zhang, S.; Zhangc, K.; Li, B.; Zhang, G., Highly efficient electrochemically driven water oxidation by graphene-supported mixed-valent Mn_{16}-containing polyoxometalate. *Green Energy & Environ.* **2016**, Available online 19 April 2016.

5. Quintana, M.; Lopez, A. M.; Rapino, S.; Toma, F. M.; Iurlo, M.; Carraro, M.; Sartorel, A.; Maccato, C.; Ke, X.; Bittencourt, C.; Ros, T. D.; Tendeloo, G. V.; Marcaccio, M.; Paolucci, F.; Prato, M.; Bonchio, M., Knitting the Catalytic Pattern of Artificial Photosynthesis to a Hybrid Graphene Nanotexture. *ACS Nano* **2012,** *7*, 811-817.

6. Wu, J.; Liao, L.; Yan, W.; Xue, Y.; Sun, Y.; Yan, X.; Chen, Y.; Xie, Y., Polyoxometalates Immobilized in Ordered Mesoporous Carbon Nitride as Highly Efficient Water Oxidation Catalysts. *ChemSusChem* **2012,** *5* (7), 1207-1212.

7. Anwar, N.; Sartorel, A.; Yaqub, M.; Wearen, K.; Laffir, F.; Armstrong, G.; Dickinson, C.; Bonchio, M.; McCormac, T., Surface Immobilization of a Tetra-Ruthenium Substituted Polyoxometalate Water Oxidation Catalyst Through the Employment of Conducting Polypyrrole and the Layer-by-Layer (LBL) Technique. *ACS Appl. Mater. & Interfaces* **2014,** *6*, 8022-8031.

8. Toma, F. M.; Sartorel, A.; Iurlo, M.; Carraro, M.; Rapino, S.; Hoober-Burkhardt, L.; Ros, T. D.; Marcaccio, M.; Scorrano, G.; Paolucci, F.; Bonchio, M.; Prato, M., Tailored Functionalization of Carbon Nanotubes for Electrocatalytic Water Splitting and Sustainable Energy Applications

. *ChemSusChem* **2011,** *4*, 1447-1451.

9. Xiang, X.; Fielden, J.; Rodríguez-Córdoba, W.; Huang, Z.; Zhang, N.; Luo, Z.; Musaev, D. G.; Lian, T.; Hill, C. L., Electron Transfer Dynamics in Semiconductor–Chromophore–Polyoxometalate Catalyst Photoanodes. *J. Phys. Chem. C* **2013,** *117* (2), 918-926.

10. Lauinger, S. M.; Sumliner, J. M.; Yin, Q.; Xu, Z.; Liang, G.; Glass, E. N.; Lian, T.; Hill, C. L., High Stability of Immobilized Polyoxometalates on TiO_2 Nanoparticles and Nanoporous Films for Robust, Light-Induced Water Oxidation. *Chem. Mater.* **2015,** *27* (17), 5886-5891.

11. Fielden, J.; Sumliner, J. M.; Han, N.; Geletii, Y. V.; Xiang, X.; Musaev, D. G.; Lian, T.; Hill, C. L., Water Splitting with Polyoxometalate-Treated Photoanodes: Enhancing Performance through Sensitizer Design. *Chem. Sci.* **2015,** *6*, 5531-5543.

12. Li, W.; Sheehan, S. W.; He, D.; He, Y.; Yao, X.; Grimm, R. L.; Brudvig, G. W.; Wang, D., Hematite-Based Solar Water Splitting in Acidic Solutions: Functionalization by Mono- and Multilayers of Iridium Oxygen-Evolution Catalysts. *Angewandte Chemie International Edition* **2015,** *54* (39), 11428-11432.

13. Palmstrom, A. F.; Santra, P. K.; Bent, S. F., Atomic layer deposition in nanostructured photovoltaics: tuning optical, electronic and surface properties. *Nanoscale* **2015,** *7* (29), 12266-12283.

14. Johnson, R. W.; Hultqvist, A.; Bent, S. F., A brief review of atomic layer deposition: from fundamentals to applications. *Materials Today* **2014,** *17* (5), 236-246.

15. Bakke, J. R.; Pickrahn, K. L.; Brennan, T. P.; Bent, S. F., Nanoengineering and interfacial engineering of photovoltaics by atomic layer deposition. *Nanoscale* **2011,** *3* (9), 3482-3508.

16. Vannucci, A. K.; Alibabaei, L.; Losego, M. D.; Concepcion, J. J.; Kalanyan, B.; Parsons, G. N.; Meyer, T. J., Crossing the divide between homogeneous and heterogeneous catalysis in water oxidation. *Proceedings of the National Academy of Sciences* **2013,** *110* (52), 20918-20922.

17. Hu, S.; Shaner, M. R.; Beardslee, J. A.; Lichterman, M.; Brunschwig, B. S.; Lewis, N. S., Amorphous TiO_2 coatings stabilize Si, GaAs, and GaP photoanodes for efficient water oxidation. *Science* **2014,** *344* (6187), 1005-1009.

18. Yang, J.; Walczak, K.; Anzenberg, E.; Toma, F. M.; Yuan, G.; Beeman, J.; Schwartzberg, A.; Lin, Y.; Hettick, M.; Javey, A.; Ager, J. W.; Yano, J.; Frei, H.; Sharp, I. D., Efficient and Sustained Photoelectrochemical Water Oxidation by Cobalt Oxide/Silicon Photoanodes with Nanotextured Interfaces. *J. Am. Chem. Soc.* **2014,** *136*, 6191-6194.

19. Lichterman, M. F.; Shaner, M. R.; Handler, S. G.; Brunschwig, B. S.; Gray, H. B.; Lewis, N. S.; Spurgeon, J. M., Enhanced stability and activity for water oxidation in alkaline media with bismuth vanadate photoelectrodes modified with a cobalt oxide catalytic layer produced by atomic layer deposition. *J. Phys. Chem. Lett.* **2013,** *4* (23), 4188-4191.

20. McDowell, M. T.; Lichterman, M. F.; Spurgeon, J. M.; Hu, S.; Sharp, I. D.; Brunschwig, B. S.; Lewis, N. S., Improved Stability of Polycrystalline Bismuth Vanadate

Photoanodes by Use of Dual-Layer Thin TiO_2/Ni Coatings. *J. Phys Chem. C* **2014,** *118* (34), 19618-19624.

21. Strandwitz, N. C.; Comstock, D. J.; Grimm, R. L.; Nichols-Nielander, A. C.; Elam, J.; Lewis, N. S., Photoelectrochemical Behavior of n-type Si(100) Electrodes Coated with Thin Films of Manganese Oxide Grown by Atomic Layer Deposition. *The Journal of Physical Chemistry C* **2013,** *117* (10), 4931-4936.

22. Lichterman, M. F.; Carim, A. I.; McDowell, M. T.; Hu, S.; Gray, H. B.; Brunschwig, B. S.; Lewis, N. S., Stabilization of n-cadmium telluride photoanodes for water oxidation to O_2(g) in aqueous alkaline electrolytes using amorphous TiO2 films formed by atomic-layer deposition. *Energy Environ. Sci* **2014,** *7*, 3334-3337.

23. Shaner, M. R.; Hu, S.; Sun, K.; Lewis, N. S., Stabilization of Si microwire arrays for solar-driven H_2O oxidation to O_2(g) in 1.0 M KOH(aq) using conformal coatings of amorphous TiO_2. *Energy & Environ. Sci.* **2015,** *8* (1), 203-207.

24. Zhong, M.; Hisatomi, T.; Kuang, Y.; Zhao, J.; Liu, M.; Iwase, A.; Jia, Q.; Nishiyama, H.; Minegishi, T.; Nakabayashi, M.; Shibata, N.; Niishiro, R.; Katayama, C.; Shibano, H.; Katayama, M.; Kudo, A.; Yamada, T.; Domen, K., Surface Modification of CoOx Loaded BiVO4 Photoanodes with Ultrathin p-Type NiO Layers for Improved Solar Water Oxidation. *Journal of the American Chemical Society* **2015,** *137* (15), 5053-5060.

25. Li, C.; Wang, T.; Luo, Z.; Zhang, D.; Gong, J., Transparent ALD-grown Ta2O5 protective layer for highly stable ZnO photoelectrode in solar water splitting. *Chemical Communications* **2015,** *51* (34), 7290-7293.

26. Lapides, A. M.; Sherman, B. D.; Brennaman, M. K.; Dares, C. J.; Skinner, K. R.; Templeton, J. L.; Meyer, T. J., Synthesis, characterization, and water oxidation by a molecular chromophore-catalyst assembly prepared by atomic layer deposition. The "mummy" strategy. *Chemical Science* **2015,** *6* (11), 6398-6406.

27. Geletii, Y. V.; Botar, B.; Kögerler, P.; Hillesheim, D. A.; Musaev, D. G.; Hill, C. L., An All-Inorganic, Stable, and Highly Active Tetraruthenium Homogeneous Catalyst for Water Oxidation. Selected as the VIP Article by the reviewers and editor. *Angew. Chem. Int. Ed.* **2008,** *47*, 3896-3899.

28. Le Formal, F.; Tetreault, N.; Cornuz, M.; Moehl, T.; Gratzel, M.; Sivula, K., Passivating surface states on water splitting hematite photoanodes with alumina overlayers. *Chemical Science* **2011,** *2* (4), 737-743.

29. McKone, J. R.; Lewis, N. S.; Gray, H. B., Will Solar-Driven Water-Splitting Devices See the Light of Day? *Chem. Mater.* **2014,** *26*, 407-414.

IMMOBILIZATION METHODS FOR BINDING POLYOXOMETALATES ONTO SURFACES FOR WATER SPLITTING APPLICATIONS

CHAPTER 4

Stability Assessment of Water Oxidation Catalysts and Conclusions

Published in part in: Lauinger S. M., Yin, Q., Geletii, Y. V., Hill, C. L. "Polyoxometalate Multi-Electron Catalysts in Solar Fuel Production" *Advances in Inorganic Chemistry*. **2017**, 69, 117-154.

As a main contributor of this work; with Yimu Hu, Elliot N. Glass, Kevin P. Sullivan, Marika Wieliczko, Mooeung Kim, Yurii Gelettii, and Craig L. Hill*. S. Lauinger designed and collected the catalytic experiments, light-driven oxygen measurements, and SEM and EDX measurements. E. Glass, Yimu Hu, and M. Wieliczko contributed the syntheses and FTIR characterization. Foxy Probe O_2 measurements collected by Quishi Yin. K. Sullivan performed the V^{51} NMR, M. Kim and Y. Geletii measured the stopped-flow kinetics.

4.1 Abstract

Polyoxometalate (POM) water oxidation catalysts (WOCs) have been examined for several years as the mechanism for POM-catalyzed water oxidation remains unclear in most cases. Stability of these catalysts is not straightforward, and new techniques and experimentation have been developed to better understand POM WOC functioning under turnover conditions. To date there has not been much early-reaction-time kinetics and quantification of generated oxygen due to lack of experimental design and instrumentation. In the artificial light-driven water oxidation systems, the photosensitizer component is one of the limiting and challenging factors for efficient water oxidation and catalyst stability assessment. Thus, the use of light-absorbing electrodes as substrates for POM WOCs has been investigated in other studies to circumvent the inherent decomposition that happens with these photosensitizer compounds.

4.2 Introduction

The stability of WOCs has long been a critical issue for the development of both practical and model water splitting systems.[1-9] For traditional heterogeneous WOCs, these issues often present as stability against corrosion under certain water oxidation conditions.[10-11] Under different conditions of pH, applied potential, and chemical environments, solid-state catalysts may well dissolve into solution. At the time of writing this chapter, one of the holy grails for WOCs is the discovery of an acid-compatible earth-abundant-element WOC.[8-10]

Similar concerns about stability also apply for molecular WOCs.[3-7, 12] For such catalysts, however, one is much more concerned with the stability of the organic ligands

that support the transition metal active sites. Organic and organometallic ligands as well as organic substituents are susceptible to both hydrolytic and oxidative degradation.[4-5, 7] Unfortunately the lack of organic ligand stability not only limits the turnover number (TON) but less appreciated is that oxidative removal of organic ligands can facilitate formation of the metal oxide (e.g. RuO_2 and CoO_x for WOCs based on those metals), and these metal oxides are also known WOCs.

The development of POMs as WOCs potentially overcomes these traditional shortcomings of coordination compound or organometallic WOCs. POM WOCs such as **Co_4P_2** comprise fully oxidized (d^0) metal oxide polyanions functioning as multi-dentate ligands for one or more d-electron transition metals involved in the multi-electron redox processes (e.g. oxidation of H_2O to O_2). Thus, such POMs are stable to oxidative degradation. POMs are soluble and experimentally similar to metal oxides. At the same time, these discrete cluster anions are distinct from transition metal oxides as they bear high charges that are electrostatically compensated by high numbers of counter cations.

The extensive use of crystallization to obtain pure single crystalline structures of POMs may further exacerbate the misconception that POMs are simply "soluble transition metal oxides": in aqueous solution, equilibria of numerous polyanionic metal oxide and/or metal hydroxides are frequently operable.[13-14] The synthetic steps taken to produce different POMs usually involve shifting the chemical equilibrium via adjustments in pH, temperature, chemical potential and counter-cations. Historically, many POM systems are famously challenging to characterize due to their complexity. As many as 40 different species may be present in a single equilibrium model.[13-14] Thus, it is not surprising that certain crystalline POM species may revert back to equilibrium species upon dissolution,

especially since some POM equilibrations may be slower than POM catalyst syntheses in aqueous solution themselves.

Most of the POM WOCs listed in Table 1.1 have not been adequately characterized with respect to the easily overlooked factors noted above: pH, solution potential, and other ionic species present. The likely existence of different pK_a values for some of these POMs alone should give us pause in identifying the "active species" in a POM WOC system. While we have developed a preliminary Pourbaix diagram for the $\mathbf{Ru_4Si_2}$ system, this type of information is rarely found in the POM literature.[15] There have been recent efforts to construct such diagrams even for well-known electrocatalysts such as CoO_x.[16] Given the lack of detailed study on the speciation of POM WOCs, questions must be raised about what one means when stating that certain POMs are WOCs. It is not unreasonable to think that different solution phase species including different protonation states, oxidation states, and possible dimer variants of these POMs may be the principal "active species" instead of the crystalline starting material.

More precisely, we take "thermodynamic stability" of these POMs to mean that solubilizing these POMs does not lead to significant decomposition of the overall polyanionic structure within the timeframe of the water oxidation reactions under study. At the very least, Table 1 gives a list of metastable species that have been shown to be active in water oxidation reactions under turnover conditions. It is now appropriate to reflect upon the last few decades of POM chemistry and realize that while our understanding of POM self-assembly and equilibration has come a long way since the seminal studies on the H-Mo-V-P systems,[13, 17-19] there is still much that we do not know about the speciation of POMs in solution.

The oxidative stability of POM WOCs relate to their stability under catalytic turnover conditions. Due to the oxidatively robust nature of the POM framework itself, the most likely decomposition pathway available to most homogeneous POM WOC systems is the leaching of the redox-active transition metal ions directly into the solution, forming metal-aqua, metal hydroxide, and/or metal oxide species. However, under various conditions, all four forms of metal-oxo species can be converted into each other and may, at times, exist in equilibrium.[20] This makes stability analyses of POM WOC systems particularly daunting and identification of the principal "active species" ambiguous.

A prime example of such a case lies in the scrutiny of the $\mathbf{Co_4P_2}$ and $\mathbf{Co_4V_2}$ system. Stracke et el. demonstrated that $\mathbf{Co_4P_2}$ does indeed decompose to form cobalt oxide films on the working electrode under electrocatalytic conditions, experimental conditions that were not used in the original paper.[21] Given the extensive number of cobalt complexes that may serve as precursors for the electrodeposition of cobalt oxide under potentiostatic or voltage cycling conditions,[22] it is reasonable to believe that a similar process may indeed take place when applied to $\mathbf{Co_4P_2}$. While the exact mechanism that leads to the oxidative instability of the $\mathbf{Co_4P_2}$ under electrocatalytic conditions is unknown, we may nevertheless speculate that under oxidative conditions, Co^{III} may rapidly exchange ligands. In the presence of an electrophilic electrode surface, Co^{III} could form Co-O-X bonds that eventually lead to the leaching of the cobalt ions and formation of a cobalt oxide film on the electrode surface. Alternatively, given the high potential of these electrochemical systems, an alternative potential decomposition pathway involves the oxidative breakdown of the tungstate framework via the formation of a peroxotungstate species leading to a

complete degradation of **Co_4P_2** with accompanying full release of hydrated freely-diffusing cobalt ions.

Ultimately, Vickers *et al*. demonstrated that the **Co_4P_2** model system is indeed the main WOC under homogeneous reaction conditions, showing that it is oxidatively stable when paired with a homogeneous oxidant and that the electrolytic decomposition of **Co_4P_2** at an electrode surface does not apply to the homogeneous reaction conditions reported initially.[23] This paper explains many criteria that can be used to distinguish between homogeneous and heterogeneous water oxidation catalysis and molecular WOCs in general (and POM WOCs in particular). A new protocol for the extraction of highly-negatively-charged POM WOCs using tetra-*n*-heptylammonium nitrate dissolved in toluene to identify the active species for water oxidation was also established that should now be used to examine the oxidative stability of all new and old POM WOCs in homogeneous systems.

The careful examination of **Co_4P_2** stability and inquiries into the question, "what is the main active species?" by multiple research groups culminated in several established techniques and procedures that are useful for the study of POM WOCs and molecular catalysts in general. In addition, recent advances in heterogenizing molecular WOCs on electrode surfaces provide protocols and criteria to assess the stability, rates, and molecular nature of immobilized WOCs.[24]

4.3 Experimental

4.3.1 General

All reagents were used as purchased. Copper(II) sulfate anhydrous ($CuSO_4$, > 99.99%), barium chloride dihydrate ($BaCl_2 \cdot 2H_2O$, > 99%), sodium hydroxide (NaOH, >

85%) and potassium hydroxide (KOH, >99.99%) were purchased from Sigma-Aldrich. Hydrous niobium oxide (Nb_2O_5) was acquired from Reference Metals Company Inc. All solutions were prepared using Milli-Q nanopure water (18.2 MΩ.cm resistivity) unless stated otherwise. $K_7HNb_6O_{19}\cdot 13H_2O$ was synthesized and purified according to a previous method.[25] FTO glass (Pilkington TEC15, ~15Ω/sq resistance) was purchased from Hartford Glass Company, Inc.

4.3.2 Instrumentation

All UV-Vis spectroscopy was performed with an Agilent 8453 spectrometer at room temperature using a quartz cell with a 1 cm pathlength. ^{51}V NMR was collected on an INOVA 500 (600 MHz) NMR. Each sample contained 5 mM V-containing compound in 10% D_2O/H_2O. NMR data collection averaged 512 scans with 0.5 relaxation delay with a pulse width of 10. Single crystal X-ray diffraction were collected at Emory University. Crystals selected were coated with Paratone N oil and suspended on a small fiber loop and dried on a nitrogen gas stream on a Bruker D8 APEX II CCD sealed tube diffractometer with a graphite monochromated MoKα radiation (0.71073 Å). The Fourier transform infrared spectroscopy (FTIR) spectra were recorded using 2% by weight KBr pellets in the range 4000–400 cm^{-1} on a Nicolet 6700 FT-IR spectrometer. Electrochemical experiments were conducted with a Pine WaveDriver 20 Bipotentiostat. For the base compatible POM WOC, a three-electrode system was equipped with a working electrode, a platinum wire counter electrode, and Ag/AgCl (1 M KCl) reference electrode (CH-Instruments) (0.235 vs. NHE) and cyclic voltammetry experiments were conducted in a one-compartment cell with 10 mL of electrolyte solution, while controlled

potential electrolysis measurements were conducted with a total of 15-20 mL of total electrolyte solution in a closed two-compartment anaerobic cell (30 mL total volume, each compartment separated by a Nafion film without *iR* compensation) that was purged with N_2 for at least 20 minutes prior to electrolysis. Glassy carbon (0.071 cm^2) disk electrode: Prior to the experiments, the glassy carbon electrode was polished with 0.05 μm Al_2O_3 slurry, followed by sonication in distilled water for ~30 seconds to remove debris and then were thoroughly rinsed with Milli-Q ultrapure water.Scanning electron microscopy and energy dispersive X-ray spectroscopy (SEM-EDX) data was conducted at the Clemson University Advanced Materials Center with three Hitachi transmission electron microscopes (STEM HD2000, TEM H7600T, and TEM 9500) and scanning electron microscopes (SEM 3400, SU-6600, and S4800) equipped with EDX.

4.3.3 Sacrificial oxidant kinetic measurements

Reaction kinetics were measured using a SF-61 stopped-flow instrument (Hi-Tech Scientific, U.K.). One syringe in the stopped-flow apparatus was filled with deaerated solutions of reduced POM and diluted with oxygen-free buffer solution. The second syringe was filled with Cu(II) in the same oxygen-rich buffer solution. In all stopped-flow kinetic measurements, the concentrations of the syringes were doubly concentrated to the desired final mixed solution concentration. The fittings of kinetic curves were performed using COPASI 4.13 (Build 87) software.

4.3.4 Light-driven water oxidation reactions

Reactions were carried out in a cylindrical cuvette containing 2 mL of liquid with a rubber stopper. A magnetic bar was stirred at a rate of 5000 RPM on the flat side of the cuvette. After purging the system of N_2 and O_2 using Ar gas, the solution was then exposed to light for the desired length of time. A 250-μL gas tight syringe replaced 100 μL Ar with 100 μL of headspace from the cuvette, of which 50 μL was injected into the GC. Calibrations of the cuvette for the moles of O_2 produced were conducted as described previously.[26] An Agilent 7890A gas chromatography (GC) system comprising a HP-MOLESIEVE capillary column (30m x 0.535 mm x 25.00 μm), thermal conductivity detector with Ar carrier gas was used to quantify O_2 before and during catalytic light-driven water oxidation experiments.

4.3.5 Synthesis of Co_4V_2

The Wu et al., synthesis of $[Co_4(H_2O)_2(VW_9O_{34})_2]^{10-}$•30 H_2O was described in published works.[27] V_2O_5 (1.5 mmol) was dissolved in a 1 M sodium acetate buffer, pH 4.8. The solution was heated to 70 ºC and 9 mmol of Na_2WO_4•$2H_2O$ and 2 mmol of $Co(NO_3)_2$•$6H_2O$ were added under gentle stirring for 40 minutes until dissolved. The solution was allowed to cool to room temperature. Note that in this synthesis, there is a 3:2:9 molar ratio of V:Co:W.

The Lv et al., synthesis of $[Co_4(H_2O)_2(VW_9O_{34})_2]$•$35H_2O$ was described in published works,[28] and adapted from the previously described method by Wu et al. $Co(NO_3)_2$*$6H_2O$ and Na_2WO_4•$2H_2O$ was dissolved in 0.5 M sodium acetate buffer, pH 4.8 and stirred prior to adding $NaVO_3$. The solution was heated to 80 ºC for 2 hours and then

allowed to cool to room temperature before filtering and precipitating. This synthesis method utilized a 5:2:9 molar ratio of V:Co:W.

4.3.6 Synthesis of $Co_2M_2P_2$ Complexes

The synthesis was adapted from the published method of $[M'_2M_2(PW_9O_{34})_2]^{12-}$ by Hou et al.[29] $Na_2WO_4 \bullet 2H_2O$ (76 mmol) and 8.5 mmol Na_2HPO_4 were dissolved in DI water. For $Na_2Co_2(PW_9O_{34})_2$, $Co(NO_3)_2 \bullet 6H_2O$ was added under stirring and the solution was adjusted to pH 7.5 using 6 M HCl at 90 ºC for one hour. After cooling, the product was crystallized out with 40 mmol KCl. For $Na_2Ni_2(PW_9O_{34})_2$, $Ni(NO_3)_2 \bullet 6H_2O$ was used in place of the $Co(NO_3)_2 \bullet 6H_2O$. For $Na_2Mn_2(PW_9O_{34})_2$ and $Na_2Zn_2(PW_9O_{34})_2$, 5.5 mmol of $Mn(CH_3COO)_2 \bullet 4H_2O$ and 5.5 mmol $Zn(NO_3)_2 \bullet 6H_2O$ was added to the solution in place of $Co(NO_3)_2 \bullet 6H_2O$, respectively. Each Na_2M_2 POM (M=Co, Ni, Mn, Zn) was added to 1.0 M $CoCl_2$ solution and gently stirred at 70 ºC until a red-purple solution formed. Ten equivalents of CsCl were dissolved in 1 mL of NPH_2O and then added dropwise to the POM solution until precipitation occurred. The mixture was allowed to cool to room temperature prior to filtering the purple powder. $[Co_2(H_2O)_2M_2(PW_9O_{34})_2]^{10-}$. FTIR-ATR: **$Co_2Co_2P_2$**, 1036 (s), 961 (w), 932 (m), 883 (w), 830 (v), 773 (w), 588 (m), 513 (m), 415.7 (s) cm^{-1}; **$Co_2Ni_2P_2$**, 1038.2 (s), 1021.4 (s), 961 (w), 944 (s), 910 (m), 887 (m), 835 (v), 737 (m), 592 (w), 508 (m), 411.8 (s) cm^{-1}; **$Co_2Zn_2P_2$**, 1035 (s), 959 (w), 938 (s), 884 (s), 830 (v), 772 (m), 733 (w), 588 (m), 513 (m), 413 (s) cm^{-1}; **$Co_2Mn_2P_2$**, 1034 (s), 960 (w), 938 (s), 881 (s) 831 (v), 771 (m), 725 (w), 586 (m), 513 (m), 413 (s) cm^{-1}.

4.4 Results and Discussion

4.4.1. Stability and kinetics of water oxidation of $Co_4V_2W_{18}O_{68}^{10-}$

Folkman and Finke have critiqued the polyoxometalate water oxidation catalyst, **Co_4V_2**, by its synthesis, characterization,[30] and electrochemical stability.[31] The synthesis of this compound was first reported by Wu et al.,[27] and then replicated by Lv et al.[28] In both of these publications, the procedure for synthesis of the **Co_4V_2** resulted in little of the target POM due to stoichiometric ratios of the vanadium, cobalt, and tungsten components. The side products (*cis*-$[V_2W_4O_{19}]^{4-}$ and $[VW_5O_{19}]^{3-}$) using this route are dominant over the active WOC, **Co_4V_2**. In a new synthesis developed by Marika Wieliczko (MK), an excess of vanadium precursors are used and the main product is **Co_4V_2**, verified by ^{51}V NMR and single crystal XRD. Furthermore, replacing the sodium salt with tetrabutylammonium (TBA) salt of **Co_4V_2** generates a more stable compound when dissolved in acetonitrile.

When beginning with a mixed system of **Co_4V_2**, *cis*-$[V_2W_4O_{19}]^{4-}$, and $[VW_5O_{19}]^{3-}$ there is a difference in the water oxidation activity as noticed by the light-driven kinetics in Figure 4.1(a) and (b). Compared to the new synthesis prepared by MK, the purity of the **Co_4V_2** WOC appears to be consistent with less co-products. There is no significant change in light-driven water oxidation kinetics when the catalyst is aged for 2 hours (Figure 4.2). The co-products, *cis*-$[V_2W_4O_{19}]^{4-}$ and $[VW_5O_{19}]^{3-}$ are not active for water oxidation as shown in Figure 4.3.

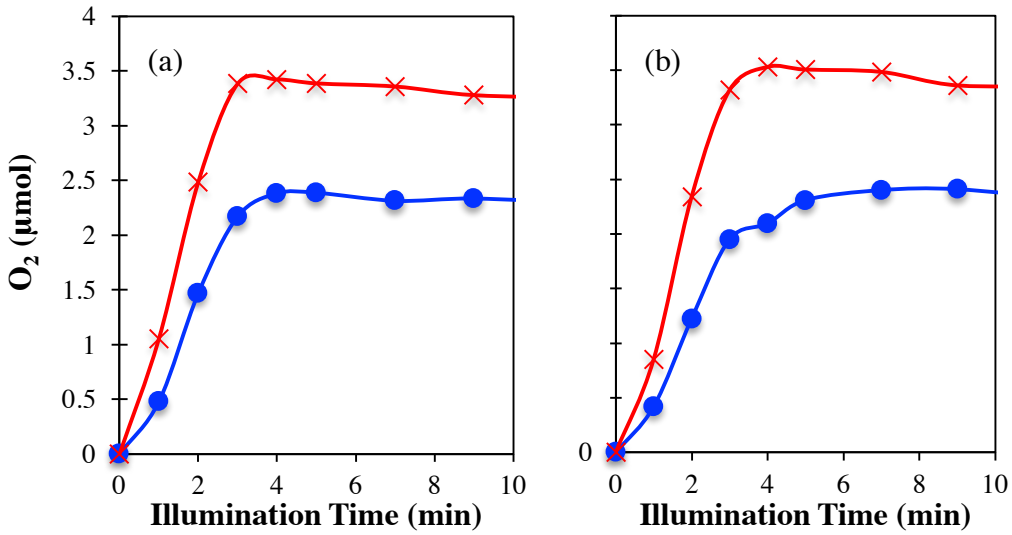

Figure 4.1 Light-driven water oxidation oxygen measurements using **Co_4V_2** (blue circles) and aging for 2 hours (red x's) prepared by synthesis methods of (a) Wu et al., and (b) Lv et al. Conditions: 440 nm LED, 20 mW, 8 µM **Co_4V_2**, 1.0 mM $[Ru(bpy)_3]Cl_2$, 5.0 mM $Na_2S_2O_8$, 80 mM sodium borate buffer, pH 9.

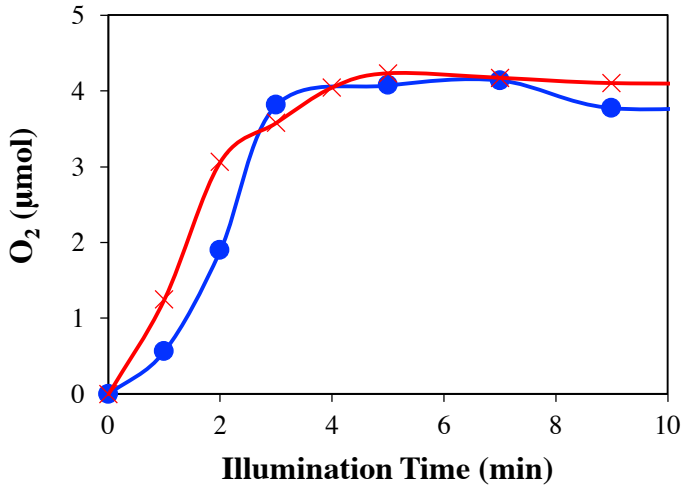

Figure 4.2 Light-driven oxygen measurements of Co_4V_2 (blue circles) and aging for 2 hours (red x's) prepared by synthesis method of MK. Conditions: 440 nm LED, 20 mW, 8 µM Co_4V_2, 1.0 mM $[Ru(bpy)_3]Cl_2$, 5.0 mM $Na_2S_2O_8$, 80 mM sodium borate buffer, pH 9.

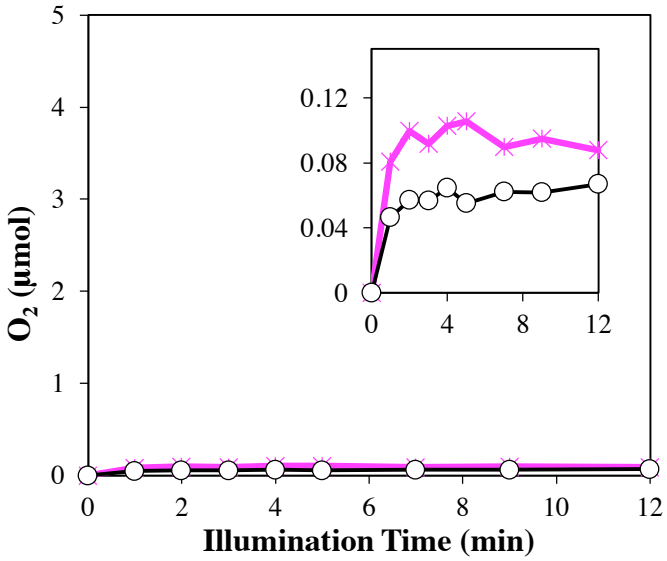

Figure 4.3 Light-driven oxygen measurements of *cis*-$[V_2W_4O_{19}]^{4-}$ (magenta stars) and $[VW_5O_{19}]^{3-}$ (black open circles). Inset: oxygen measurements with expanded y axis values. Conditions: 440 nm LED, 20 mW, 8 µM **Co_4V_2**, 1.0 mM $[Ru(bpy)_3]Cl_2$, 5.0 mM $Na_2S_2O_8$, 80 mM sodium borate buffer, pH 9.

Upon dissolution in an aqueous system, POMs can be constantly changing due to reversible acid-base equilibria. In buffered conditions, the POM speciation is controlled by pH, but can be further altered by temperature, chemical potential and counter-cations. The presence of a small amount of side-products is hard to limit in aqueous conditions (Figure 4.4). Using TBA-**Co_4V_2** in organic media avoids the presence of co-products by freezing the hydrolytic breakdown of POMs as seen in the ^{51}V NMR in Figure 4.5.

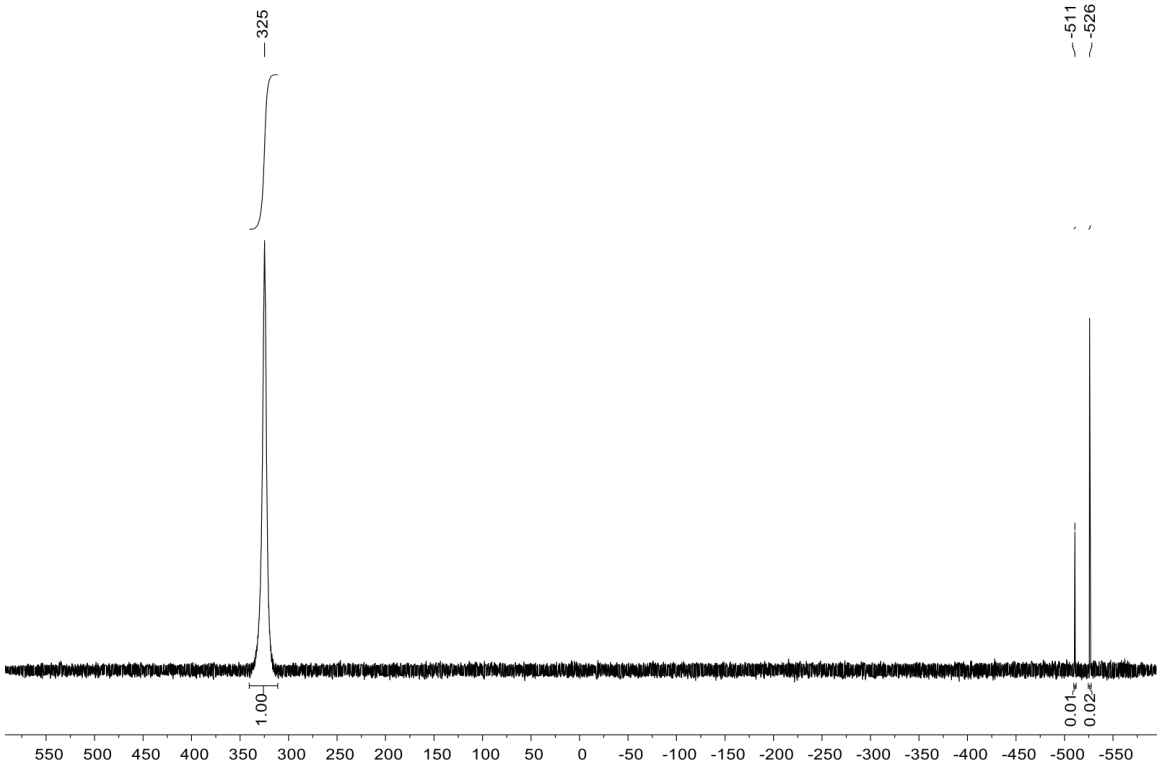

Figure 4.4 ^{51}V NMR of $Na_{10}Co_4V_2W_{18}O_{28}$ •$26H_2O$ (+325 ppm) with small amounts of $K_2V_2W_4O_{19}$•$8H_2O$ (-511 ppm) and $TMA_3VW_5O_{19}$ (-526 ppm).

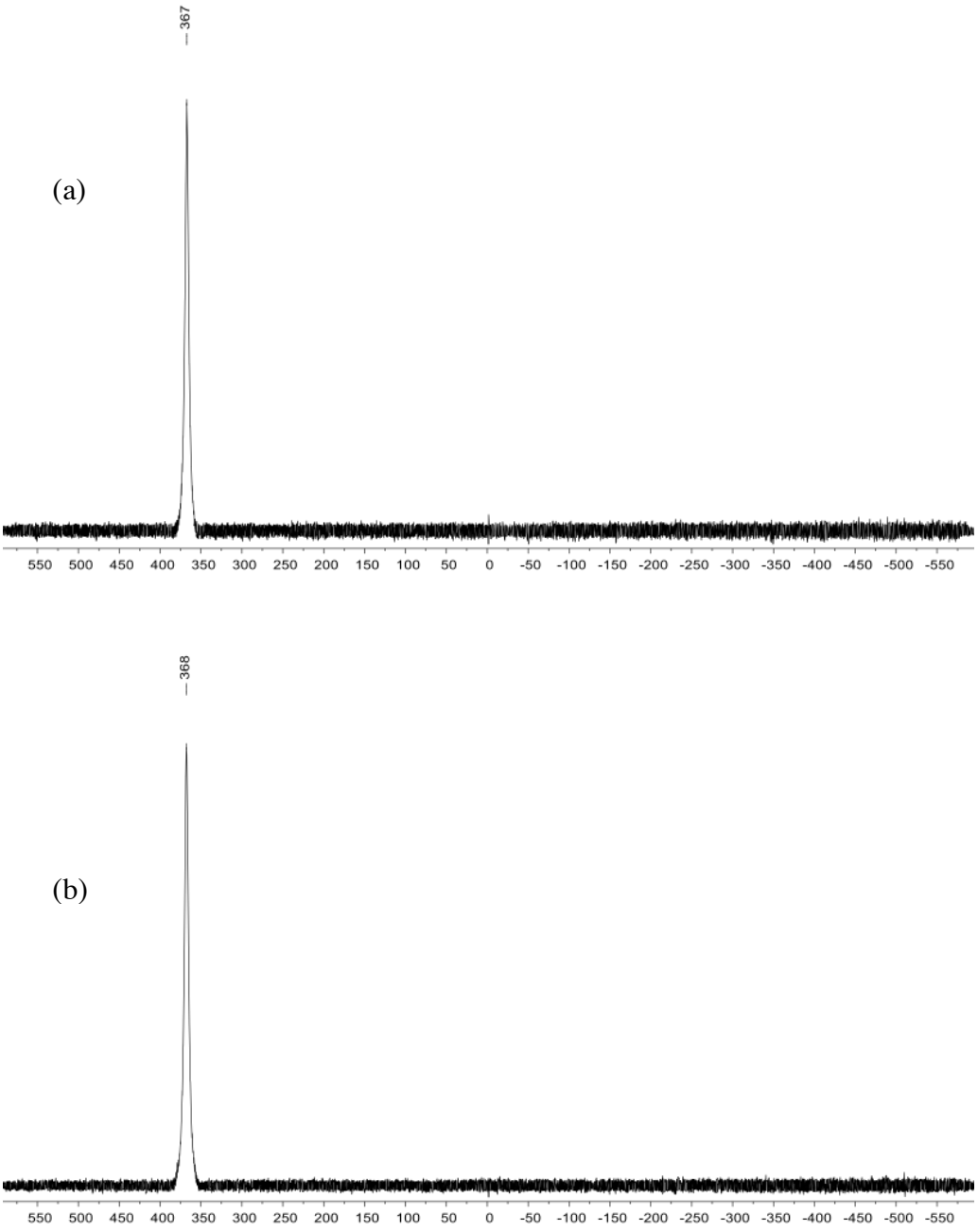

Figure 4.5 ^{51}V NMR of $TBA_7H_3Co_4V_2W_{18}O_{28}$ (+367 ppm) after (a) 30 minutes after dissolution and (b) 50 days after dissolution.

It is well-documented that Co-containing POMs are unstable in certain aqueous buffers, especially phosphate buffers, due to the strong competing complexation of Co

ions by phosphate buffer anions, resulting in decomposition of Co-POMs (**Co_4P_2** and **Co_4V_2**).[32] In the ^{31}P NMR study of **Co_4V_2** decomposition into $Co(II)_{aq}$ ions with phosphate buffer, the Co(II) can bind $H_2PO_4^-$ and HPO_4^{2-}, and these paramagnetic, larger species result in ^{31}P NMR line broadening.[31]

Similar to the way in which pH and buffers anions can perturb the system of POM WOCs, the use of Co-chelating reagents such as dimethylglyoxime (DMG) and bipyridine (bpy) can also affect the speciation of POMs by forming Co(II) DMG or bpy complexes. Therefore, the stability assessment of the M(II)-containing POMs is not clear with DMG and bpy. Instantaneous mixing of the POM with bpy results in reduced light-driven water oxidation activity as seen in Figure 4.6(a), but with aging together in buffer, the activity is slightly restored with the formation of a new complex and possibly excess $Co(II)_{aq}$ from the decomposition of the POM (Figure 4.6(b)).

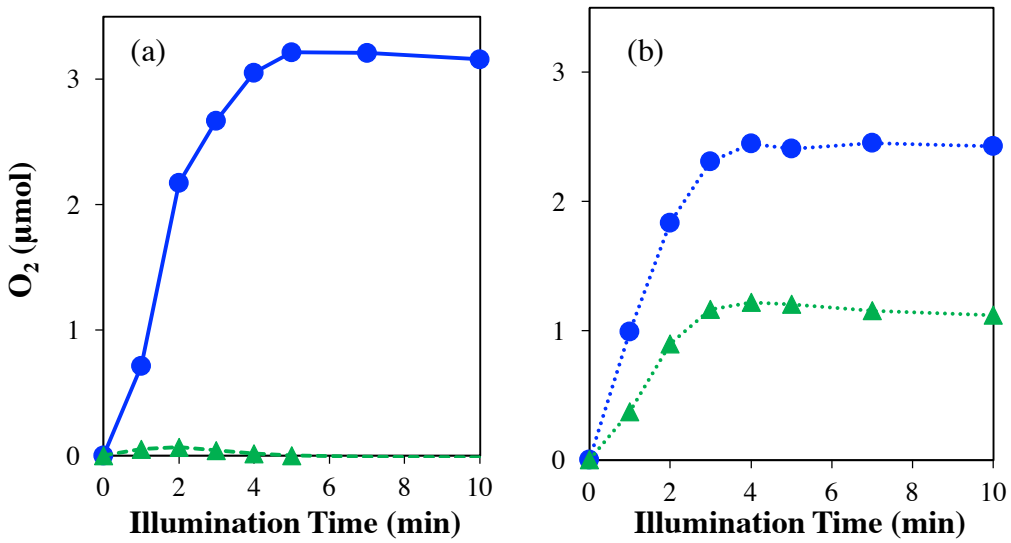

Figure 4.6 Light-driven water oxidation oxygen measurements using **Co_4V_2** (blue circles) and **Co_4V_2** mixed with 10 equivalents of bpy per Co atom (green triangles), (a) with 0 minutes of mixing and (b) aging for 1 hour. Conditions: 440 nm LED, 20 mW, 2

μM **Co_4V_2**, 8 μM bpy, 1.0 mM $[Ru(bpy)_3]Cl_2$, 5.0 mM $Na_2S_2O_8$, 80 mM sodium borate buffer, pH 9.

The sacrificial oxidant, $Ru(bpy)_3^{3+}$ has been used in many studies to assess the kinetics of light-driven water oxidation.[33] Because light-driven water oxidation oxygen measurements are susceptible to bpy ligand oxidation, it is necessary to also study the kinetics of the consumption of $Ru(bpy)_3^{3+}$ to complete the picture of the water oxidation kinetics. For a closer look at the water oxidation of $Co(II)_{aq}$ compared to **Co_4V_2**, the kinetic curves were collected under sacrificial oxidant [$Ru(bpy)_3^{3+}$] and light-driven oxygen measurements shown in Figure 4.7 (a) and (b).

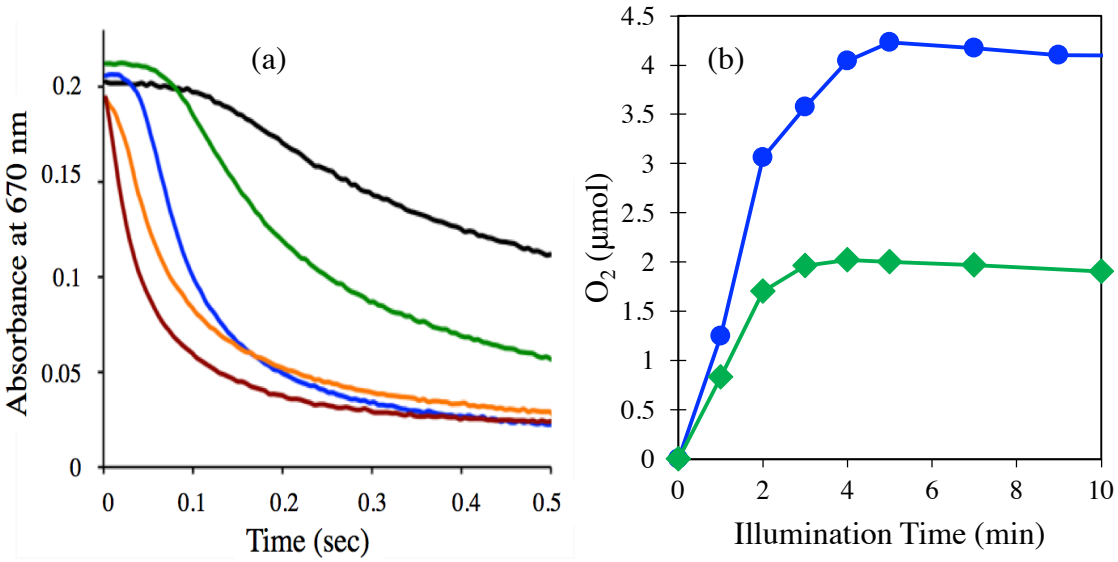

Figure 4.7 (a) Kinetics of $[Ru(bpy)_3]^{3+}$ reduction, measured at 670 nm, catalyzed by solutions of $Co(II)_{aq}$ and **Co_4V_2** in 80 mM sodium borate buffer, pH 9.0. The stock solution of the catalyst were aged for 1 hour in 160 mM sodium borate buffer, pH 9 and then mixed with 1 mM $[Ru(bpy)_3]^{3+}$. Co(II) (1 μM; black), 2 μM Co(II) (green), 4 μM

Co(II) (blue), 1 μM **Co_4V_2** (orange), 2 μM **Co_4V_2** (red). (b) light-driven oxygen measurements of 8 μM Co(II) (green diamonds) and 8 μM **Co_4V_2** (blue circles). Conditions: 440 nm LED, 20 mW, 1.0 mM $[Ru(bpy)_3]Cl_2$, 5.0 mM $Na_2S_2O_8$, 80 mM sodium borate buffer, pH 9.

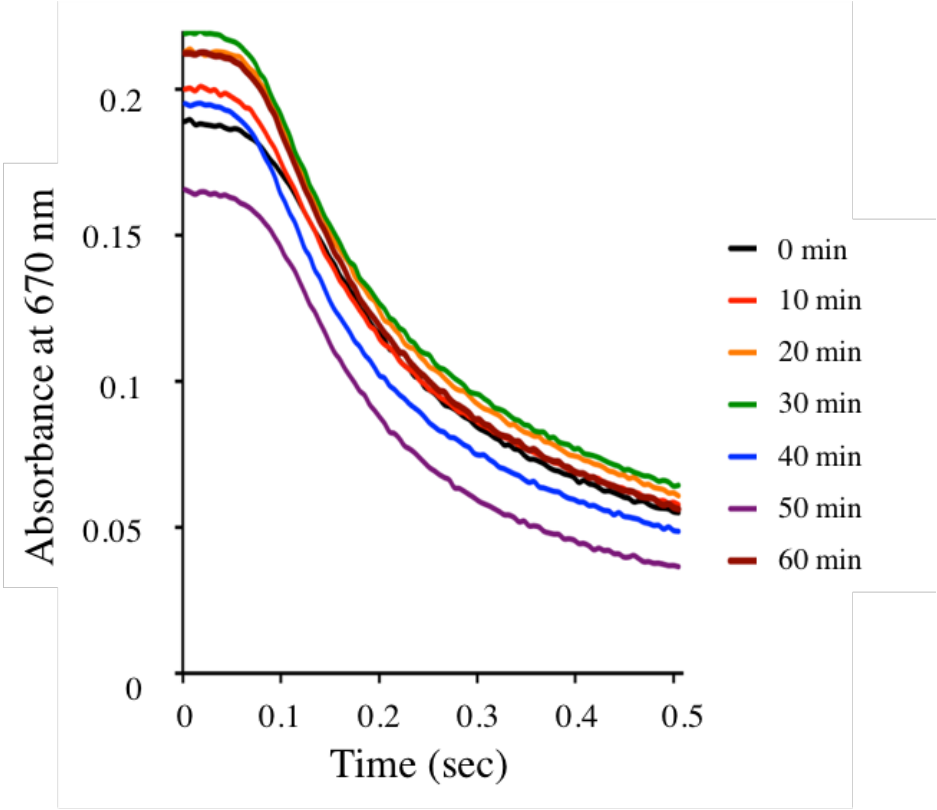

Figure 4.8 Kinetics of $[Ru(bpy)_3]^{3+}$ reduction, measured at 670 nm, catalyzed by solutions of 2 μM $Co(II)_{aq}$ and 0.5 mM $[Ru(bpy)_3^{3+}]$ in 80 mM sodium borate buffer, pH 9.0. The stock solution of the catalyst were aged for 1 hour in 160 mM sodium borate buffer, pH 9 and then mixed with 1 mM $[Ru(bpy)_3]^{3+}$.

4.4.2. Early-time kinetics of $[Co_2(M)_2(PW_9O_{34})_2]^{10-}$, M = Co^{II}, Ni^{II}, Mn^{II}, Zn^{II} in light-driven oxygen generation reactions with oxidant consumption

POM catalysts containing cobalt have led to much research on the role of the Co_4O_4 core and other variables.[34] For **Co_4P_2**[7] and **Co_4V_2**[7, 28] in particular, the influence of the P^V and V^V heteroatoms in the ligand may play a role in making these compounds such active WOCs. To probe the effect of the electronic structure on the activity and stability of these Co-POMs, transition metals Ni, Mn, and Zn have been incorporated centrally into the Co_4O_4 core. These mixed transition-metal sandwich POM WOCs were synthesized and assessed for their structure and early-time water oxidation kinetics. The syntheses involved a modification of the known method for preparation of $[Na_2M_2(PW_9O_{34}]^{12-}$, where M = Co^{II}, Ni^{II}, Mn^{II}, and Zn^{II}; sodium is exchanged for lithium in the external belt positions followed by convertion of these complexes into $[Co_2M_2(H_2O)_2(PW_9O_{34})_2]^{10-}$ (**$Co_2M_2P_2$**) by dissolving each M^{II} complex in a concentrated $CoCl_2$ solution. However, single-crystal X-ray diffraction revealed that **$Co_2Ni_2P_2$** is the only true mixed-metal POM. In contrast, the Co^{II}, Mn^{II}, and Zn^{II} derivatives reverted to **Co_4P_2** and other species (Figure 4.9). The FTIR-ATR spectra in Figure 4.10 also indicate that the Ni^{II} had remained in the central positions of the four-metal belt unit that exists in **$Co_2Ni_2P_2$** as determined by the shift in low frequency peaks and the split in the peak at 1032 cm^{-1}.

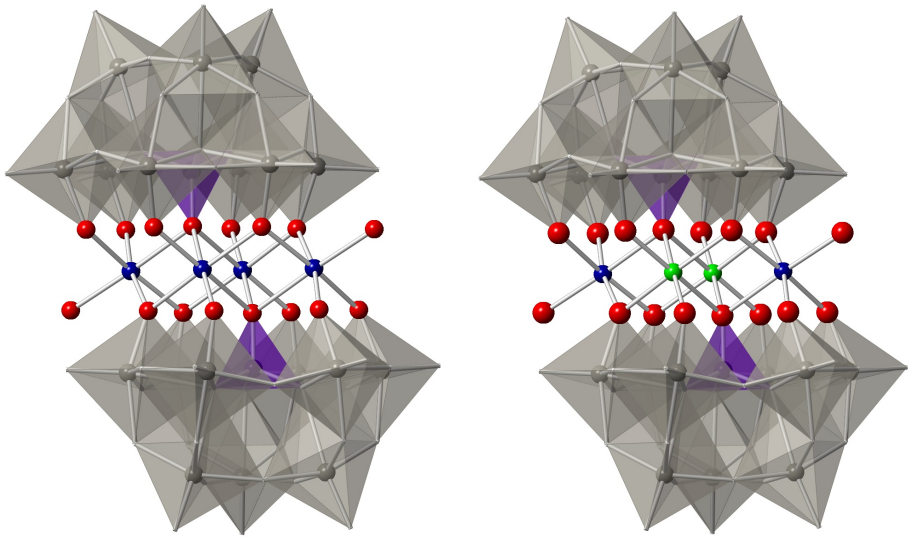

Figure 4.9 X-ray crystal structure of (a) $\mathbf{Co_4P_2}$ and (b) $\mathbf{Co_2M_2P_2}$, M= Co^{2+}, Zn^{2+}, Mn^{2+}, and Ni^{2+}. Color scheme: Co, blue; O, red; Co, Zn, Mn, or Ni, green; WO_6, gray.

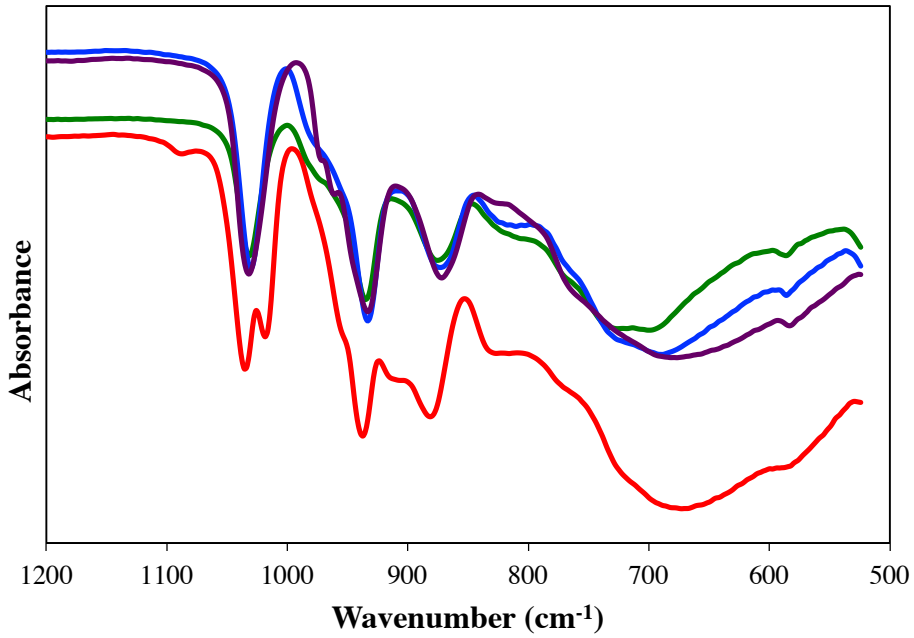

Figure 4.10 FTIR-ATR of $\mathbf{Co_2Co_2P_2}$ (purple), $\mathbf{Co_2Zn_2P_2}$ (green), $\mathbf{Co_2Mn_2P_2}$ (blue), and $\mathbf{Co_2Ni_2P_2}$ (red).

Interestingly, there is a yet-unexplainable difference in the **$Co_2Co_2P_2$**, **$Co_2Zn_2P_2$**, and **$Co_2Mn_2P_2$** light-driven oxygen evolution kinetic measurements. Because these three compounds are a mix of the **Co_4P_2** POM and other species, they should exhibit similar rates for oxygen generation; however, they all show varying degrees of activity. One trend remains constant—the **$Co_2Ni_2P_2$** has reduced water oxidation activity in both the light-driven oxygen evolution (Figure 4.11) and oxidant consumption kinetics (Figure 4.12).

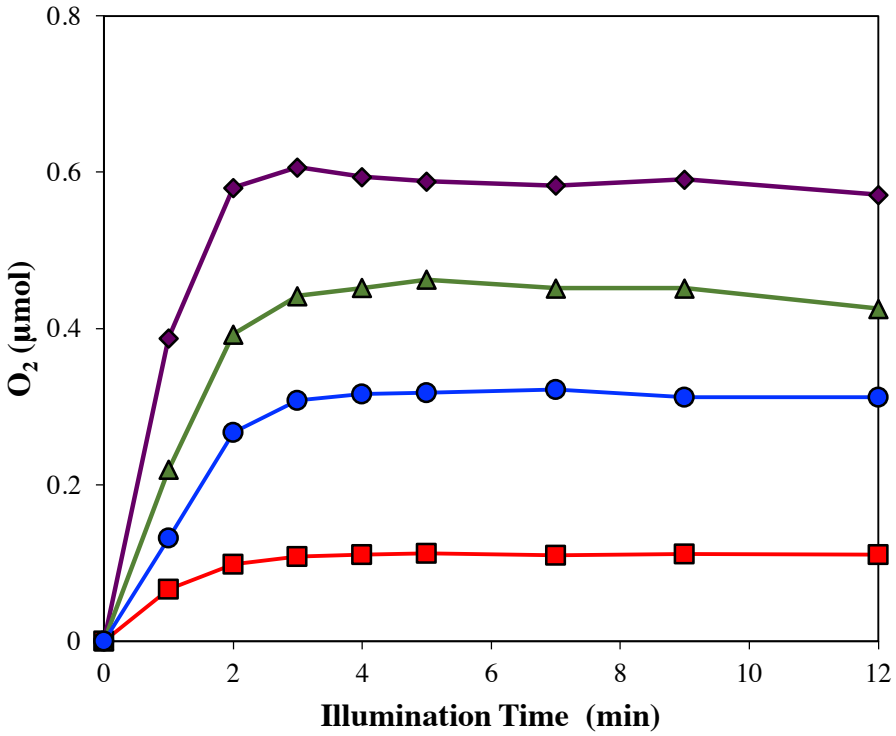

Figure 4.11 Light-driven water oxidation oxygen measurements of **$Co_2Co_2P_2$** (purple diamonds), **$Co_2Zn_2P_2$** (green triangles), **$Co_2Mn_2P_2$** (blue circles), and **$Co_2Ni_2P_2$** (red squares). Conditions: 80 mM sodium borate buffer, pH 9.0, 1 mM $[Ru(bpy)_3]Cl_2$, 5 mM $Na_2S_2O_8$, 5.2 μM $[Co_2M_2]$, 440 nm LED, 20 mW.

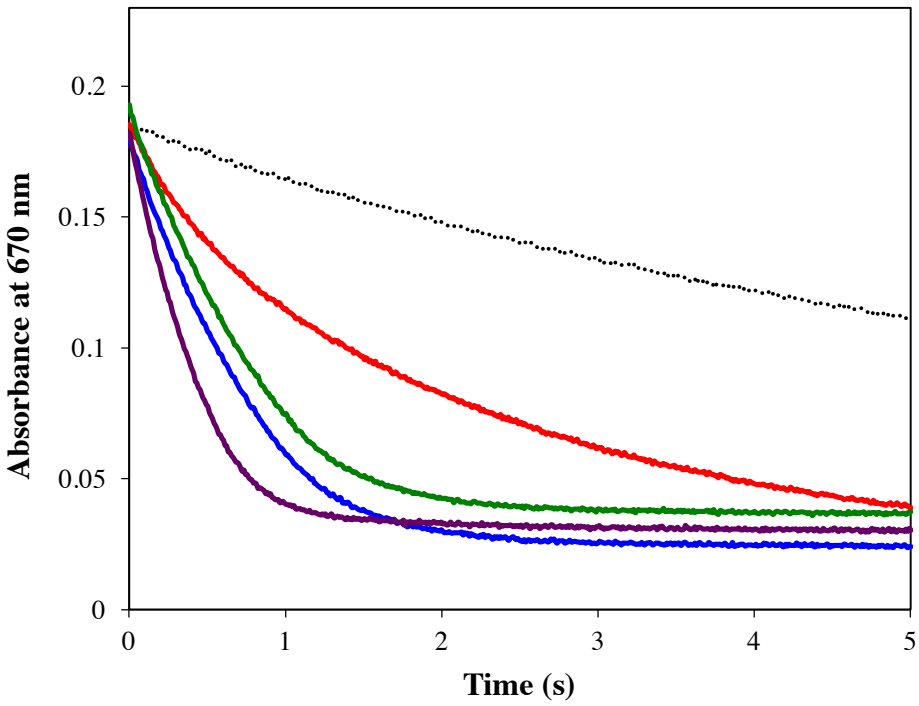

Figure 4.12 Kinetics of $[Ru(bpy)_3]^{3+}$ reduction, measured at 670 nm, catalyzed by solutions of buffer (dotted black line), **$Co_2Co_2P_2$** (purple line), **$Co_2Zn_2P_2$** (green line), **$Co_2Mn_2P_2$** (blue line), and **$Co_2Ni_2P_2$** (red line). Conditions: 80 mM sodium borate buffer, pH 9.0, 1 mM $[Ru(bpy)_3]Cl_2$, 5 mM $Na_2S_2O_8$, 5.2 μM [**$Co_2M_2P_2$**], The stock solution of the catalyst were aged for 1 hour in 160 mM sodium borate buffer, pH 9 and then mixed with 1 mM $[Ru(bpy)_3]^{3+}$.

Although these mixed metal POM WOCs have not been synthesized as desired, a direct comparison of **$Co_2Co_2P_2$** and **$Co_2Ni_2P_2$** reveals the effect of altering the electronic structure of the Co_4O_4 core. Further work comparing **$Co_2Zn_2P_2$** and **$Co_2Mn_2P_2$** is underway and will elucidate how the Co_4O_4 core and the POM WOCs can be altered to make faster and more stable catalysts.

4.4.3 Base-compatible POM WOC, $[H_9Cu_{25}O_8(Nb_7O_{22})_8]^{28-}$

Water oxidation in very high and very low pH's is a difficult task in terms of catalyst stability. At lower pH's, the potential required to oxidize water is extremely high and there are very few systems that function at high pH's. In alkaline conditions, the stability of the system is further inhibited and water splitting activitiy is slow. Reported here is the first POM WOC system capable of water oxidation at pH 13. This WOC system, henceforth "**$Cu_{25}Nb_{56}$**" (X-ray structure in Figure 4.13) was characterized as a homogenous electrocatalyst. **$Cu_{25}Nb_{56}$** was shown to be a stable molecular catalyst in five ways. First, the UV-vis spectra of this catalyst in solution before and after 24 hours of electrochemical measurements remained unchanged (Figure 4.14). The absorption for copper at 670 nm would have shifted if the POM decomposed and formed aqueous or uncomplexed Cu(II) ions.

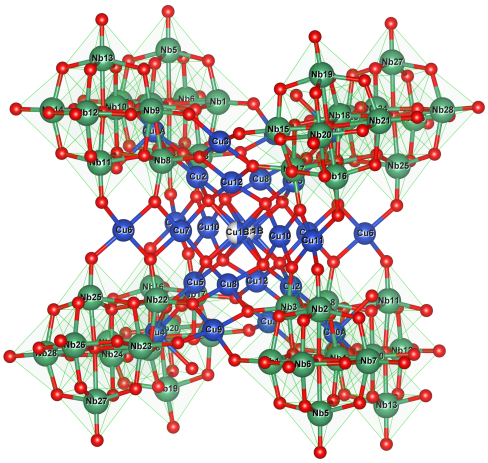

Figure 4.13 X-ray crystal structure of the first base-compatible POM WOC, $[H_9Cu_{25}O_8(Nb_7O_{22})_8]^{28-}$ (**$Cu_{25}Nb_{56}$**). Color scheme: Nb, green; Cu, blue; O, red.

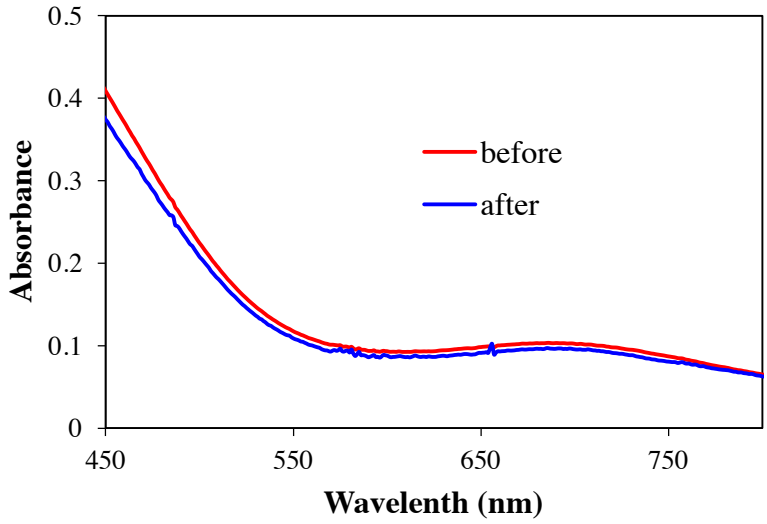

Figure 4.14 UV-Vis spectrum of $\mathbf{Cu_{25}Nb_{56}}$ before (red line) and after (blue line) 24 h electrolysis. Conditions: 1 mM $\mathbf{Cu_{25}Nb_{56}}$ catalyst in 0.1 M KOH (pH = 13) was used in bulk electrolysis. The solution was diluted 10 times by 0.1 M KOH for UV-Vis spectroscopy. There was no significant change in the absorption spectrum after a 24 h electrolysis period.

In a second stabilization experiment, FTIR spectra shows small changes to the POM WOC before and after bulk electrolysis (Figure 4.15). In both spectra, the vibrational frequencies for the framework of the Nb-O polyoxoniabate are found in 1200 – 400 cm^{-1} region, which suggests that the recovered catalyst remains intact.

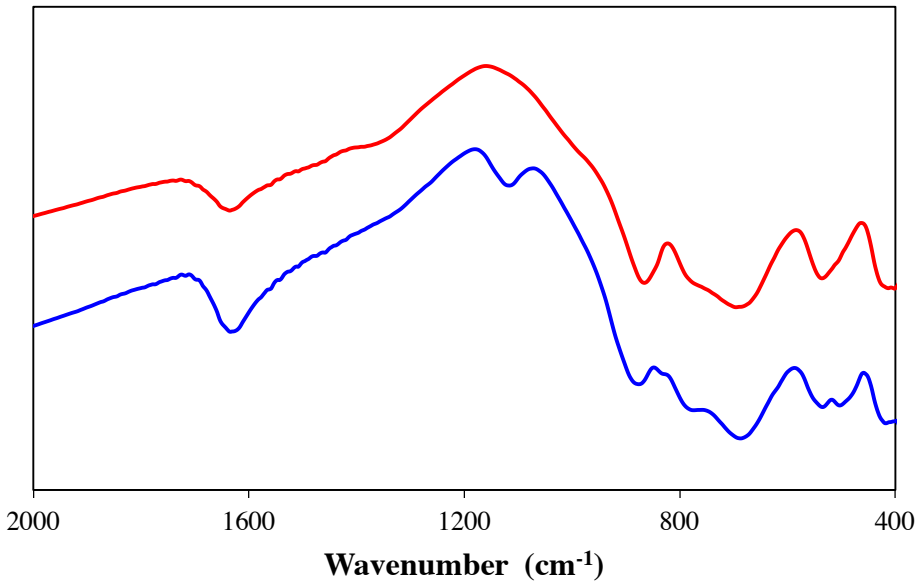

Figure 4.15 FT-Infrared spectrum of $\mathbf{Cu_{25}Nb_{56}}$ before (blue) and after (red, the green precipitate re-isolated from a "post-catalysis" solution) 24 h bulk electrolysis.

When the catalyst was immobilized on glassy carbon electrodes, consecutive electrochemical measurements after long-term bulk electrolysis resulted in unchanged glassy carbon surfaces under water oxidation turnover conditions. Successive CV measurements shown in Figure 4.16 reveal catalyst stability properties during electrochemical experiments. In a separate electrochemical experiment, the homogenous catalyst was left in solution and a polished FTO working electrode was used for bulk electrolysis with the potential held at 1.25 V vs. NHE. The stability of the catalyst in solution was assessed through CV comparison before and after 24 hour bulk electrolysis (Figure 4.17 and 4.18). Furthermore, electrodeposition of copper or copper oxides on the FTO working electrode would be expected if decomposition of the catalyst were occurring. SEM/EDX measurements in Table 4.1 reveal the absence of Cu on the surface of the FTO

working electrode. Finally, the homogenous electrocatalyst was confirmed to oxidize water as measured by a Neofox oxygen probe over 12 hours of bulk electrolysis in Figure 4.19.

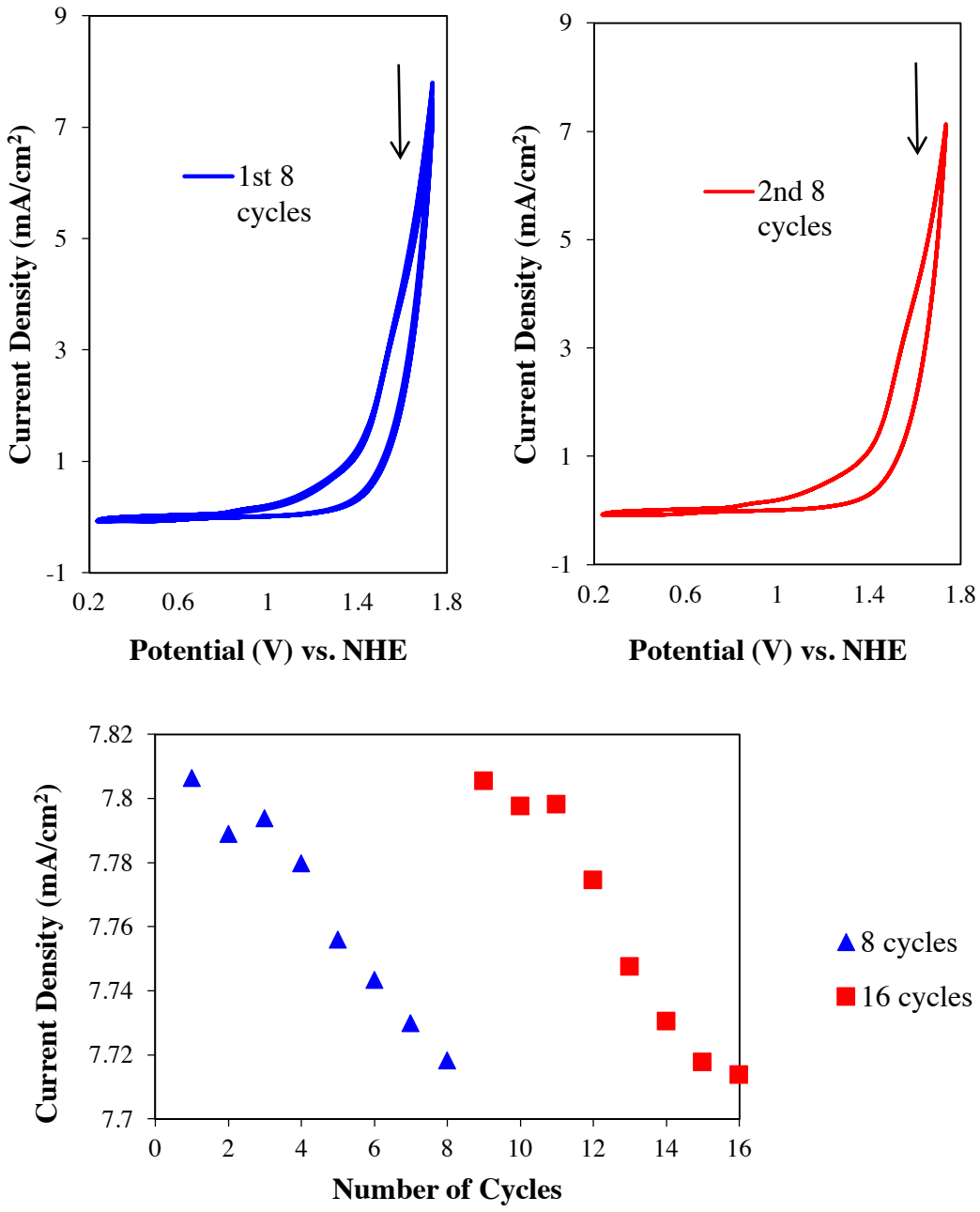

Figure 4.16 (Top) Two series of 8 continuous scan cycles of 1 mM $\mathbf{Cu_{25}Nb_{56}}$ in 0.1 M KOH (pH 13). No change in CV shape was observed during the multiple scans. (Bottom)

The plots of peak/plateau current density variations with the scan cycle number. Condition: glassy carbon working electrode (0.071 cm^2), scan rate 50 mV/s.

The current density was decreased following the scan cycles due to the generation of O_2 gas bubbles. Therefore, the glassy carbon working electrode was shaken slightly to remove the gas bubbles attached on the electrode surface prior to the following series of CVs.

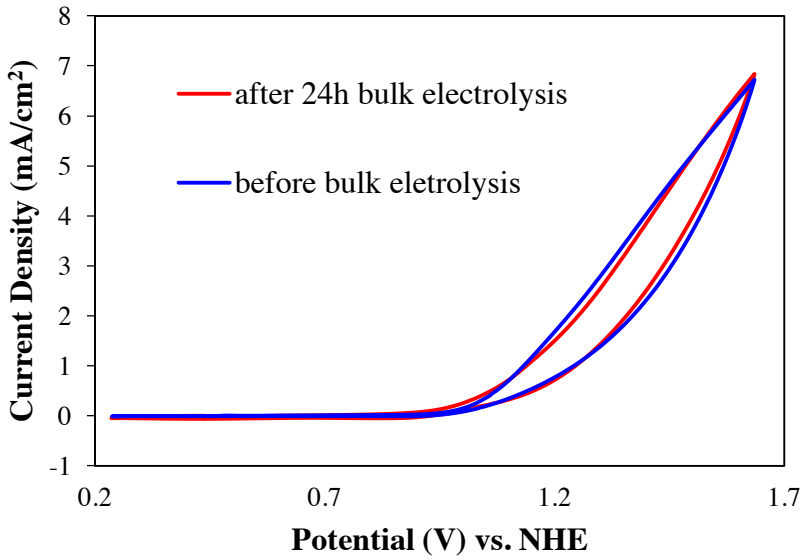

Figure 4.17 CVs of **$Cu_{25}Nb_{56}$** before (blue) and after (red) 24 hours of electrolysis at pH 13. Conditions: 0.1 M KOH, 1.25 V vs. NHE, FTO working electrode, A = 0.56 cm^2.

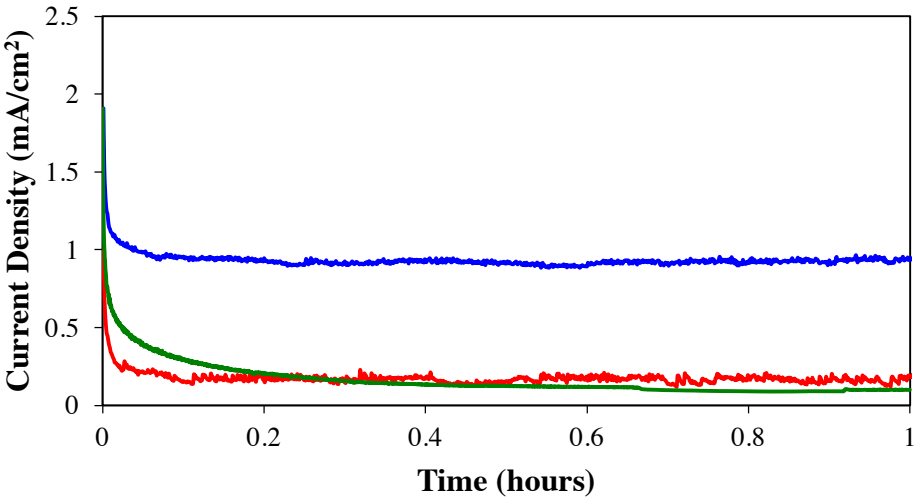

Figure 4.18 Catalytic current obtained upon 24 h bulk electrolysis at controlled potential (E = 1.25 V vs. NHE) with (red) and without (blue) 1 mM $\mathbf{Cu_{25}Nb_{56}}$ in 0.1 M KOH with FTO working electrode (A = 0.56 cm^2). After bulk electrolysis, the same electrode was rinsed continuously with DI water for 5 minutes (but not polished) before being used for bulk electrolysis in 0.1 M KOH without catalyst at E = 1.25 V.

Table 4.1 EDX analysis of FTO working electrode with $\mathbf{Cu_{25}Nb_{56}}$ in solution with no Cu electrodeposition

	Time			
Element	**0 hrs**	**6 hrs**	**12 hrs**	**24 hrs**
O	67.88	69.68	69.18	67.5
Si	6.72	8.1	7.74	6.22
Cu	0	0	0	0
Sn	25.4	22.22	23.08	26.28

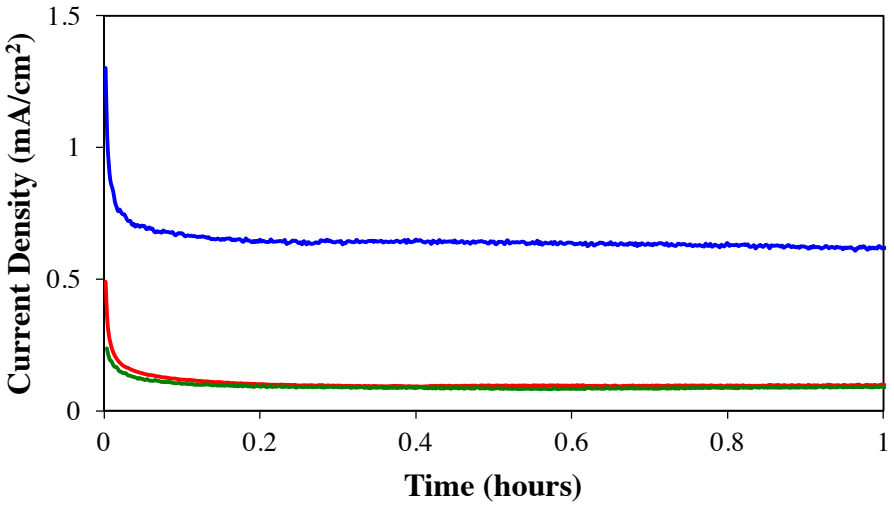

Figure 4.19 Current density obtained during bulk electrolysis at E = 1.25 V vs. NHE with (red) 1 mM $\mathbf{Cu_{25}Nb_{56}}$. After electrolysis, the GC working electrode was rinsed continuously with DI water for 5 minutes then used for electrolysis (E = 1.25 V vs. NHE) in 0.1 M KOH (green). No enhanced catalytic current was observed for washed electrode when compared with freshly polished GC working electrode in 0.1 M KOH buffer with $\mathbf{Cu_{25}Nb_{56}}$ (blue).

The electrochemical water oxidation activity of $\mathbf{Cu_{25}Nb_{56}}$ was measured by oxygen probe when immobilized on an FTO working electrode (Figure 4.20). The current that was passed through the electrode was used to determine the Faradaic efficiency. To ensure the system was not leaking ambient air inside, the system was purged with N_2 almost every hour.

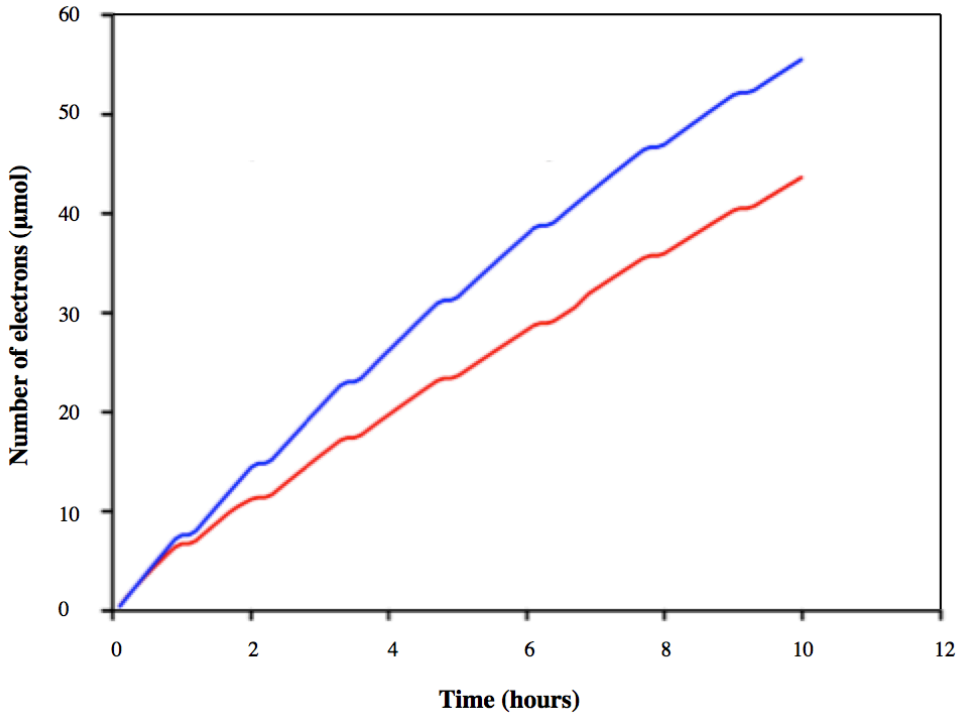

Figure 4.20 Oxygen measurements of $\mathbf{Cu_{25}Nb_{56}}$ using Neofox oxygen probe (red line) and Faradaic yield (blue line) in 0.1 M KOH at 1 V vs. Hg/HgO, FTO working electrode. Plateaus are indicative of pauses during electrocatalysis where the solution was purged with nitrogen.

4.5 Conclusions

POM catalyst development is an integral part of the broader efforts on renewable energy research. The molecular nature of these metal oxide polyanions (polyoxometalates, "POMs") continue to present unique opportunities in the investigation of water splitting systems. Moving forward, there is substantial interest for further advancements in POM WOC design for different catalytic conditions as well as their immobilization. At the same time, investigations have shown that we must pay significant attention to the stability of the catalysts, especially when heterogenized on electrode surfaces. Studying the POM

speciation and the mechanism of catalysis isn't straightforward, but is essential for garnering fundamentally useful insights into catalysis by POM-based systems and, by extension, many heterogeneous metal oxide systems. The explosion in POM WOC studies in the last 6 years is a testament to the intrinsic intellectual and potential practical value of this research.

4.6 References

1. Artero, V.; Fontecave, M., Solar fuels generation and molecular systems: is it homogeneous or heterogeneous catalysis? *Chemical Society Reviews* **2013,** *42* (6), 2338-2356.

2. Crabtree, R. H., Resolving Heterogeneity Problems and Impurity Artifacts in Operationally Homogeneous Transition Metal Catalysts. *Chem. Rev.* **2012,** *112*, 1536-1554.

3. Fukuzumi, S.; Hong, D., Homogeneous versus Heterogeneous Catalysts in Water Oxidation. *European Journal of Inorganic Chemistry* **2014,** *2014* (4), 645-659.

4. Lv, H.; Geletii, Y. V.; Zhao, C.; Vickers, J. W.; Zhu, G.; Luo, Z.; Song, J.; Lian, T.; Musaev, D. G.; Hill, C. L., Polyoxometalate water oxidation catalysts and the production of green fuel. *Chem. Soc. Rev.* **2012,** *41*, 7572-7589.

5. Stracke, J. J.; Finke, R. G., Distinguishing Homogeneous from Heterogeneous Water Oxidation Catalysis when Beginning with Polyoxometalates. *ACS Catalysis* **2014,** *4* (3), 909-933.

6. Sumliner, J. M.; Lv, H.; Fielden, J.; Geletii, Y. V.; Hill, C. L., Polyoxometalate multi-electron transfer catalytic systems for water splitting. *Eur. J. Inorg. Chem.* **2014,** *4*, 635-644.

7. Yin, Q.; Tan, J. M.; Besson, C.; Geletii, Y. V.; Musaev, D. G.; Kuznetsov, A. E.; Luo, Z.; Hardcastle, K. I.; Hill, C. L., A fast soluble carbon-free molecular water oxidation catalyst based on abundant metals. *Science* **2010,** *328*, 342-345.

8. Walter, M. G.; Warren, E. L.; McKone, J. R.; Boettcher, S. W.; Mi, Q.; Santori, E. A.; Lewis, N. S., Solar Water Splitting Cells. *Chem. Rev.* **2010,** *110* (11), 6446-6473.

9. Kudo, A.; Miseki, Y., *Chem. Soc. Rev.* **2009,** *38*, 253-278.

10. Guerrini, E.; Trasatti, S., Electrocatalysis in Water Electrolysis. In *Catalysis for Sustainable Energy Production*, Wiley-VCH Verlag GmbH & Co. KGaA: 2009; pp 235-269.

11. Kanan, M. W.; Nocera, D. G., In Situ Formation of an Oxygen-Evolving Catalyst in Neutral Water Containing Phosphate and Co^{2+}. *Science* **2008,** *321*, 1072-1075.

12. Artero, V.; Fontecave, M., Solar fuels generation and molecular systems: is it homogeneous or heterogeneous catalysis? *Chem. Soc. Rev.* **2012,** *42*, 2338-2356.

13. Pettersson, L., Equilibria of Polyoxometalates in Aqueous solution. In *Topics in Molecular Organization and Engineering - Polyoxometalates: From Platonic Solids to Anti-Retroviral Activity*, Pope, M. T.; Müller, A., Eds. Kluwer Academic Publishers: Netherlands, 1993; pp 27-40.

14. Pope, M.; Müller, A., *Topics in Molecular Organization and Engineering*. ER Academic Publishers: Boston, 1994; Vol. 10.

15. Ogo, S.; Miyamoto, M.; Ide, Y.; Sano, T.; Sadakane, M., Hydrothermal and solid-state transformation of ruthenium-supported Keggin-type heteropolytungstates [XW11O39{Ru(ii)(benzene)(H2O)}]n- (X = P (n = 5), Si (n = 6), Ge (n = 6)) to ruthenium-substituted Keggin-type heteropolytungstates. *Dalton Transactions* **2012,** *41* (33), 9901-9907.

16. Gerken, J. B.; McAlpin, J. G.; Chen, J. Y. C.; Rigsby, M. L.; Casey, W. H.; Britt, R. D.; Stahl, S. S., Electrochemical Water Oxidation with Cobalt-Based Electrocatalysts from pH 014: The Thermodynamic Basis for Catalyst Structure, Stability, and Activity. *J. Am. Chem. Soc.* **2011,** *133*, 14431-14442.

17. Polyoxometalates: From Platonic Solids to Anti-Retroviral Activity. . In *Top. Mol. Organ. Eng.*, Pope, M. T.; Müller, A., Eds. 1994; Vol. 10.

18. Kim, K. C.; Pope, M. T., Cation-Directed Structure Changes in Polyoxometalate Chemistry. Equilibria between Isomers of Bis(9)-tungstophosphatodioxouranate(VI) Complexes. *J. Am. Chem. Soc.* **1999,** *121* (37), 8512-8517.

19. Thiel, J.; Molina, P. I.; Symes, M. D.; Cronin, L., Insights into the Self-Assembly Mechanism of the Modular Polyoxometalate "Keggin-Net" Family of Framework Materials and Their Electronic Properties. *Crystal Growth & Design* **2012,** *12* (2), 902-908.

20. Hill, C. L.; Vickers, J. W.; Sumliner, J. M.; Lv, H.; Geletii, Y. V. In *Importance of buffer in the design and study of solar fuel production*, 247th ACS National Meeting & Exposition, Dallas, TX, United States, March 16-20, ENFL-146., 2014.

21. Stracke, J. J.; Finke, R. G., Electrocatalytic Water Oxidation Beginning with the Cobalt Polyoxometalate $[Co_4(H_2O)_2(PW_9O_{34})_2]^{10-}$: Identification of Heterogeneous CoO_x as the Dominant Catalyst. *J. Am. Chem. Soc.* **2011,** *133*, 14872-14875.

22. Roger, I.; Symes, M. D., First row transition metal catalysts for solar-driven water oxidation produced by electrodeposition. *Journal of Materials Chemistry A* **2016,** *4* (18), 6724-6741.

23. Vickers, J. W.; Lv, H.; Sumliner, J. M.; Zhu, G.; Luo, Z.; Musaev, D. G.; Geletii, Y. V.; Hill, C. L., Differentiating Homogeneous and Heterogeneous Water Oxidation Catalysis: Confirmation that $[Co_4(H_2O)_2(\alpha\text{-}PW_9O_{34})_2]^{10-}$ Is a Molecular Water Oxidation Catalyst. *J. Am. Chem. Soc.* **2013,** *135* (38), 14110-14118.

24. Sheehan, S. W.; Thomsen, J. M.; Hintermair, U.; Crabtree, R. H.; Brudvig, G. W.; Schmuttenmaer, C. A., A molecular catalyst for water oxidation that binds to metal oxide surfaces. *Nat. Commun.* **2015,** *6*, 6469.

25. Nyman, M.; Alam, T. M.; Bonhomme, F.; Rodriguez, M. A.; Frazer, C. S.; Welk, M. E., Solid-state Structures and Solution Behavior of Alkali Salts of the $[Nb_6O_{19}]^{8-}$ Lindqvist Ion. *J. Cluster Sci.* **2006,** *17* (2), 197-219.

26. Huang, Z.; Luo, Z.; Geletii, Y. V.; Vickers, J.; Yin, Q.; Wu, D.; Hou, Y.; Ding, Y.; Song, J.; Musaev, D. G.; Hill, C. L.; Lian, T., Efficient Light-Driven Carbon-Free Cobalt-Based Molecular Catalyst for Water Oxidation. *J. Am. Chem. Soc.* **2011,** *133*, 2068-2071.

27. Li, B.; Yan, Y.; Li, F.; Xu, L.; Bi, L.; Wu, L., Synthesis, crystal structure, and properties of two sandwich-type tungstovanadates. *Inorg. Chim. Acta* **2009,** (362), 2796-2801.

28. Lv, H.; Song, J.; Geletii, Y. V.; Vickers, J. W.; Sumliner, J. M.; Musaev, D. G.; Kögerler, P.; Zhuk, P. F.; Bacsa, J.; Zhu, G.; Hill, C. L., An Exceptionally Fast Homogeneous Carbon-free Cobalt-based Water Oxidation Catalyst. *J. Am. Chem. Soc.* **2014,** *136* (26), 9268-9271.

29. Hou, Y.; Xu, L.; Cichon, M. J.; Lense, S.; Hardcastle, K. I.; Hill, C. L., A New Family of Sandwich-Type Polytungstophosphates Containing Two Types of Metals in the Central Belt: $M'_2M_2(PW_9O_{34})_2^{12-}$ (M' = Na or Li, M = Mn^{2+}, Co^{2+}, Ni^{2+},and Zn^{2+}). *Inorg. Chem.* **2010,** *49*, 4125-4132.

30. Folkman, S. J.; Kirner, J. T.; Finke, R. G., Cobalt Polyoxometalate Co4V2W18O6810–: A Critical Investigation of Its Synthesis, Purity, and Observed 51V Quadrupolar NMR. *Inorganic Chemistry* **2016,** *55*, 5343-5355.

31. Folkman, S. J.; Finke, R. G., Electrochemical Water Oxidation Catalysis Beginning with Co(II) Polyoxometalates: The Case of the Precatalyst Co4V2W18O6810–. *ACS Catalysis* **2017,** *7* (1), 7-16.

32. Goberna-Ferrón, S.; Soriano-López, J.; Galán-Mascarós, J. R.; Nyman, M., Solution Speciation and Stability of Cobalt-Polyoxometalate Water Oxidation Catalysts by X-ray Scattering. *Eur. J. Inorg. Chem.* **2015**, 2833-2840.

33. Vickers, J. W.; Sumliner, J. M.; Lv, H.; Morris, M.; Geletii, Y. V.; Hill, C. L., Collecting meaningful early-time kinetic data in homogeneous catalytic water oxidation with a sacrificial oxidant. *Phys. Chem. Chem. Phys.* **2014,** *16* (24), 11942-11949.

34. Ayingone Mezui, C. S.; de Oliveira, P.; Teillout, A.-L.; Marrot, J.; Berthet, P.; Lebrini, M.; Mbomekallé, I. M., Synthesis, Structure, and Magnetic Electrochemical

Properties of a Family of Tungstoarsenates Containing Just CoII Centers or Both CoII and FeIII Centers. *Inorg. Chem.* **2017,** *56* (4), 1999-2012.